U.S. DEPARTMENT OF COMMERCE • John T. Connor, Secretary

ENVIRONMENTAL SCIENCE SERVICES ADMINISTRATION
Robert M. White, Administrator

Weather Bureau

TECHNICAL NOTE 3-NSSL-24

Papers on Weather Radar, Atmospheric Turbulence, Sferics and Data Processing

CHARLES G. CLARK
WILLIAM E. COBB
J. T. DOOLEY
KATHRYN C. GRAY
WILLIAM C. HERRMANN
EDWIN KESSLER
GILBERT D. KINZER
SHASHI M. KULSHRESTHA
JEAN T. LEE
CHARLES H. MEEKS
BYRON B. PHILLIPS
LESLIE D. SANDERS
JACK L. TEAGUE
NEIL B. WARD
KENNETH E. WILK

WASHINGTON, D.C.
August 1965

PREFACE

The National Severe Storms Laboratory was established at Norman, Okla. by the United States Weather Bureau in January 1964. The present report collects many of the results of the first year's in-house investigations; authors are NSSL staff except where otherwise indicated.

This report should reveal much of the character of our program to the meteorological community and provide bases for useful discussion before some completed studies will be proposed for formal publication. We hope that these works will suggest to discerning readers the nature of unsolved problems suitably posed and relevant to national needs.

More generally than in the formal literature, these notes represent studies which may still be incomplete, but they indicate the scope of the program and its probable future development. Already, some of the techniques described herein are being changed. This is true, for example, of weather radar data collections, which should become more comprehensive and nearly automatic and provide digital data of improved accuracy and reliability.

The United States Weather Bureau NSSL program reflects the cooperative efforts and substantial support of the Federal Aviation Agency, National Aeronautics and Space Administration, U. S. Air Force, U. S. Army, Department of Agriculture, and various groups within U. S. Weather Bureau. The Office of Naval Research and Atomic Energy Commission, and units of commerce and education under Government contracts or other arrangements, have also participated in the program.

The interactions of various meteorological processes are complex and their setting is vast. Development of substantially improved syntheses of theories and observations, and applications, requires a multidisciplinary approach involving considerable resources.

Edwin Kessler
Director, NSSL

CONTENTS

WSR-57 REFLECTIVITY MEASUREMENTS AND HAIL OBSERVATIONS

Neil B. Ward, Kenneth E. Wilk, and William C. Herrmann

ABSTRACT

Hail reports of volunteer observers are related to the maximum intensities of the associated radar echoes. Eighty-five percent of hail occurrences in Oklahoma is associated with equivalent radar reflectivity factors Z_e, greater than $10^5 mm^6 m^{-3}$. With Z_e less than 10^4, hail is rare and small.

1. INTRODUCTION

The relationship of radar reflectivity measurements to hail occurrences in thunderstorms has been studied by several investigators. Donaldson [1] found that hail in Massachusetts is often associated with a reflectivity peak aloft where $Z_e > 10^5 mm^6 m^{-3}$ (Z_e is discussed on pp. 33 ff). This was confirmed in Texas by Inman and Arnold [2] and in Illinois by Wilk [3]. A significant restriction common to these studies, however, was the use of X-band radars.

Geotis [4] provided comparative data for a 10-cm. radar. His findings are that height-variations of reflectivity do not furnish a unique indication of hail, but that hail is indicated by low level equivalent reflectivities exceeding $5 \times 10^5 mm^6 m^{-3}$.

2. RECENT STUDIES WITH THE WSR-57 WEATHER RADAR

Several Weather Bureau investigators have discussed the operational use of 10-cm. radars for hail identification. Conte, et al. [5] and Williams, et al. [6] combined three years of WSR-57 observations of hail-producing thunderstorms. The hail data used in these studies conducted at the Weather Bureau Airport Station at St. Louis, Mo., were obtained from volunteer observers in eastern Missouri and southwestern Illinois. The results are summarized in the frequency distribution bar graphs of figure 1. Figure 1a shows that with the antenna at zero degrees, over 90 percent of the reported hail occurrences are accompanied by core reflectivity factors $Z_e > 10^4 mm^6 m^{-3}$. Figure 1b indicates that the reflectivity distribution narrows when hail is related to maximum reflectivities aloft and that

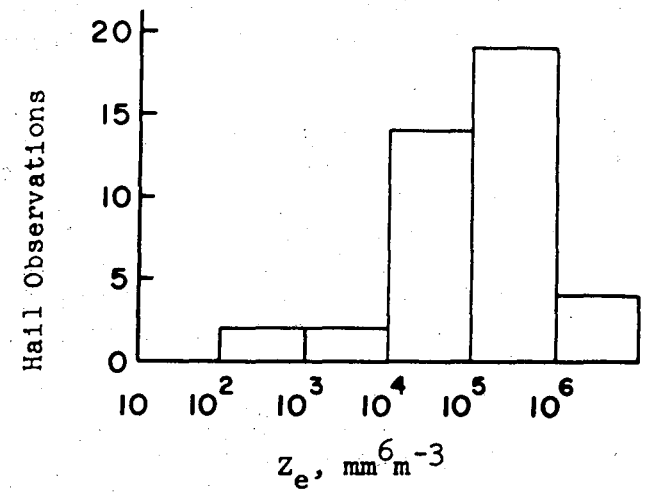

a. Maximum Reflectivity with antenna at zero degrees, 41 occurrences

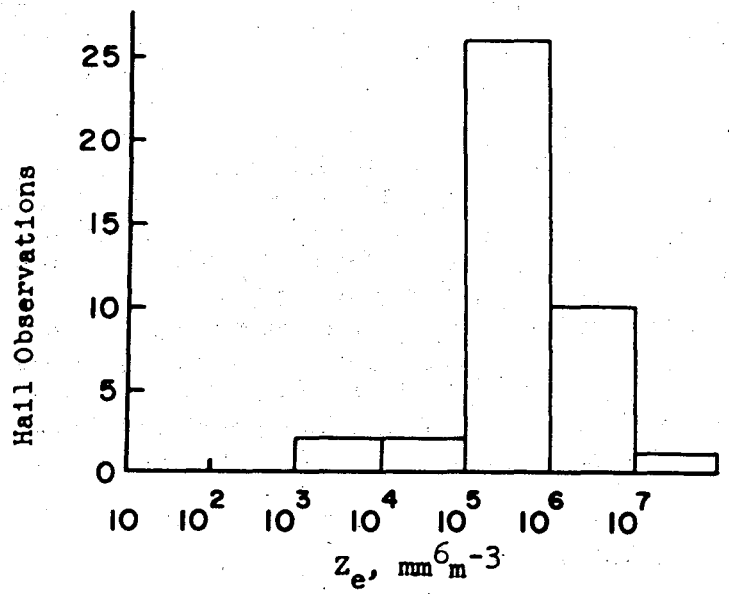

b. Maximum Reflectivity Observed at Any Elevation, 41 occurrences

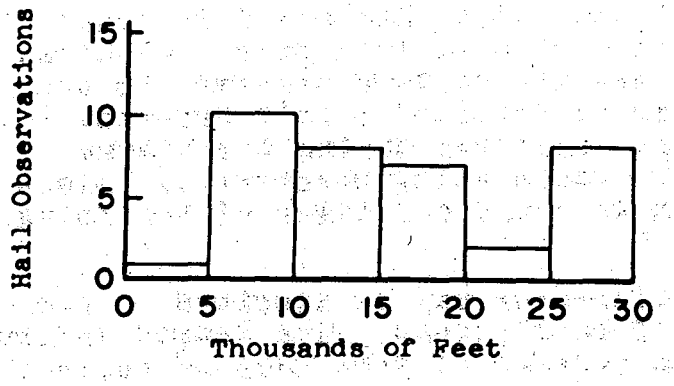

c. Height of Maximum Reflectivity, 36 occurrences

Figure 1. - Hail frequency in relation to the radar reflectivity of storm cores (after Conte, Williams, et al. [5]).

90 percent of hail occurrences are associated with Z_e's greater than 10^5 mm.^{6} m^{-3} aloft. The very broad distribution of heights of reflectivity maxima is shown in figure 1c.

Six severe storm reflectivity profiles studied by Hamilton [7] at WBAS, Kansas City, Mo., indicate that reflectivity maxima occur aloft at S-band in association with surface hail, but are not as sharply defined as at X-band.[1] The average height of maximum reflectivity for these data shown in figure 2 is about 19,000 ft. Note that Z_e is in the range $10^5 < Z_e < 10^6$ except for profile No. 6, which corresponds to the largest hail and the shortest distance from the radar.[2]

Extensive convective echo data collected by Whalen [8] at WBAS, Minneapolis shows that reflectivity maxima with Z_e between 10^4 and 10^7 often occur near 12,000 ft. However, a large percentage of cases show uniform reflectivity from the surface to about 10,000 ft. with Z_e decreasing above that level. A comparison of the St. Louis, Kansas City, and Minneapolis data suggests that the height of maximum Z_e in thunderstorms tends to be lower at higher latitudes.

Reflectivity maxima aloft have not yet been wholly explained, but probably result from a combination of factors. Accumulation of large raindrops and hailstones in strong updrafts and some melting of hail at low altitudes probably partially account for the observed maxima aloft. The wider beamwidth of the 10cm. radar contributes to the differences in maximum reflectivity seen by the CPS-9 and the WSR-57. Attenuation of 3-cm. energy in high liquid water contents at low altitudes may reduce the 3-cm. echo relative to that returned from aloft since attenuation by frozen hydrometeors is smaller.

3. NSSL DATA

Point hail data have been correlated with specific radar reflectivity values over a 30-county area in central Oklahoma. The reflectivity measurements are the maximum observed in the particular storms corresponding to particular hail reports. The hail sizes are the "average" observed during the storms (subjectively determined by the cooperating observers). Since the cooperative observers tend to round off times of beginning

---

[1] Some, but not all, of the differences may be ascribed to the wider beamwidths (2°) of the S-band radars. The X-band radars discussed in the hail studies referenced here have 1° beamwidths.

[2] At short range relatively enhanced reflectivities may result because the beam is more nearly filled by narrow hail shafts.

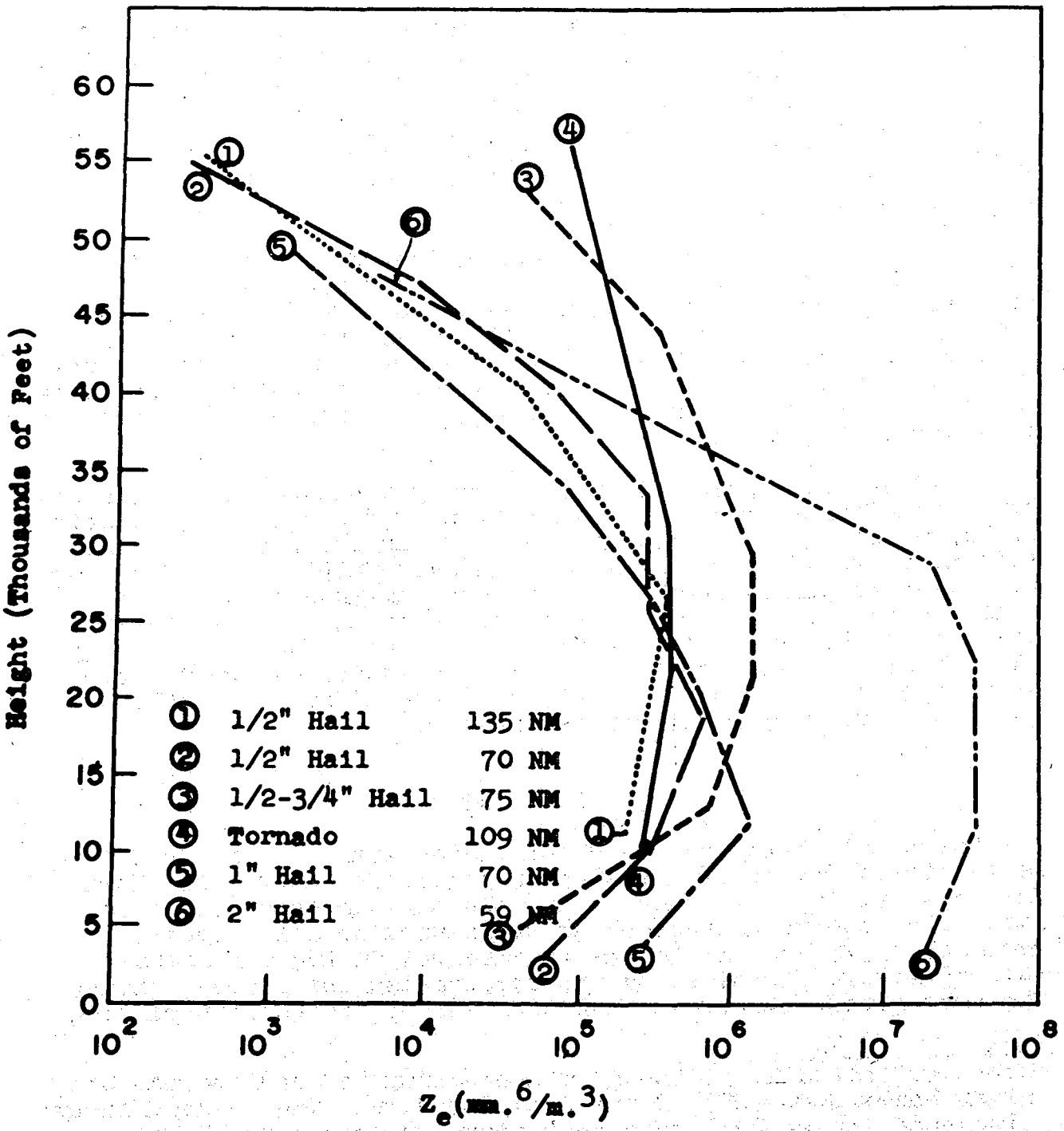

Figure 2. - Vertical profiles of Z_e in the cores of severe storms (after Hamilton [7]).

and ending of an event to the nearest 5 or 10 minutes, our ability to relate simultaneous radar echoes and hail is correspondingly limited. Fifty-three percent of the times of hail reported by observers end in the digit zero, 33 percent end in 5, and the other digits each appear about 2 percent of the time.

In 1963, Watts, et al. [8] of NSSL, published data collected during 1962 and 1963 relating hail size to radar reflectivity. With additional data obtained in 1964, the sample is perhaps the largest of its type collected to date. Table 1 shows the frequency distribution of hail sizes defined by 368 reports, no two of which refer to the same storm at time intervals closer than 7 minutes.

Table 1. - 368 Hail Reports, 1962 - 64

Average Diameter (inches)	Number of Reports	% of Total
1/4	160	43.5
1/2	115	31.2
3/4	53	14.4
1 or greater	40	10.9

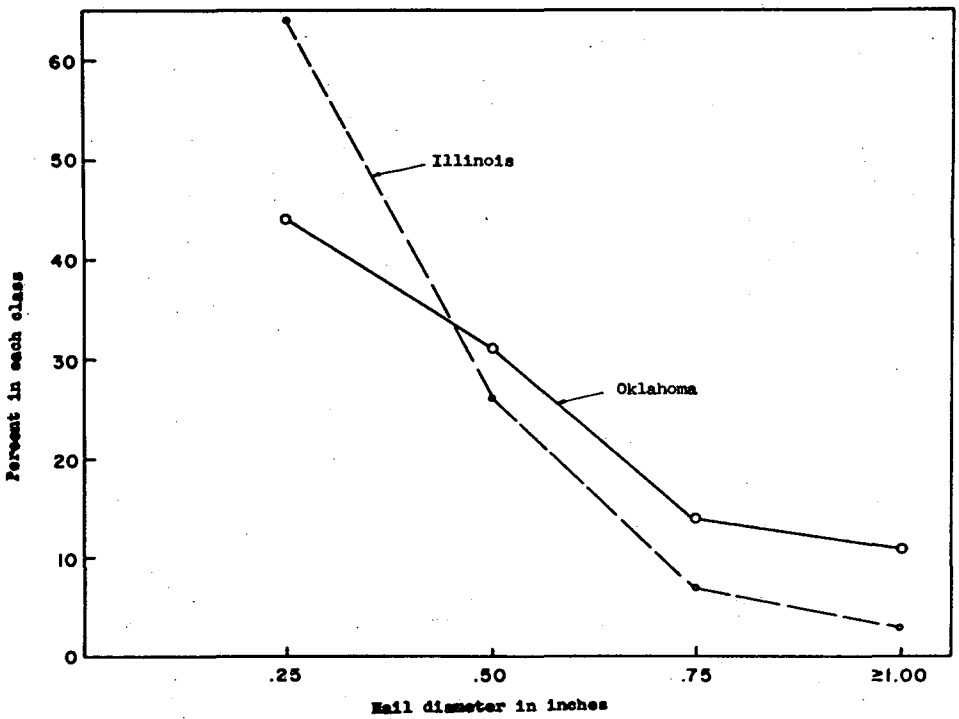

Figure 3. - Frequency of hail in four classes in Oklahoma (NSSL data) and in Illinois [9].

Figure 3 shows relative frequencies of different sizes of hail reported by cooperating observers in Oklahoma and Illinois [9]. To the extent that the Oklahoma and Illinois observers have equal tendencies to emphasize reports of larger hail, it seems that large hail is proportionately more common in Oklahoma.

Figure 4 shows the distribution of Oklahoma hail occurrences in relation to the maximum core reflectivity of the hail-producing thunderstorms as observed with the NSSL radar. Note that about 85 percent of the hail-producing storms are identified by Z_e's above 10^5mm.^{6} m.$^{-3}$ In the small fraction of cases which occurred with Z_e less than 10^5, 73 percent of hail diameters were only 1/4 inch or less.

In general, the frequency of occurrence of echoes decreases with increasing maximum echo intensity. Therefore, the ascending portion of the bar graph in figure 4 is probably related to an increasing likelihood that the specified echo intensities contain hail. The descending portion of the bar graph is probably closely related to a decreasing frequency of severe echoes of progressively greater intensity, practically all of which contain hail. Unfortunately, we are not yet able to say with certainty what proportion of echoes of specified intensity are associated with hail; the statistical analyses of radar data discussed on p. 99 in this report should contribute to answers to this question.

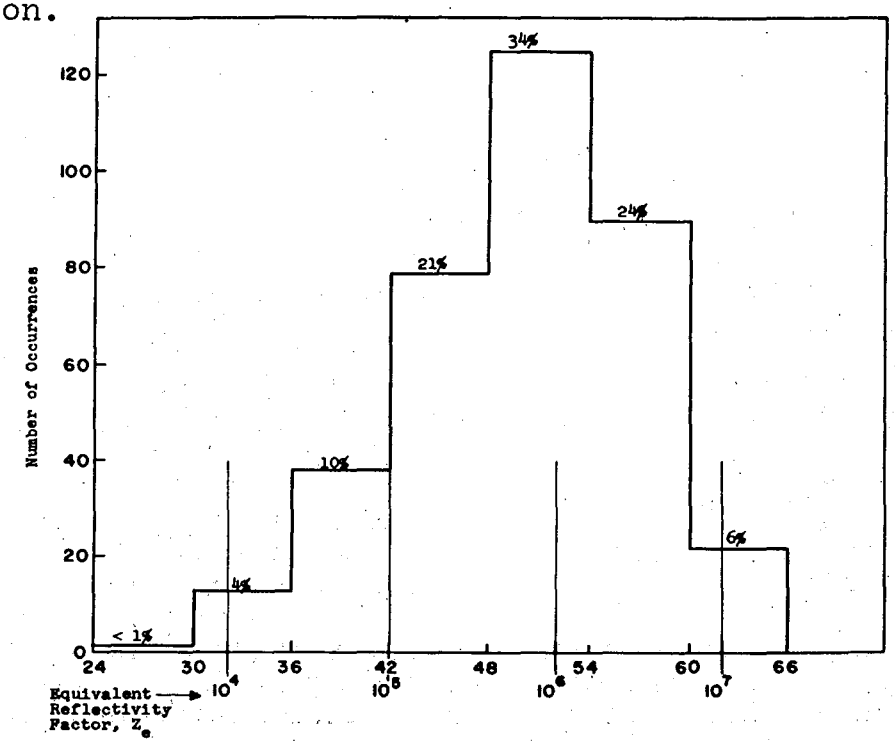

Figure 4. - Distribution of Oklahoma hail in relation to the radar reflectivity of storm cores. The abscissa shows the radar gain reduction in db. which reduces the indicated Z_e to threshhold detection on the PPI when the WSR-57 MDS is -105 dbm.

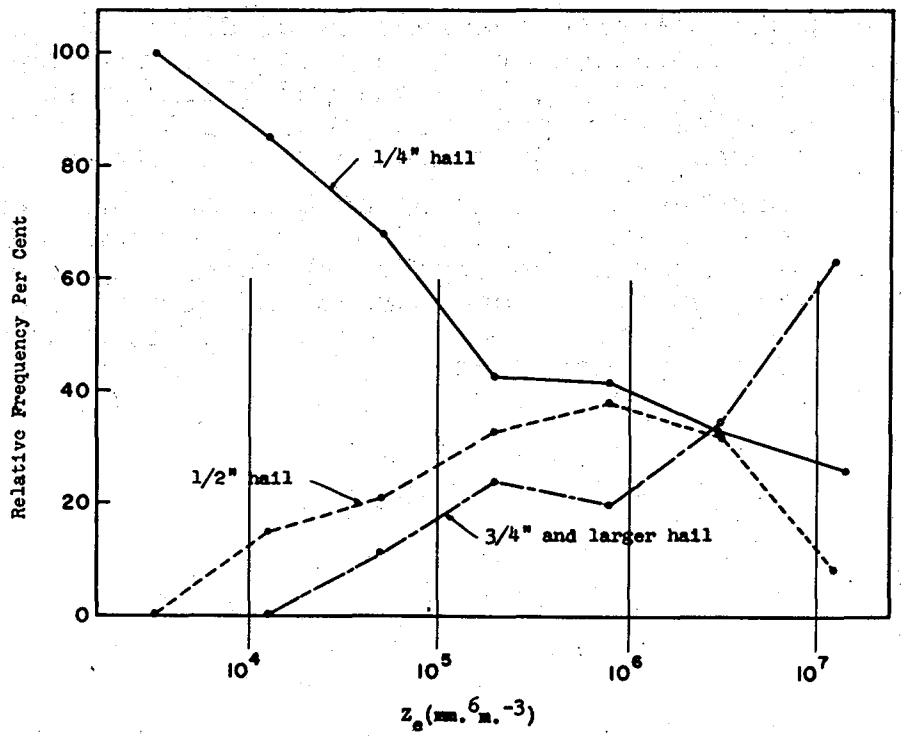

Figure 5. - Relative frequency of three size categories of Oklahoma hail in relation to Z_e of storm cores.

Figure 5 shows how the hail occurrences reported with different echo intensities are distributed with size. Practically all of the hail reported when $Z_e \leq 10^4$ is 1/4 inch or smaller in diameter. When $Z_e = 10^7$, nearly two-thirds of the reported hail is 3/4 inch in diameter or larger. As before, figure 5 does not indicate what fraction of radar echoes of given intensity have associated hail. However, the NSSL experience with the program of aircraft penetrations has led us to believe that most Oklahoma echoes for which Z_e is 10^5 or more contain significant hail somewhere, and that much less than half of echoes for which $Z_e = 10^4$ contain hail. We hope to refine these estimates in a later study.

It may be noted that, in the absence of hail, $Z_e = 10^4 mm.^6 m.^{-3}$ corresponds to a rainfall rate of about 1/2 in./hr. and $Z_e = 10^6$ corresponds to about 8 in./hr., in accordance with $Z = 200\ R^{1.6}$ where R is in mm./hr. The same vigorous updrafts required to accumulate water contents associated with rates of cloudburst intensity are effective in forming hail. In tropical climates, where the melting level is at higher altitudes, and high water vapor contents extend to greater heights than in central and northeastern United States, we expect that hail is not commonly associated with the smaller values of Z_e associated with hail in this report.

4. SUMMARY AND CONCLUSIONS

The 10-cm. radar data indicate that storm reflectivity at low levels or aloft is an index of the occurrence and size of hail. Hail occurs occasionally with radar reflectivities as low as $10^4 mm.^6 m.^{-3}$; in these cases hail is usually not larger than 1/4 inch in diameter. As the reflectivity increases, the probability that hail occurs and that it is large increases, although further study is required to determine with reasonable certainty the proportion of observed echoes of different intensities which contain hail. Most hail reports in Oklahoma are associated with echoes whose reflectivity factor Z_e is about $10^6 mm.^6 m.^{-3}$, and most echoes where $Z_e \leq 10^5$ probably contain some significant hail.

REFERENCES

1. Donaldson, R. J., Jr., "Radar Reflectivity Profiles in Thunderstorms," Journal of Meteorology, vol. 18, 1961, pp. 292-305.

2. Inman, R. L. and J. E. Arnold, "Thunderstorm Characteristics," Chapter II of Utilization of AN/CPS-9 Radar in Weather Analysis and Forecasting, Final Report, Contract AF 19(604)-6136, A&M College of Texas, 1961, pp. 8-73.

3. Wilk, K. E., "Radar Reflectivity Observations of Illinois Thunderstorms," Proceedings Ninth Weather Radar Conference, American Meteorological Society, Boston, 1961, pp. 127-132.

4. Geotis, S. G., "Some Radar Measurements of Hail," Proceedings Ninth Weather Radar Conference, American Meteorological Society, Boston, 1961, pp. 133-138.

5. Conte, J. J. and Radar Staff, "Radar Determination of Hail Occurrence," Progress Report No. 14, WSR-57 Radar Program, U. S. Weather Bureau, 1964.

6. Williams, W. E. and Radar Staff. "Radar Determination of Hail Occurrence," Progress Report No. 15, WSR-57 Radar Program, U. S. Weather Bureau, 1965.

7. Hamilton, R. E., "Thunderstorm Reflectivity Profiles," Progress Report No. 13, WSR-57 Radar Program, U. S. Weather Bureau, 1963.

8. Watts, W. L., D. Sirmans, and J. T. Dooley, "WRL Techniques with Field Station Applications," Progress Report No. 13, WSR-57 Radar Program, U. S. Weather Bureau, 1963.

9. Wilk, K. E. "Research Concerning Analysis of Severe Thunderstorms," Final Report, Contract No. AF 19(604)-4940, Illinois State Water Survey, 1961, 68 pp.

THUNDERSTORM TURBULENCE AND RADAR ECHOES 1964 DATA STUDIES

J. T. Lee

ABSTRACT

Two specially instrumented aircraft, an F-100 and an F-11 made 78 flights through thunderstorms in Oklahoma. Turbulence parameters recorded by the aircraft are compared with concurrent data from a ground based radar. Severe turbulence is almost wholly confined to target storms in which the maximum radar reflectivity factor Z_e is $10^4 mm.^6 m.^{-3}$ or higher, but turbulence is not generally confined to the reflectivity cores. There is some evidence that turbulence is more severe in echoes which combine high reflectivities with large gradients of reflectivity, although the former factor is more significant.

1. INTRODUCTION

Atmospheric turbulence in and near convective clouds is still a relatively unexplored phenomenon. Conditions which signify severe turbulence hazardous to aircraft operations need to be determined. This paper discusses observed associations between turbulence experienced by aircraft and characteristics of ground based radar echoes. Knowledge of these relationships may be applied to increase aircraft safety while effectively utilizing air space in the vicinity of strong convection.

2. DESIGN OF PROGRAM

The following guide lines were established for the 1964 season to promote collection of statistically meaningful turbulence data by the aircraft.

1. Sampling is concentrated at the 25,000 ft. flight level.

2. Thunderstorms penetrated are in optimum radar range (i.e., 20 to 100 n. mi. radius of Norman).

3. Thunderstorms chosen for penetration should not contain core reflectivity factors[1] (Z_e) exceeding $10^5 mm.^6 m.^{-3}$.

---

[1]The equivalent radar reflectivity factor Z_e is discussed on p. 33 of this report.

4. Thunderstorms satisfying (2) and (3) are sampled on a random basis.

During the 1964 season, the F-100's normal operating pressure altitude was restricted to 25,000 ft. because of a special, externally carried, instrument package. This single altitude was chosen for penetrations in order to obtain abundant data there and have high probability that the conditions sampled are representative of the whole population of turbulence occurrences at this altitude. These data should be a standard for comparison with data collected later at different, especially higher, altitudes.

Guide line number two was established to permit quantitative use of radar. The lower range limit is beyond the pattern of "ground clutter" and meaningful resolution of precipitation distributions near the aircraft is obtainable inside the upper range limit.

The third guide line is based on data which indicate that where the radar reflectivity equals or exceeds $10^5 mm.^6 m.^{-3}$, observed surface hail commonly has a diameter 3/4 in. or larger.[2] Naturally, the occurrence of such hail at the ground reflects the presence of similar or larger hail aloft. Hail of this size encountered in flight may damage the structure of even high-performance military aircraft [1].

Guide line number four was selected in an effort to minimize sampling bias. However, due to limitations of aircraft range, restricted flight areas and other similar factors, its application was subjective.

3. DATA ACQUISITION

Since this program treats relationships between ground-based radar observations and turbulence experienced by aircraft within thunderstorms, the radar observations had to be coordinated in time with aircraft flight paths. As described in the paper by Dooley and Clark on p.122 in this report, an automatic step-attenuating and antenna elevating program is being used with the NSSL WSR-57 radar to probe the atmosphere systematically. One complete probing cycle requires about 7 min.

The aircraft operations are similar to those described by Van Thullenar [2]. Two aircraft participated in the 1964 program. An F-100 F aircraft of the U. S. Air Force Aeronautical Systems Division, flown by an Air Force pilot, was

---

[2] See preceding paper in this report.

instrumented with gust vanes, accelerometer, and other sensing equipment little different from that described by Underwood [3]. An F-11 Navy fighter with a Navy pilot carried a NASA accelerometer, standard air speed, altitude and free air temperature probes and other equipment. Figure 1 shows a typical photograph of the WSR-57 radar scope, the corresponding digitized radar printout and the time history of the turbulence encountered by the penetration aircraft. In this study, the aircraft paths were converted to i-j coordinates and superimposed on the digitized radar printout as shown in the figure. The digitizing and processing of the radar data at NSSL is described by Gray and Wilk elsewhere in this report.

4. DATA ANALYSIS

As noted above, specific guide lines were established; some deviations from these were necessary as synoptic conditions varied. Table 1 lists the number of penetrations made by the F-100 and F-11 at the various altitudes. This list includes only those cases in which data recording equipment was functioning satisfactorily. Figure 2 shows the altitude distribution of the number of miles flown during penetrations. Sixty-seven percent of the total miles flown were at 25,000 ft. (±2,500) and 81 percent were at or above 20,000 ft. (±2,500 ft.)

Table 1. - Number of flights (storm penetrations made at indicated altitudes ±2,500 ft.) during the 1964 season

Altitude	F-100	F-11	Total
25,000	21	31	52
20,000	15	1	16
15,000	1	5	6
10,000 ft. or below	1	3	4
	38	40	78

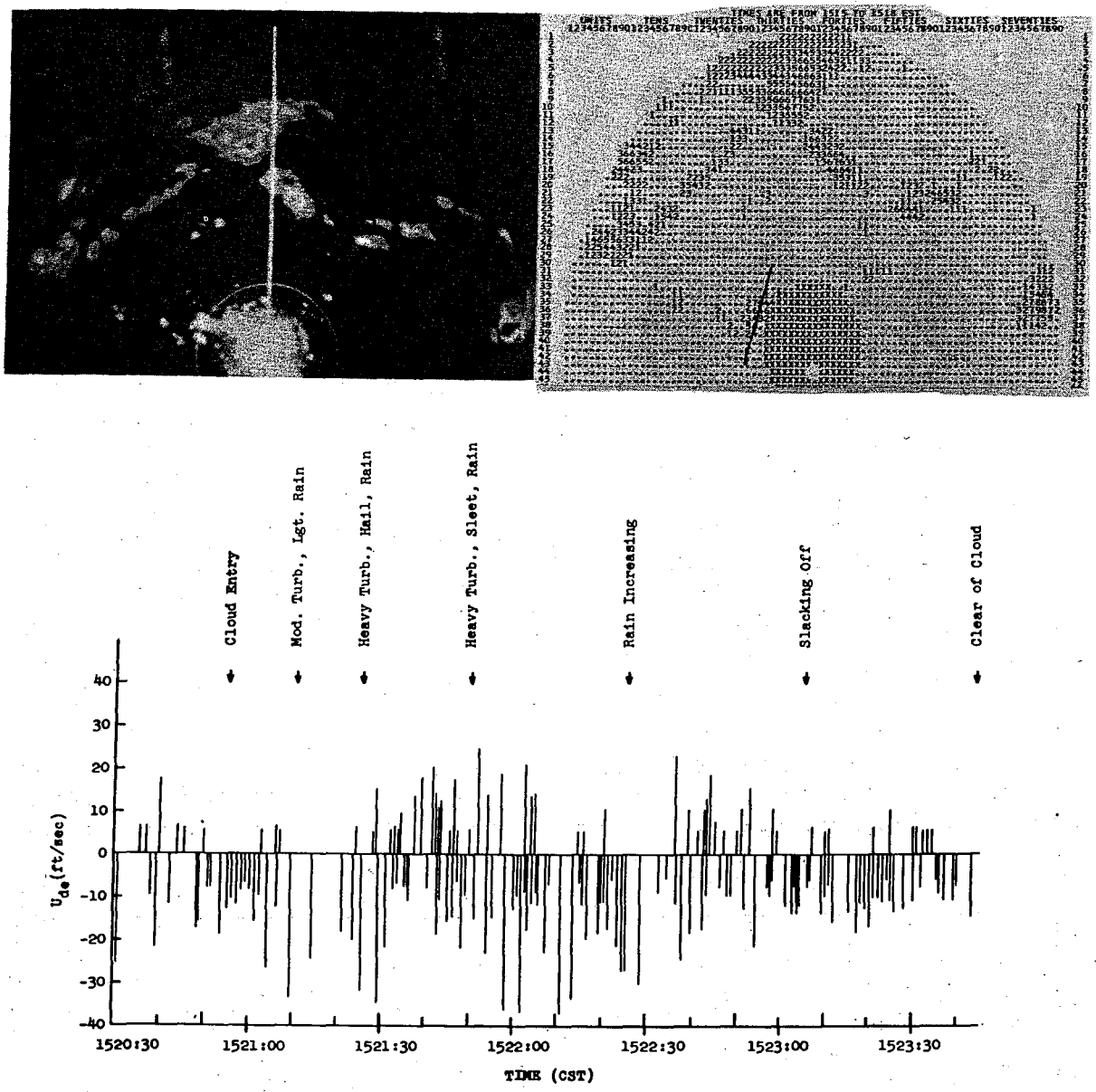

Figure 1. - Composite showing (a) upper left, photo of radar scope presentation at 1520 CST, May 1, 1965; (b) upper right, the printout of digitized data with the aircraft track superimposed -- numbers in printout indicate intensity of echo [(Number - 1) x 6 = db above noise]; and (c) below, the time history of the derived gust velocities including selected examples of the pilot's comments.

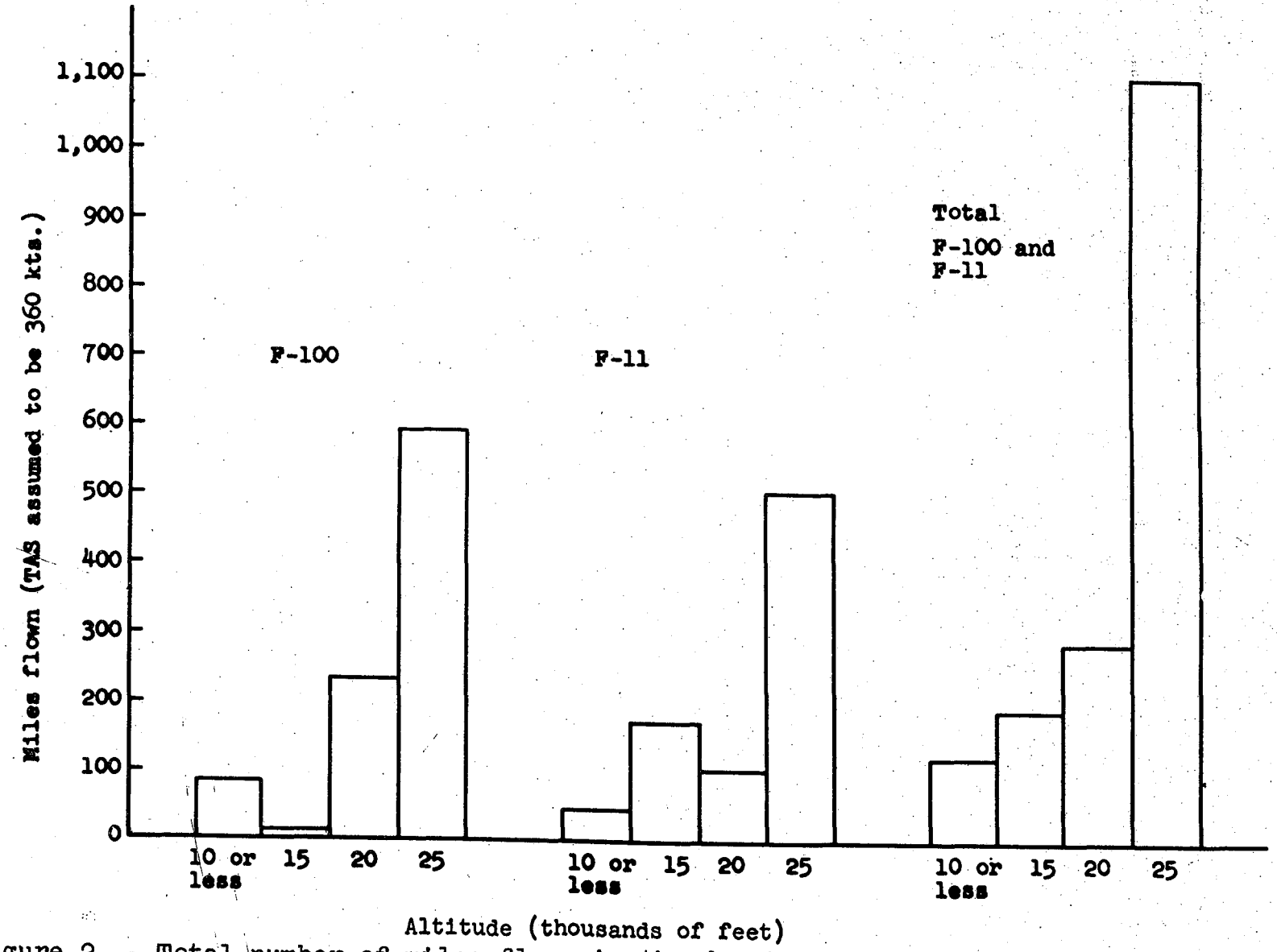

Figure 2. - Total number of miles flown in thunderstorms during spring 1964 as a function of altitude to the nearest 5000-ft.

Various descriptions have been given of deviations of the instantaneous wind from the mean flow. Our concern here is with that relatively narrow portion of the motion spectrum significant to aircraft flight; the derived gust velocity (U_{de}) is the standard used in this report. Derived gust velocities are computed by the method of Pratt [4] and plotted as time histories. For a given aircraft, air speed, weight and pressure altitude, U_{de} is proportional to the acceleration of the aircraft perpendicular to the plane formed by its flight axes. The magnitude and distribution of U_{de} are fair measures of the turbulence "felt" by the pilot. Figure 3 compares the pilot's subjective evaluations of turbulence encountered on particular penetrations with the computed maximum U_{de} for that penetration. Figure 4 compares the pilot's evaluation with the standard deviation of U_{de}. Note that the distribution of the F-11 pilot's characterization is very similar to that of the F-100 pilot's.

Figures 3 and 4 show two penetrations ("a" and "b" in the figures) which lie outside the general distribution. These are two successive runs. The recorder data indicate, as do the flight observer's classification, only light or moderate turbulence. However, the pilot's classification is "moderate to severe." Considering the systematic correspondence of the recorder data to human experience otherwise evident in figures 3 and 4, one must acknowledge the existence of other factors, such as fatigue, in the subjective evaluation. To reduce this subjectivity, the maximum derived gust velocity and standard deviation of derived gust velocity are used exclusively below as measures of turbulence encountered.

The standard deviation (σU_{de}) values can be roughly divided into turbulence categories (table 2) light, moderate, severe, and extreme paralleling the classification by derived gust velocities [5]. These intervals establish a basis for quick comparisons with earlier flight data.

Figure 5 shows the standard deviation of U_{de} vs. the maximum radar intensity of the penetrated cell. The ordinate is the maximum storm reflectivity factor (Z_e) observed by the radar operator at the time of aircraft penetration. Figure 6 is similar, but in this case the ordinate is the maximum Z_e derived from digitized radar data. Estimates derived from digitized data tend to be lower because the echo must cover 50 percent of the area of a square (2.5 miles square or 6.25 $mi.^2$) to be recorded. The next lower intensity step (6 db. lower) was recorded in a number of cases when the area of

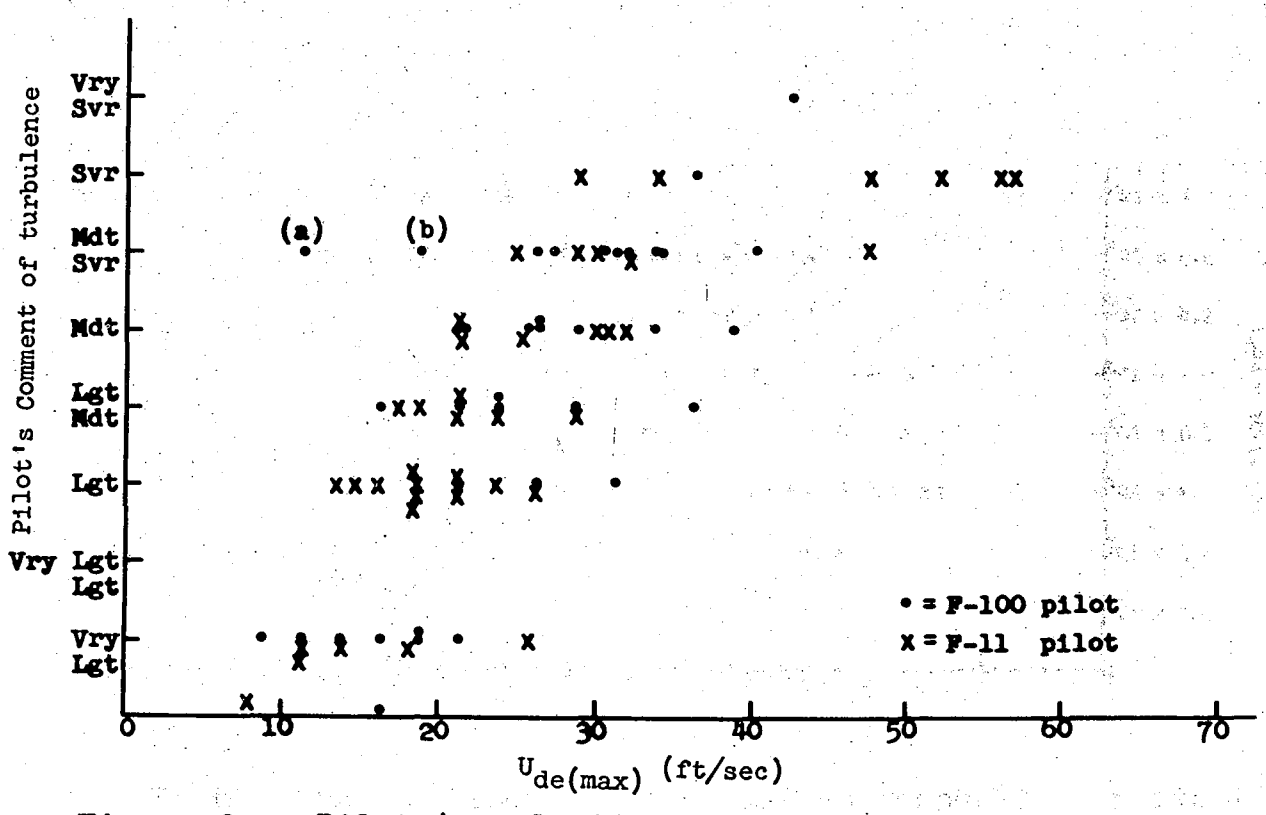

Figure 3. - Pilots' evaluation of turbulence as a function of the maximum derived gust velocities [$U_{de(max)}$].

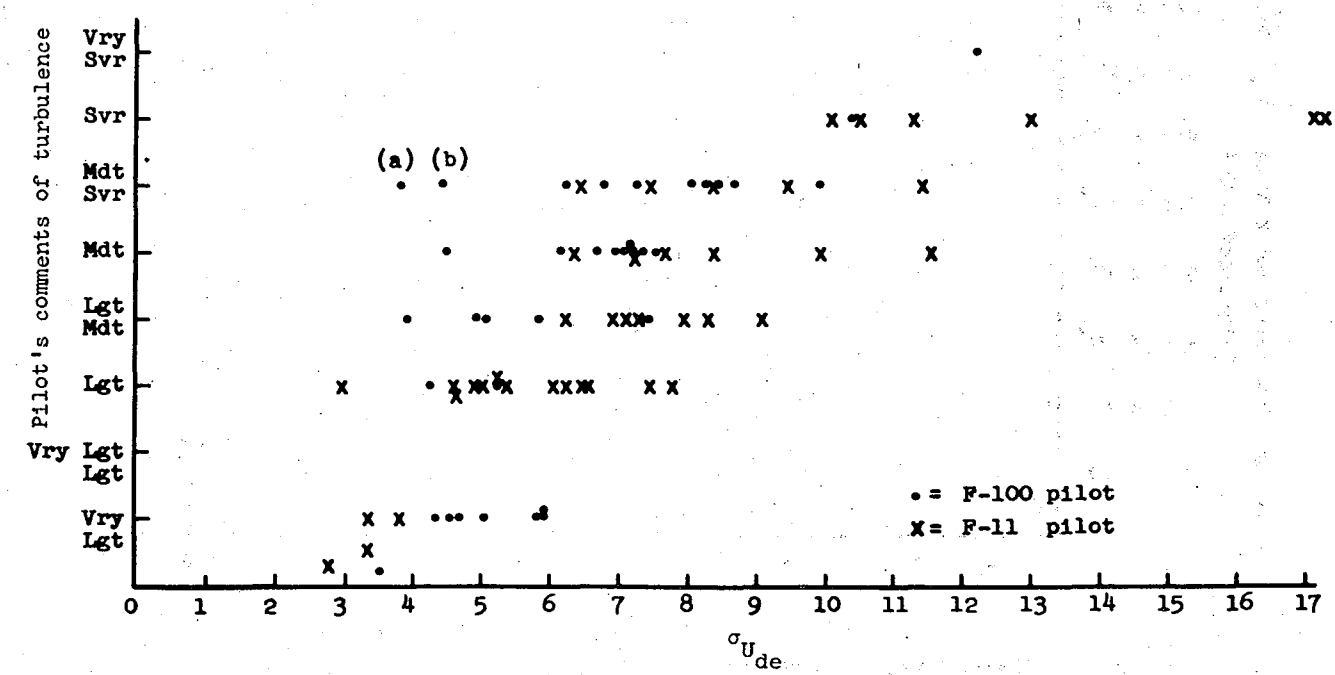

Figure 4. - Pilots' evaluation of turbulence encountered as a function of the standard deviation of the derived gust velocities ($\sigma_{U_{de}}$).

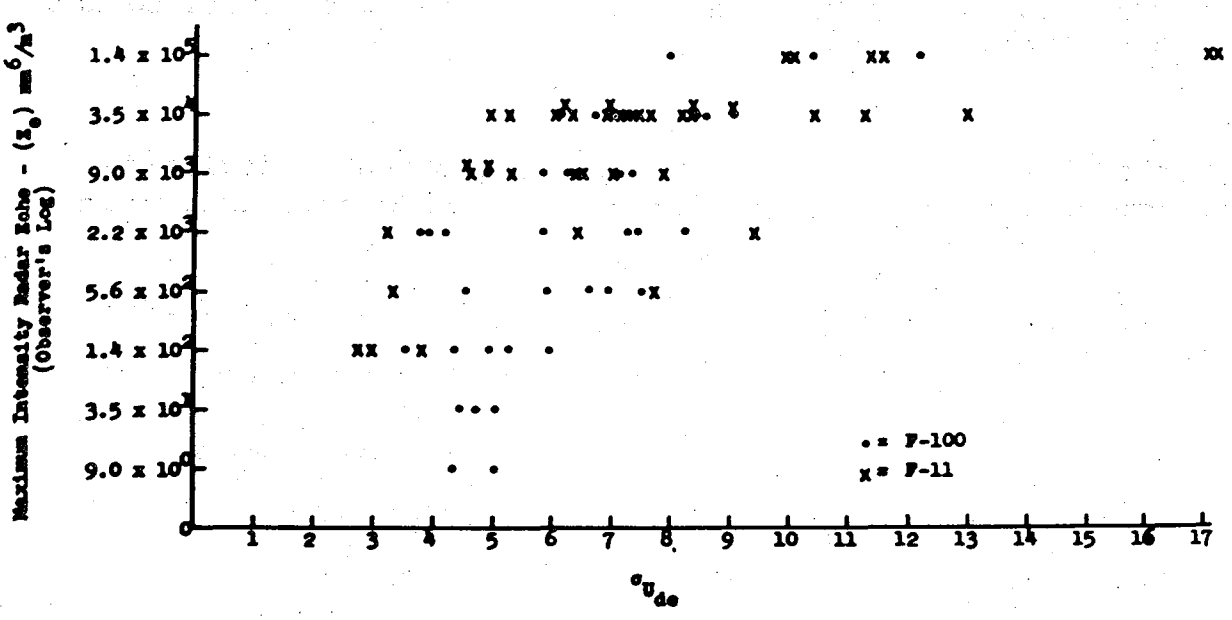

Figure 5. - Standard deviation of the derived gust velocities during each penetration as a function of the radar operator's determination of maximum radar reflectivity (Z_e) of the echo being penetrated.

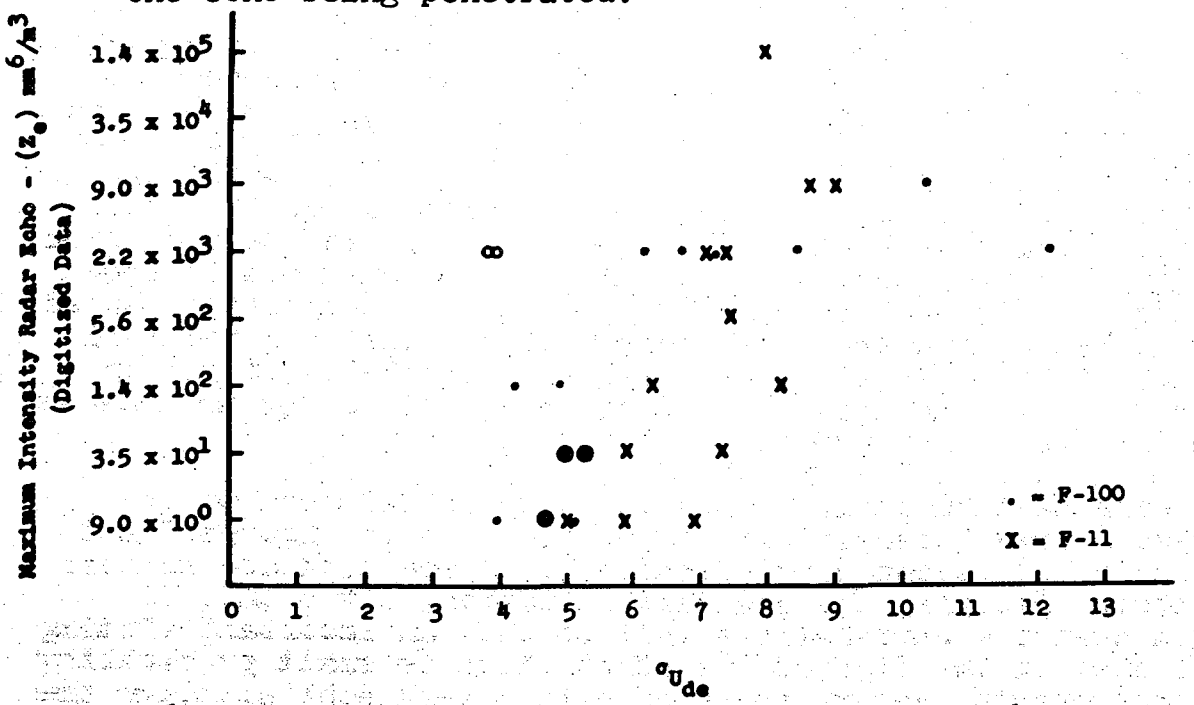

Figure 6. - Standard deviation of the derived gust velocities of each penetration related to the maximum radar reflectivity (Z_e) determined from the digitized radar scope printout.

maximum echo was small. In this study both the radar operators' observations and digitized data are used because digitized data are not available for all flights.

Table 2. - Turbulence categories using standard deviation

Turbulence Category	$\sigma_{U_{de}}$ ft. sec.$^{-1}$	Accepted U_{de} Values
Light	0 —> 6	Less than 20 fps
Moderate	6 —> 8	20-35 fps
Severe	8 —> 15	35-50 fps
Extreme	Above 15 (Max. measurement)	Above 50 fps

Kessler, Lee and Wilk [6] have discussed possible physical bases for the statistical nature of the correspondence between turbulence and radar echo intensities. Figures 5 and 6 show the statistical character of the association between turbulence and radar echo intensities for the 1964 flights. The first part of table 3 lists correlation of derived gust velocities and the radar echo intensity for data derived from flights by different aircraft and by different methods from the radar. These are typically about 0.6. Correlation based on the F-100 data are consistently higher than for the F-11 data; this may reflect the presence on the F-100 of better instruments which are used to obtain values for parameters in the data reduction program.

The maximum derived gust velocity in relation to the maximum echo intensity of storms is shown in figures 7 and 8 and in the second part of table 3. These data are similar to those involving the standard deviation. It should be noted that the correlations fail to show an important finding indicated in the figures, viz., that there is small probability of encountering severe turbulence in a weak echo although the scatter of the data is large.

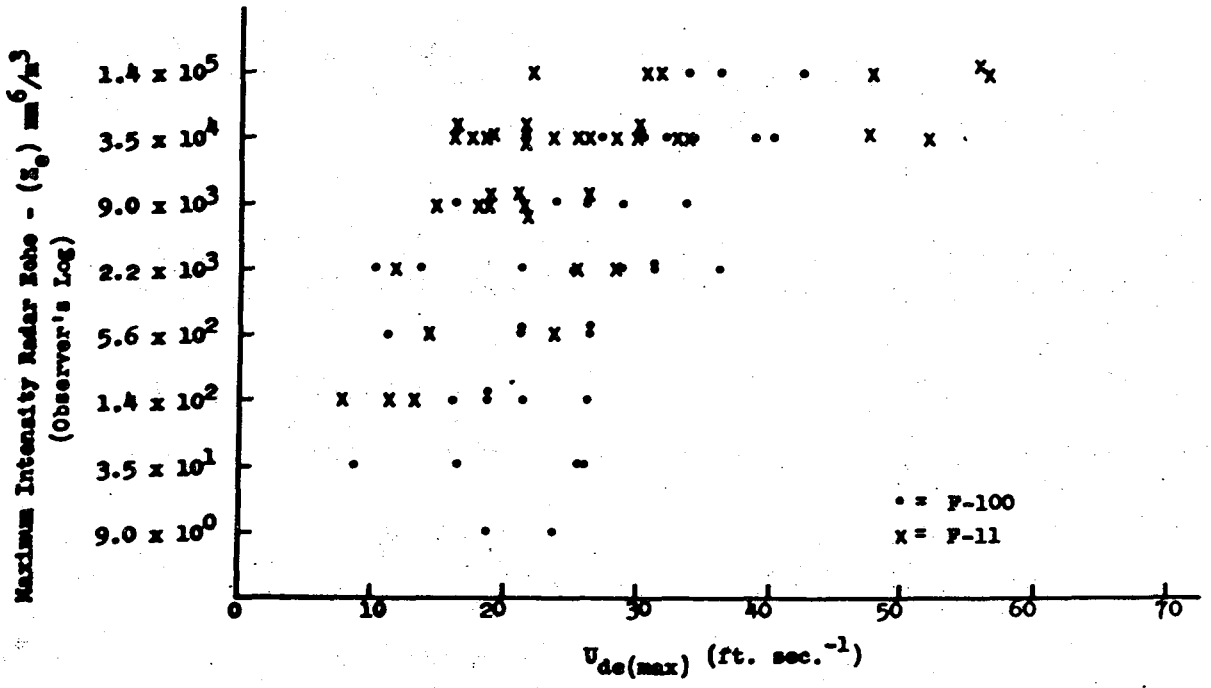

Figure 7. - Maximum derived gust velocity for each penetration related to the radar operator's determination of the maximum radar reflectivity (Z_e) of the echo being penetrated.

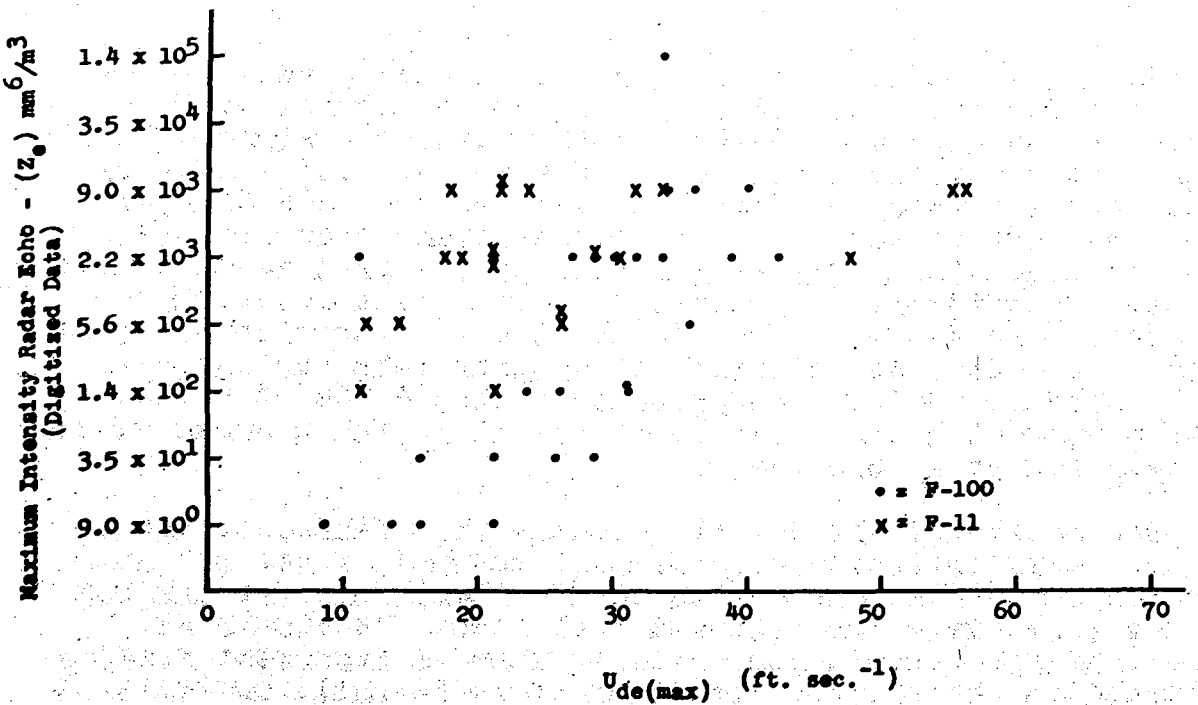

Figure 8. - Maximum derived gust velocity for each penetration related to maximum radar reflectivity (Z_e) as determined from the digitized radar scope printout.

Table 3. - Correlation between turbulence measurement and maximum radar echo intensity

Aircraft	Turbulence Measurement	Maximum Radar Reflectivity Determined by:	Correlation Coefficient
F-100	$\sigma_{U_{de}}$	Radar operator	0.693
F-11	$\sigma_{U_{de}}$	Radar operator	0.533
Combined	$\sigma_{U_{de}}$	Radar operator	0.635
F-100	$\sigma_{U_{de}}$	Digitized Radar Data	0.542
F-11	$\sigma_{U_{de}}$	Digitized Radar Data	0.566
Combined	$\sigma_{U_{de}}$	Digitized Radar Data	0.514
F-100	$U_{de(max)}$	Radar operator	0.629
F-11	$U_{de(max)}$	Radar operator	0.591
Combined	$U_{de(max)}$	Radar operator	0.530
F-100	$U_{de(max)}$	Digitized Radar Data	0.644
F-11	$U_{de(max)}$	Digitized Radar Data	0.465
Combined	$U_{de(max)}$	Digitized Radar Data	0.464

The author considered whether a combination of the maximum derived gust velocity and the standard deviation of the derived gust velocity would increase the correlation with the echo intensity. Since the maximum U_{de} may be one large displacement during an otherwise smooth flight, this single displacement may be unrealistically emphasized in the data already presented. Thus the correlation of: (1), the product of the maximum U_{de} and the standard deviation with maximum radar reflectivity $[U_{de(max)} \cdot \sigma U_{de}$ vs. $Z_{e(max)}]$ and (2),

the product of the maximum U_{de} and the variance of U_{de} with maximum radar reflectivity [$U_{de(max)} \cdot \sigma^2 U_{de}$ vs. $Z_{e(max)}$] were computed. However, these results were actually poorer than those discussed above and this approach was not pursued further.

Some of the literature [7] discusses the correspondence between turbulence and the gradient of the radar echo reflectivity ($\frac{dZ}{dx}$). In this study the aircraft paths are converted to i-j coordinates and superimposed on the radar scope printout as illustrated in figure 1. From such data, the average gradient ($\overline{\frac{dZ}{dx}}$) and the maximum gradient ($\frac{dZ}{dx}$ max) are computed for each penetration and compared with the turbulence measurements (table 4). Only the correlation coefficient between $\frac{dZ}{dx}_{(max)}$ and U_{de} or σU_{de} for the F-100 approaches the value of the correlation coefficient between U_{de} and echo intensity. The other correlations seem to be operationally insignificant.

To test further the gradient of radar reflectivity as a measure of turbulence, $\frac{dZ}{dx}_{(max)}$ and $\overline{\frac{dZ}{dx}}$ were each combined with $Z_{e(max)}$, $U_{de(max)}$, and σU_{de}. The multiple correlation coefficients for the various combinations are shown in table 5. Comparison with table 3 shows that this procedure results in some improvement in the correlations. This suggests that the echo intensity variations and associated vertical air velocity variations may be resolved by radar on a scale meaningful for aircraft flight. Discussion relevant to this topic is contained in [6] and in the paper by Kessler on p. 99 in this report. Effective operational use of echo gradients and reflectivities in combination is a difficult problem requiring development of new data processing and analysis techniques.

Figure 9 shows the distribution of derived gust velocities recorded during the 1964 season. A reference path length of 10 n. mi. is chosen for compatibility with previous years' data [6]; this is also the approximate radius of the storm echoes penetrated. In addition to the composite average, figure 9 shows the cumulative frequency of derived gust velocities for the cases where $Z_{e(max)}$ equals $1.4 \times 10^5 mm.^6 m.^{-3}$ and $5.6 \times 10^2 mm.^6 m.^{-3}$ (corresponding to 48 and 24 db.). These data are further detailed in figure 10. It is readily seen that the probability of recording a gust velocity greater than 35 ft. $sec.^{-1}$ is very small in echoes whose maximum radar

Table 4. - Linear correlation coefficient for turbulence and radar reflectivity gradients

Aircraft	Turbulence	Reflective Gradient	Correlation Coefficient
F-100	$\sigma_{U_{de}}$	Average	0.336
F-11	$\sigma_{U_{de}}$	Average	0.226
Combined	$\sigma_{U_{de}}$	Average	0.315
F-100	$\sigma_{U_{de}}$	Maximum	0.543
F-11	$\sigma_{U_{de}}$	Maximum	0.135
Combined	$\sigma_{U_{de}}$	Maximum	0.322
F-100	$U_{de(max)}$	Average	0.494
F-11	$U_{de(max)}$	Average	0.197
Combined	$U_{de(max)}$	Average	0.241
F-100	$U_{de(max)}$	Maximum	0.651
F-11	$U_{de(max)}$	Maximum	0.141
Combined	$U_{de(max)}$	Maximum	0.302

Table 5. - Multiple Correlations 1964

Aircraft	x	y	z	$r_{x(yz)}$
F-100	$\sigma_{U_{de}}$	$Z_{e(max)}$	Avg. Gradient	0.693
F-11	$\sigma_{U_{de}}$	$Z_{e(max)}$	Avg. Gradient	0.536
Combined	$\sigma_{U_{de}}$	$Z_{e(max)}$	Avg. Gradient	0.636
F-100	$\sigma_{U_{de}}$	$Z_{e(max)}$	Max. Gradient	0.775
F-11	$\sigma_{U_{de}}$	$Z_{e(max)}$	Max. Gradient	0.533
Combined	$\sigma_{U_{de}}$	$Z_{e(max)}$	Max. Gradient	0.636
F-100	$U_{de(max)}$	$Z_{e(max)}$	Avg. Gradient	0.663
F-11	$U_{de(max)}$	$Z_{e(max)}$	Avg. Gradient	0.591
Combined	$U_{de(max)}$	$Z_{e(max)}$	Avg. Gradient	0.557
F-100	$U_{de(max)}$	$Z_{e(max)}$	Max. Gradient	0.792
F-11	$U_{de(max)}$	$Z_{e(max)}$	Max. Gradient	0.593
Combined	$U_{de(max)}$	$Z_{e(max)}$	Max. Gradient	0.531

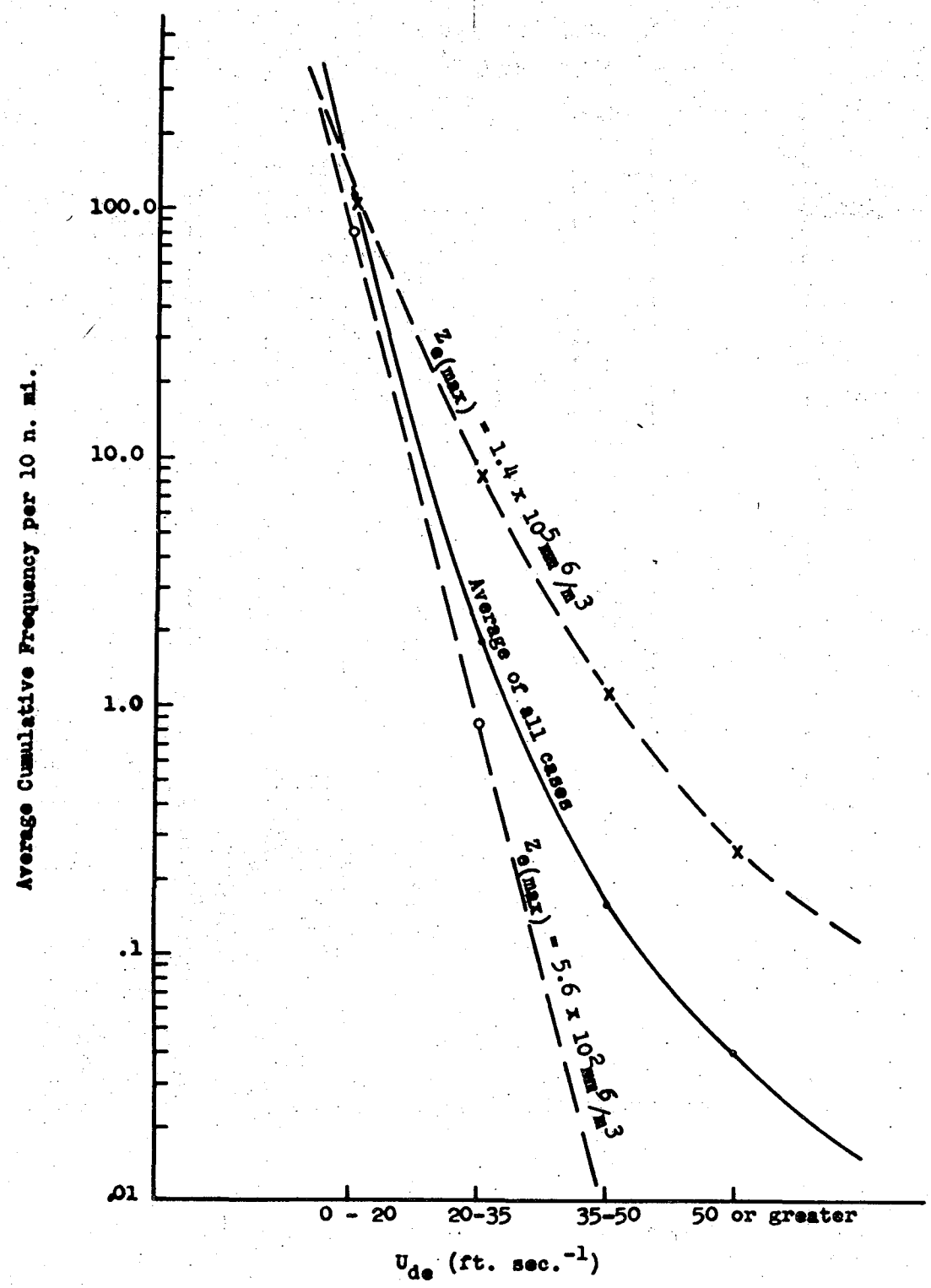

Figure 9. - Average cumulative frequency of derived gust velocities (U_{de}) per 10 n. mi. of flight in thunderstorms.

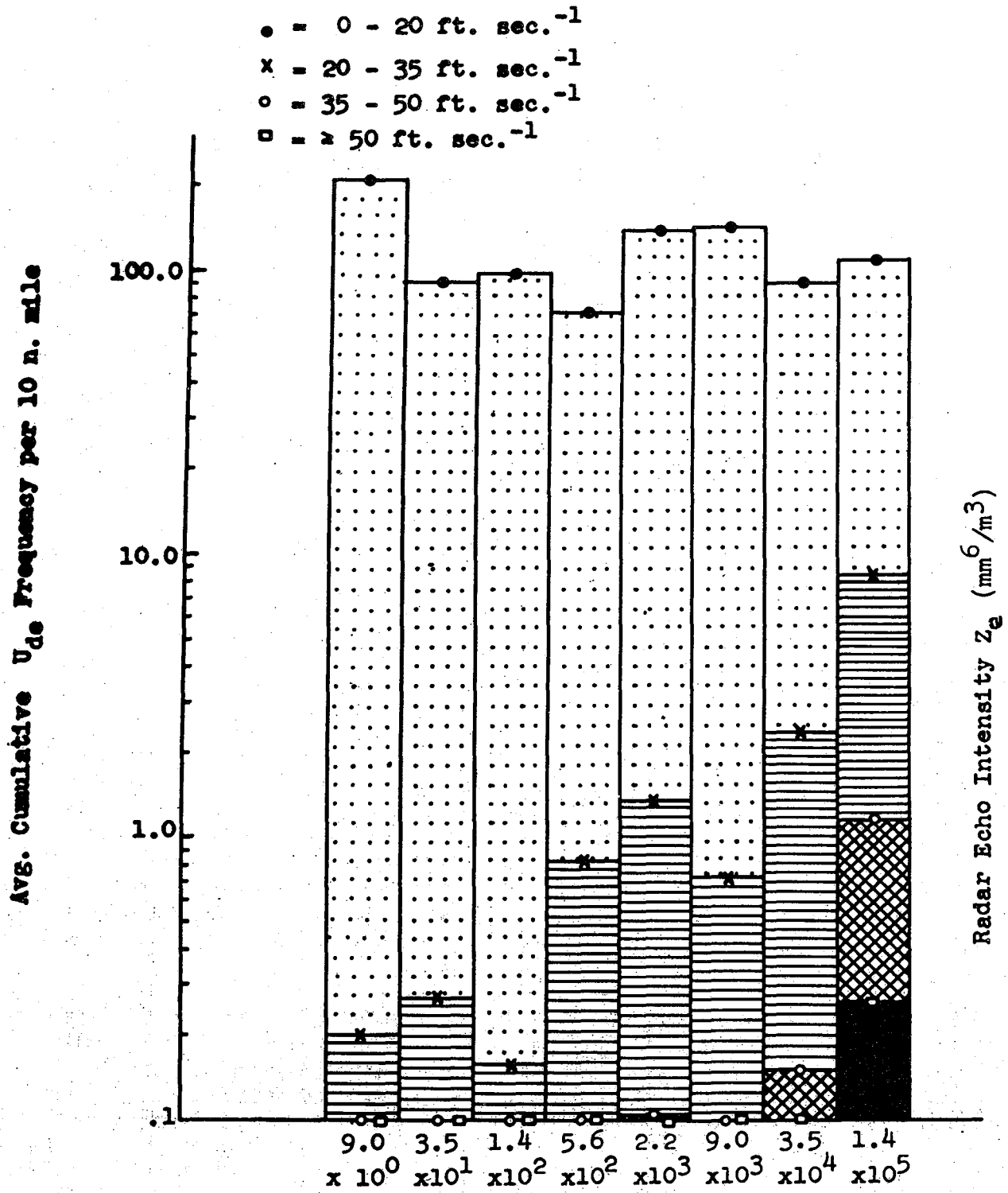

Figure 10. - Average cumulative frequency of derived gust velocities per 10 n. mi. as a function of the maximum reflectivity of the radar echo being penetrated. Dotted area indicates U_{de} 0 to 20 ft. sec.$^{-1}$ (light turbulence); horizontal stripes signify 20 to 35 ft. sec.$^{-1}$ (moderate turbulence); cross-hatched area represents 35 to 50 ft. sec.$^{-1}$ (severe turbulence); and solid area represents 50 ft. sec.$^{-1}$ or more (extreme turbulence).

reflectivity is less than $10^4 mm.^6 m.^{-3}$. However, the probability of severe turbulence rises very rapidly as this intensity value is exceeded. No U_{de}'s greater than 35 ft. $sec.^{-1}$ were encountered when Z was 5 x $10^2 mm.^6 m.^{-3}$ or less. Table 6, derived from these data, estimates the probabilities of derived gust velocities per nautical mile of flight in echoes of various intensities. Since most of these data are based on observations at 25,000 ft. the applicability of table 6 to higher altitudes remains to be determined.

The distribution of turbulence encountered within thunderstorms as a function of the distance from the area of maximum reflectivity is indicated in figures 11 and 12. Only those flights in which values of $U_{de} \geq 20$ fps (moderate turbulence or greater) occurred at least once are considered. Figure 11 shows the occurrence of $U_{de} \geq 20$ fps as determined from the time histories of turbulence in 2.5 mile block intervals, referenced to the distance from $Z_{e(max)}$ of the storm being penetrated. Fifty-seven percent of the flights experienced moderate turbulence in the area of $Z_{e(max)}$. Moderate turbulence was encountered at least once per 2.5 mile block nearly 20 percent or more of the time whenever the aircraft were within the cloud and were within 15 miles from the center of maximum intensity.

Figure 12 shows the maximum distance from the area of $Z_{e(max)}$ when the first occurrence of $U_{de} \geq 20$ fps was recorded. Data beyond 15 miles is based on only four flights. These data indicate that moderate turbulence was often encountered in the cell prior to entry into the center of $Z_{e(max)}$.

The rate of growth of areas of maximum intensity is discussed in the paper by Lee [8]. Rate of growth is not investigated here because of limitations in data processing. This should be considered in future studies.

At least one other point of interest is evident in figure 10. Note that for all except very weak echoes, the total number of derived gusts per 10 n. mi. of flights is nearly constant. The basic difference in echoes of different intensities is in the distribution of the gust intensities.

6. SUMMARY

Data from 78 storm penetrations in Oklahoma during the spring of 1964 indicate that the storm radar echo intensity has a clear statistical correspondence to the turbulence encountered by aircraft penetrating the storm. The chance of encountering severe or extreme turbulence is small (less

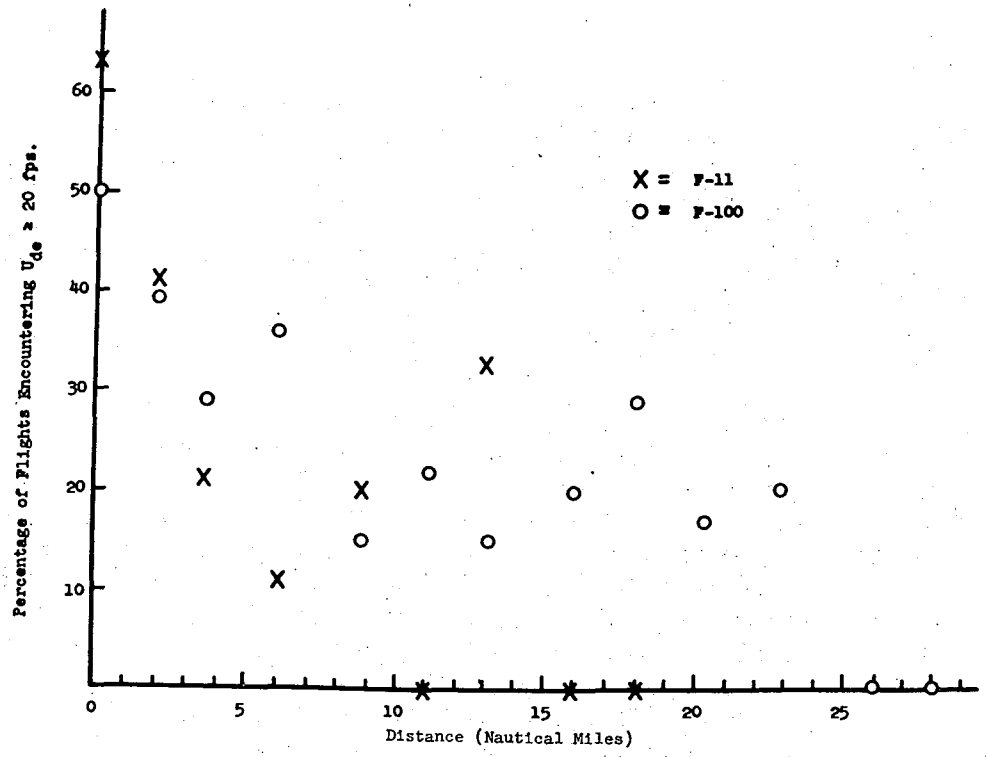

Figure 11. - Percentage of flights encountering $U_{de} \geq 20$ fps at least once in a 2.5 n. mi. block as a function of distance from $Z_{e(max)}$.

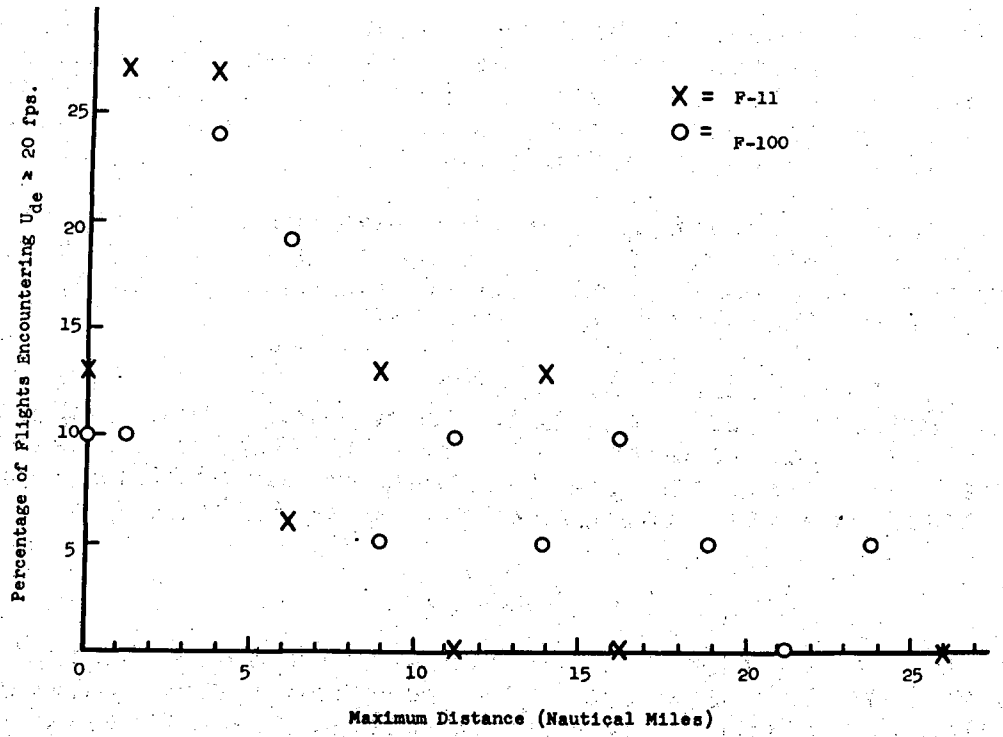

Figure 12. - Maximum distance from storm cores at which the indicated percentage of flights encountered $U_{de} > 20$ fps.

Table 6. - Smoothed probability of occurrence of derived gust velocities (U_{de}) per mile of thunderstorm flight as a function of maximum radar echo intensity (Z_e)

	Maximum radar echo intensity Z_e ($mm.^6m.^{-3}$)							
U_{de} ($ft.\ sec.^{-1}$)	9.0×10^0	3.5×10^1	1.4×10^2	5.6×10^2	2.2×10^3	9.0×10^3	3.5×10^4	1.4×10^5
0 - 19	100%	100%	100%	100%	100%	100%	100%	100%
20 - 34	.6	1.4	2.5	4.8	10	20	40	86
35 - 49	0	0	0	.07	.25	1.0	3.5	11
50 and above	0	0	0	0	0	0	0	3

than 1.0 percent) if the maximum radar reflectivity factor Z_e is less than $10^4 mm.^6m.^{-3}$. Above this value there is a rapid increase in the probabilities even though damaging hail is not expected with radar reflectivity values less than about $10^5 mm.^6m.^{-3}$. The maximum radar reflectivity of a given storm seems more indicative of turbulence than the maximum or average gradients of echo intensity based on digitized radar data. However, most correlations were improved by considering the maximum echo and echo gradients simultaneously. It should be noted that these data relate to whole storms. The maximum turbulence encountered is not necessarily in the area of maximum radar reflectivity. This study has not established criteria for flight planning by which turbulence can be reduced by flying particular paths in the vicinity of severe storms. This interesting and important topic will be considered at a later date.

REFERENCES

1. Foster, D. C., "Aviation Hail Problems," Technical Note No. 37, World Meteorological Organization, Geneva, Switzerland, 1961.

2. Van Thullenar, C. F., "The Use of Radar in the Control of National Severe Storms Project Penetration Aircraft," Proceedings, Ninth Weather Radar Conference, Kansas City, Mo., 1961, pp. 199-205.

3. Underwood, E. B., "Instrumentation and Operations for Thunderstorm Data with an F-100 Aircraft during the 1963 National Severe Storms Project," Technical Document Report No. ASD-TDR 64-77, U. S. Air Force, 1964.

4. Pratt, K. G. and W. G. Walker, "A Revised Great-Load Formula and a Re-Evaluation of V-G Data taken on Civil Transport Airplanes from 1933 to 1950." National Advisory Committee of Aeronautics Report 1206, pp. 1-4.

5. U. S. Weather Bureau. Weather Bureau Manual, Section III-B-2011, Washington, D. C., 1957.

6. Kessler, E., J. T. Lee, and K. E. Wilk, "Associations between Aircraft Measurements of Turbulence and Weather Radar Measurements." Paper presented at Spring Meeting of American Meteorological Society, Washington, D. C., April 1964. (In press, Bull. Amer. Met. Soc., Aug., 1965.)

7. Beckwith, W. B., "The Use of Weather Radar in Turbojet Operation." UAL Meteorology Circular No. 53, United Airlines, Denver, Colo., 67 pp.

8. Lee, J. T., "Thunderstorm Turbulence Measurements by Aircraft and Concurrent Radar Echo Evaluation," Unit I, Severe Storm Detection and Circumnavigation Final Report, FAA Contract ARDS-A-176, U. S. Weather Bureau, 1963.

CIRCULARLY POLARIZABLE RADAR AND HAIL DETECTION

by

Edwin Kessler and Kenneth E. Wilk

ABSTRACT

Photographs of the PPI of the ARSR-1D L-band radar have been made when echoes from rain and hail were present. No systematic differences are observed with respect to the cancellation of circular polarization by rain and hail. Since signal intensity measurements of this study were crudely made, it is conceivable that future work may reveal cancellation differences of operational interest.

The sense of rotation of circularly polarized radiation is reversed by isotropic targets such as spherical raindrops and the back scattered energy is rejected by the polarizing transmitting waveguide. Since large hail is usually markedly aspherical, circular polarization techniques have been suggested as means for identifying hail. However, a study of FAA and USWB radars [1], summarized in part here, provides some confirmation of Newell's empirical data [2] which suggest that depolarization by hail is not significantly more than by rain. The FAA-USWB radar study used an FAA ARSR-1D L-band radar. In contrast to the WSR-57, the ARSR-1D has a vertical fan-shaped beam and circular polarization capability required for air-traffic control.

The ratio of the signal received when the radar radiation is circular to that when it is plane polarized is called the cancellation ratio. Figure 1 shows the cancellation ratio in db. determined for the core of a number of echoes, in relation to the equivalent radar reflectivity factor Z_e of the echoes (p.33). Cancellation ratios and Z_e's are determined from PPI photographs at steps of the radar sensitivity as described in the papers by Dooley and Clark and by Gray and Wilk elsewhere in this report. Most of the echoes with Z_e's greater than 10^5 mm.^{6}/m.$^{-3}$ contain hail, as discussed in the paper by Ward, Wilk, and Herrmann in

a. Linear polarization, 12 db attenuation.

b. Circular polarization, no attenuation.

c. Linear polarization, 36 db attenuation.

d. Circular polarization, 24 db attenuation.

Figure 2. - ARSR-LD linear and circular polarization comparison

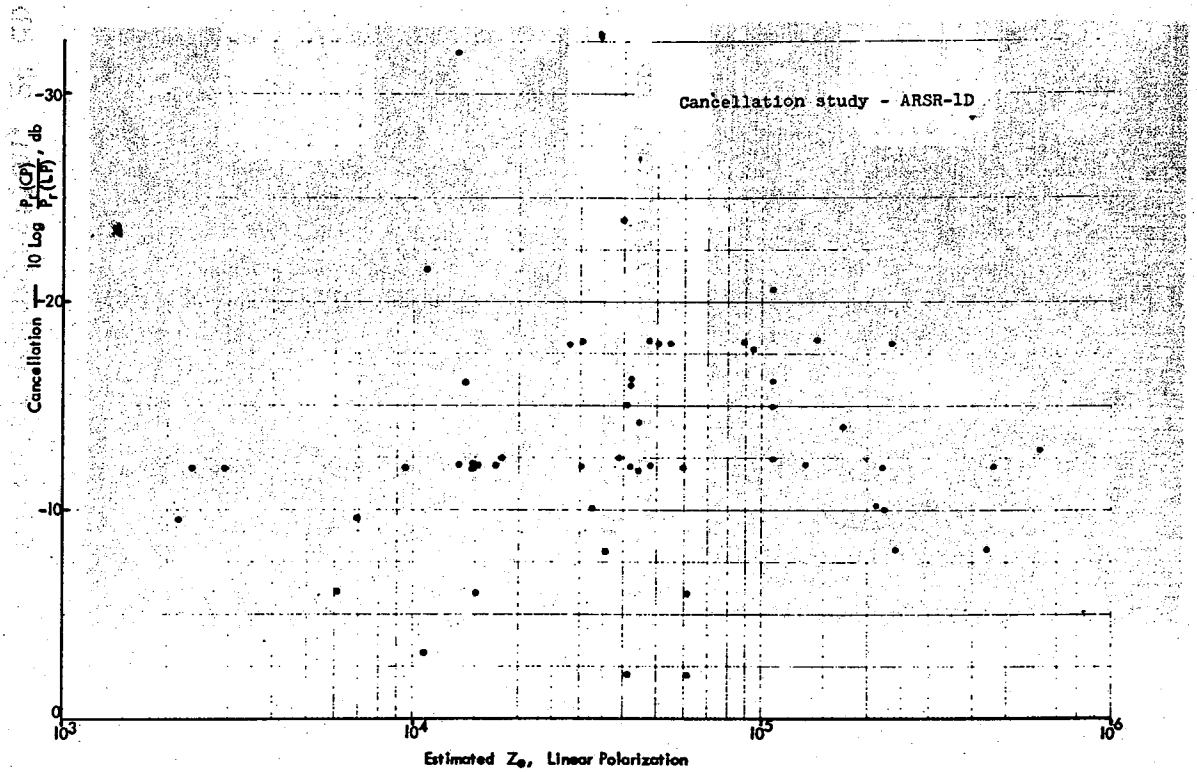

Figure 1. - Cancellation vs. Z_E in echo cores; ARSR-1D radar.

this report. Figure 1 shows that the cancellation is not systematically less for the hail echoes than for the weaker echoes which contain only rain.

In this study, failure to find a relationship between cancellation and echo strength may be attributable to at least two factors. First, such a relationship may not actually exist since large raindrops as well as hail tend to be aspherical. Also, it has recently been noted that hail having the same physical ellipticity as rain appears more spherical to the radar [2]. Therefore, significant depolarization of circular radiation should be expected only from markedly irregular hail which is sufficiently abundant to contribute most of the radar return.

Secondly, a small effect may be masked by the scatter of data in figure 1. Some of this scatter is due to changes of echo intensities during the time interval required to change polarizations with the available equipment, and some scatter is due to quantitative deficiencies inherent in the use of gain-stepped PPI photographs to measure echo intensities.

Figure 2 shows PPI photographs of the ARSR-1D made at the FAA Aeronautical Center, Oklahoma City, April 22, 1964, with and without circular polarization. The large echo 60 n.mi. north of the station is associated with a tornado at Enid, Okla. and hail larger than 2 in. in diameter; the echoes about 120 n.mi. southeast are associated with moderate showers. Examination of the whole series of photographs from which those in figure 2 are drawn confirms that the "best match" of weather echoes between displays with circular and linear polarization is given when the signal due to the linear radiation is attenuated 12 db. This is true at both high and low sensitivity settings, i.e., for both weak and strong echoes or hail and rain echoes.

In the authors' opinion, hail is fairly well identified by its intensity signature. Improved information on hail can be made available to concerned parties through improved techniques of echo intensity measurement and communication and display of data.

Although use of circular polarization may offer no important hail detection capabilities at present, it is important for air traffic control since it reduces echoes from precipitation relative to those from aircraft. Techniques for measuring the distributions of cancellation ratio more rapidly and more accurately must be used if there is to be hope of deducing operational or theoretical significance from storm polarization data.

REFERENCES

1. Wilk, K.E., Dooley, J.T., and Kessler, E.: "Weather Detection by ARSR-1D, ASR-4 and WSR-57 Radar: A Comparative Study", Technical Memo No. 1, National Severe Storms Laboratory, U.S. Weather Bureau, 1965, 20 pp.

2. Newell, R.E., Geotis, S., Stone, M.L., and Fleisher, A.: "How Round are Raindrops?" Proceedings, Fifth Weather Radar Conference, American Meteorological Society, 1961, pp. 261-268.

3. Hodson, M.C., and Peter, T.V.: "Observations of the Ellipticity of Raindrops Using a Polarized Radar System" Proceedings, Eleventh Weather Radar Conference, American Meteorological Society, 1964, pp. 188-191.

WAVE LENGTH DEPENDENCE OF THE RADAR REFLECTIVITY OF WATER AND ICE SPHERES

Shashi M. Kulshresthal and Kenneth E. Wilk

ABSTRACT

The equivalent radar reflectivity factor, Z_e , is proportional to the echo power received by a given radar. Z_e is calculated for four radar wave lengths, for ice and water spheres in a range of sizes applicable to hydrometeors.

The dependence of Z_e on the nature and size of the scatterers and on the radar wave length is discussed. It is concluded that Z_e measurements obtained with longer wave length radars are more useful in the determination of hail.

1. INTRODUCTION

Radars in general use for weather detection and air traffic control operate in the four frequency bands designated X, C, S, and L, corresponding to approximate wave lengths of 3, 5, 10, and 23 cm, respectively. This paper assesses the echo intensity at these wave lengths in relation to the size of precipitation particles.

The average received power, $\overline{P_r}$, that is returned to a radar from a beam-filling target in the absence of attenuation, is defined approximately by,

$$\overline{P_r} \approx \frac{C\,P_t}{R^2} \sum N\sigma \qquad (1)$$

where P_t is the transmitted power, R is the range to the target, and C is the radar constant containing the characteristics of the particular radar [1]. The total back-scatter cross-section, $\sum N\sigma$, is the summation of the geometric cross sections of isotropic scatterers which return the same power to the radar as the given targets (hydrometeors).

---

[1] On fellowship from the United Nations. Permanent affiliation: Indian Meteorological Service, New Delhi -3, India.

For water drops whose diameters, D, are less than about .04 times the radar wave length, the Rayleigh scattering law provides estimates of the true Mie scattering to within 10%. In such cases, the back-scattered power is proportional to the inverse fourth power of the wave length and to the summation of the sixth powers of particle diameters. This summation is called the radar reflectivity factor, Z.

$$Z = \Sigma N D^6 \tag{2}$$

For Rayleigh scattering, Z and σ are related by the expression:

$$Z = \frac{\lambda^4 \Sigma N\sigma}{\pi^5 |K|^2} \tag{3}$$

where K is a function of the complex index of refraction. It is obvious from equation (2) that Z is a more interesting meteorological parameter than σ.

For particles larger than approximately .04λ, the simple relation between Z and $\Sigma N\sigma$ in (3) is not valid. If $\Sigma N\sigma$ is known, however, equation (3) can be used to define an equivalent Z, written Z_e. By definition, this equivalent reflectivity factor is that associated with Rayleigh scatterers having the same radar cross section as the actual scatterers. Z_e is proportional to $\Sigma N\sigma$ and hence to the power received by a given radar.

2. COMPUTATION

Stephens [2] and Herman and Battan [3] have used the complete scattering equations of Gustav Mie to compute area-normalized radar cross sections of water and ice spheres for a number of wave lengths and for a wide range of sphere diameters. From these authors' tabulations we have calculated values of Z_e, using the value of $|K|^2$ appropriate for water, i.e., .93. In both rain and hail cases, therefore, our calculations present the equivalent Z's of Rayleigh-scattering water drops. Data for water spheres are readily available for wave lengths of 3.2, 5, 10, and 16 cm. For hail, the wave lengths chosen are 3.2, 5.3, 10, 16, and 23. All but 16 cm are identified with present-day operational radars.

The computed Z_e values are presented graphically in figures 1 and 2. For academic interest, both graphs are extended beyond values of meteorological significance. Raindrops are rarely larger than 7 mm and 8 cm is a practical upper limit for hail.

3. CONCLUSIONS

Figure 1 shows Z_e for single drops of the indicated diameters in a cubic meter of space. It is seen that for drop diameters $\leq$ 3 mm, Z_e does not change appreciably with change in wave length. Between diameters of 3 and 6 mm, Z_e's at S and L band are nearly the same and lie between the values for C and X band. Above 6 mm, Z_e for C band noticeably exceeds the values for the other wave lengths. However, since expected median-Z drop diameters for common rain are less than 4 mm, there are no significant differences in Z_e measured at the various wave lengths and, for sufficiently small sizes, the Rayleigh approximation is applicable. Meteorological application of Z_e data for sizes greater than 1 cm is restricted to complicated considerations of ice and water mixtures which may exist during stages of hail growth. It may be noted that effects of temperature variations are not considered in figure 1. These effects are relatively small in practical cases and have been discussed by Stephens [2].

Figure 2 shows Z_e for hail as derived from the backscattering cross section tabulations for ice spheres. At X- and C-band wave lengths, reflectivities decreased markedly below the Rayleigh approximation for hail diameters greater than 1 cm and 2 cm, respectively. The Rayleigh approximation is applicable for ice at S-band (10 cm) to a diameter of 3 cm, above which Z_e is greatly different from Z. The 16 cm Z_e curve follows the Rayleigh approximation to a diameter of nearly 5 cm. It too then deviates to lower values.

The greatest differences in Z_e for the four wave lengths in the region of observed maximum hail diameters (i.e., 2 cm to 8 cm) range from a factor of 17.5 (12 db) to 147 (22 db) between X-band and L-band. The corresponding differences between L-band and the other wave lengths are also substantial. The meteorological significance of these differences, as in the case of raindrops, is strongly dependent upon hail diameters. Hail diameters can be large enough (especially in the central United States) to cause significant differences in the Z_e values measured at the four frequency bands.

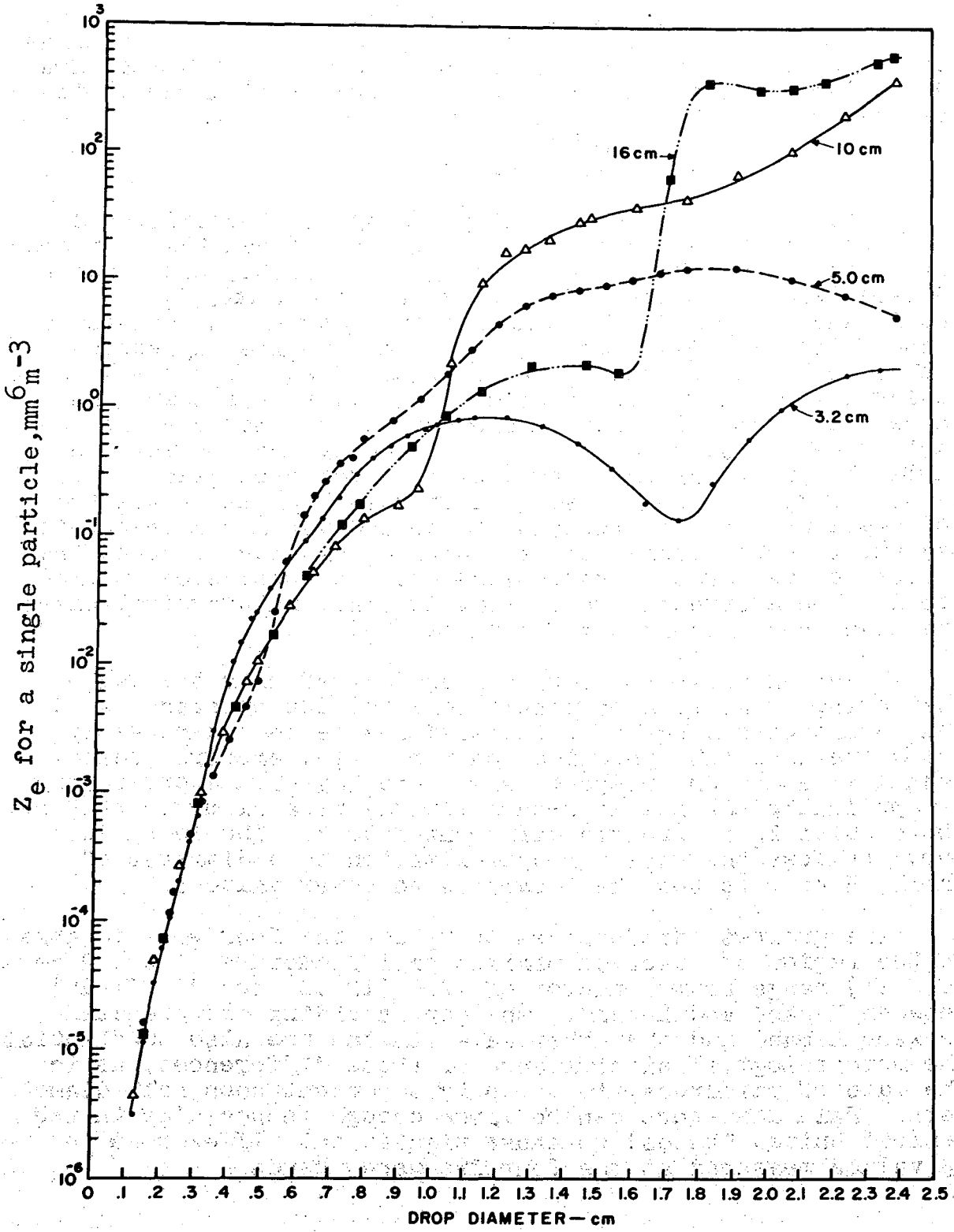

Figure 1. - Equivalent radar reflectivity for wavelengths in the range $3.2 \leq \lambda \leq 16$ cm., as a function of drop diameter (18°C).

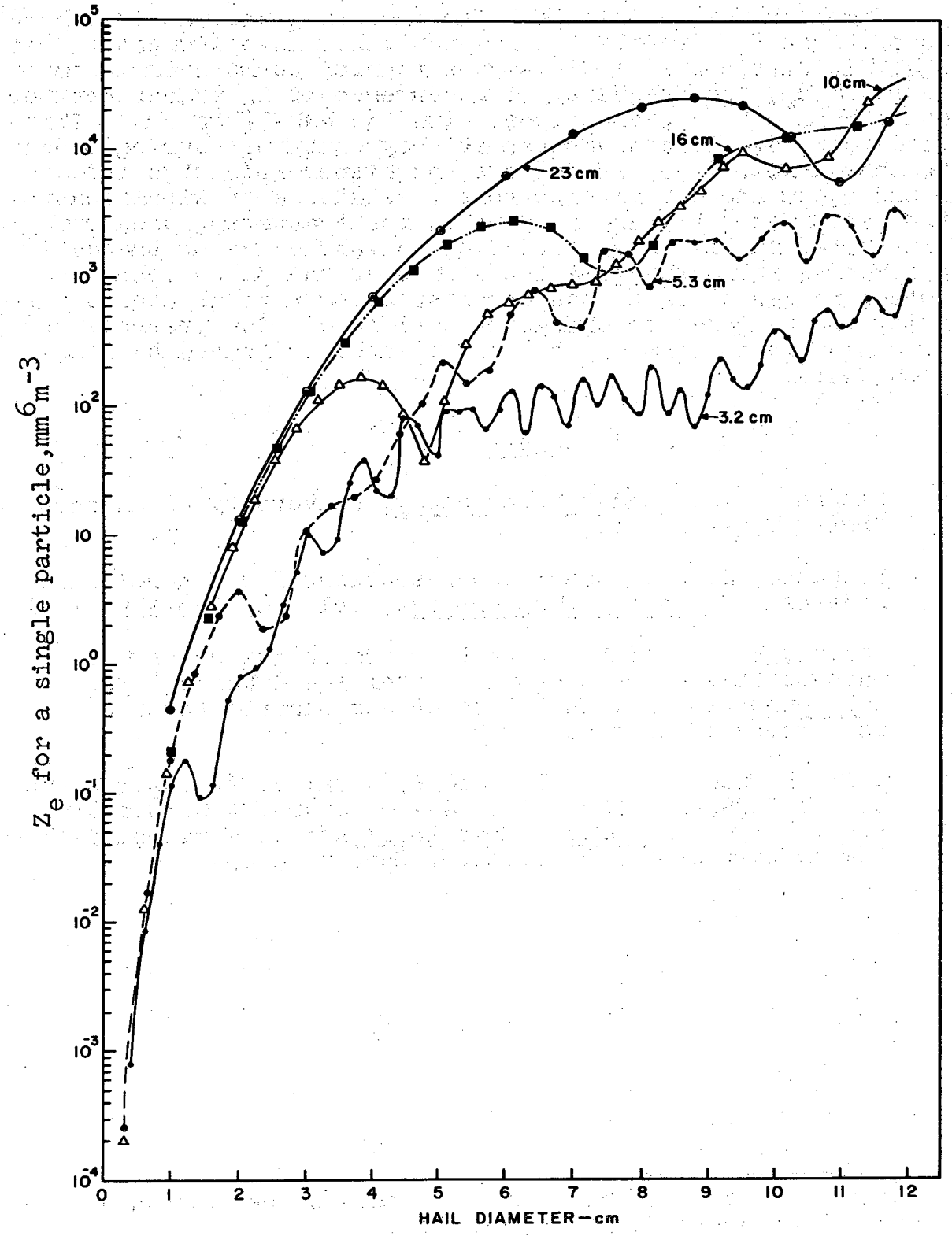

Figure 2. - Equivalent radar reflectivity for wavelengths in the range $3.2 \leq \lambda \leq 16$ cm., as a function of hail diameter (0°C).

The authors' experiences with the CPS-9 and WSR-57 radars operating at 3 cm and 10 cm, respectively, have indicated that higher Z_e's are observed in severe thunderstorms with 10 cm radars; i.e., the frequency of occurrence of Z_e values greater than $10^6 mm.^6 m.^{-3}$ appears higher with the WSR-57 radar.[2] This trend with wave length was tentatively confirmed during L-band studies at NSSL [4]. We believe the higher Z_e's observed at 10 and 23 cm are due in part to the existence of significant attenuation at 3 cm, and in part to the scattering properties illustrated in figure 2. Principal significance of the data in figure 2 is in the relative slopes of the Z_e curves. The greater ranges of Z_e values are associated with greater sensitivity of the radar to change in hail size. The presence of large hail in a storm may be most clearly indicated by long-wave radars.

REFERENCES

1. Battan, L. J., Radar Meteorology, University of Chicago Press, 1959, 161 pp.

2. Stephens, J. J., "Radar Cross-sections for Water and Ice Spheres," Journal of Meteorology, vol. 18, 348-359, 1961.

3. Herman, B. M. and L. J. Battan, "Calculations of Mie Back-scattering of Microwaves from Ice Spheres," Technical Report No. 12, Institute of Atmospheric Physics, University of Arizona, 1959.

4. Wilk, K. E., J. T. Dooley and E. Kessler, "Weather Detection by ARSR-1D, ASR-4 and WSR-57 Radars, A Comparative Study," 1964, Technical Memorandum No. 1, National Severe Storms Laboratory, U.S.Weather Bureau, 33pp.

[2] The first paper in this report discusses the correspondence between observations of Z_e and hail.

SFERICS RECEPTION AT 500 kc./sec., RADAR ECHOES, AND SEVERE WEATHER

Neil B. Ward, Charles H. Meeks, and Edwin Kessler

ABSTRACT

The response of the directional 500 kc./sec. noise meter, SPARSA, is investigated with respect to its associations with radar echoes, indications of severe storm events reported by ground observers, and turbulence experienced by aircraft. SPARSA counts appear greater with greater lightning activity and the transition of storms to severe hail stages is usually associated with increasing SPARSA count rates. However, the absolute magnitude of SPARSA counts has a complicated range dependence and is highly variable with respect to parameters such as wind and hail. The time record of SPARSA counts is typically variable and many changes are not associated with severe storm events.

The variability of sferics activity associated with severe storms demands careful investigation, from the viewpoints of both basic meteorological researchers and those who are charged with identifying and forecasting storms containing lightning and other hazards.

TABLE OF CONTENTS

1. INTRODUCTION

The electrical manifestations of storms affect aircraft operations, distribution systems for electrical power, communications, and other works of man. They hold our interest also because of probable connections between atmospheric electricity and many processes intimately connected with storm development and decay. The purported existence [1] of singular relationships between important storm features and the response of the SPARSA[1] directional detecting equipment for 500 kc./sec. sferics, led the Weather Bureau to evaluate SPARSA equipment with respect to its potential for development and utilization with radar as an operational tool for the location and short term prediction of severe thunderstorms.

Particular assertions investigated are:

1. That SPARSA can provide useful information concerning developing severe storms within 200 mi., in advance of radar indications;
2. That sferics maxima as defined by SPARSA are indicative of the onset of storms' dissipating stages;
3. That severe storm events are characteristically preceded by a very rapid increase of SPARSA-detected sferics activity;
4. That SPARSA data are a useful indicator of the storm turbulence experienced by aircraft.

Data were gathered during April, May, and June 1964 at NSSL and include SPARSA output (see below), WSR-57 film records, storm data gathered by an Air Force F-100 and a Navy F-11 aircraft, surface weather reported by 400 volunteer weather observers, and compilations of the U.S. Weather Bureau Office of Climatology.

The related study of Kohl and Miller [2] treats principally the associations between omni-directional sferics and severe weather, while the present study concerns directional sferics and particular storms identified by radar and human observers.

2. NOTE CONCERNING SPARSA EQUIPMENT

The SPARSA is a directional sferics monitor tuned to 500 kc./sec. It is intended to record automatically the sferics count rate in 64 azimuthal sectors each 5.6° wide. An additional sense circuit (SPARSA/S) can be employed to remove the 180° direction ambiguity which is otherwise present.

---

[1] Sferics pulse amplitude rate spectrum analyzer available from Litton Systems, Inc., Applied Science Division.

Data from each sector are collected during 10-sec. periods repeated at intervals of 112 sec.; the latter is the time taken for stepwise rotation of the receiver and antenna system through 45°. Data from each sector are electronically averaged according to a 10-min. time constant. The azimuthal distribution of SPARSA response is displayed as a polar diagram on a cathode ray tube (CRT) and photographed. Also displayed and photographed are polar diagrams representing the azimuthal distributions of count rate change as electronically derived. Photographs of the CRT count rate and rate-of-change displays are made at two sensitivity settings every 4 min.

SPARSA equipment was installed and calibrated by Litton personnel, who remained in attendance from April 15 through May 29. From May 29 through June 25, equipment operation was supervised by U. S. Weather Bureau personnel.

It should be noted that 500 kc./sec. is a frequency reserved for distress signals, and is normally quiet with respect to ordinary broadcasting activities of man. However, the presence of man-made broad-band radiations of diverse origins can be a significant source of interference to equipment established for sferics detection. Interference was apparently present about 15 percent of the time during NSSL data collections; the data discussed in the following sections of this report exclude these cases.[2] Also omitted from consideration are most cases where more than one discrete disturbance occurred at one azimuth.

An example of multiple sources at one azimuth, illustrative also of the means used to combine radar and sferics data, is shown in figure 1. The echo cells are labeled with the maximum radar reflectivity factor Z in $mm.^6/m.^3$. The outer contour of all echoes enclose reflectivity factors $\geq Z = 10\ mm.^6/m.^3$, while inner contours enclose approximately equal intervals of log Z. The heavy line in each section of the figure shows the azimuthal distribution of sferics count rate, and the numerals adjacent thereto indicate their range normalized values (see next section). This figure shows a developing storm which later produced large hail and a tornado and which moved between the observing site and a more distant storm. On this occasion, storm cells occurred also at opposite azimuths, and their radiations were not rejected by the SPARSA equipment because the sense circuit was not operated.

3. SPARSA RESPONSE AND RANGE

Figure 2 shows the distribution of SPARSA count rates with range for 113 severe weather reports. The observations filed by about 400 cooperative observers or tabulated in the Weather Bureau publication Storm Data describe hail, wind damage, or tornadoes sighted. The count rates are those

[2] It is admitted that some interference may have been unnoticed.

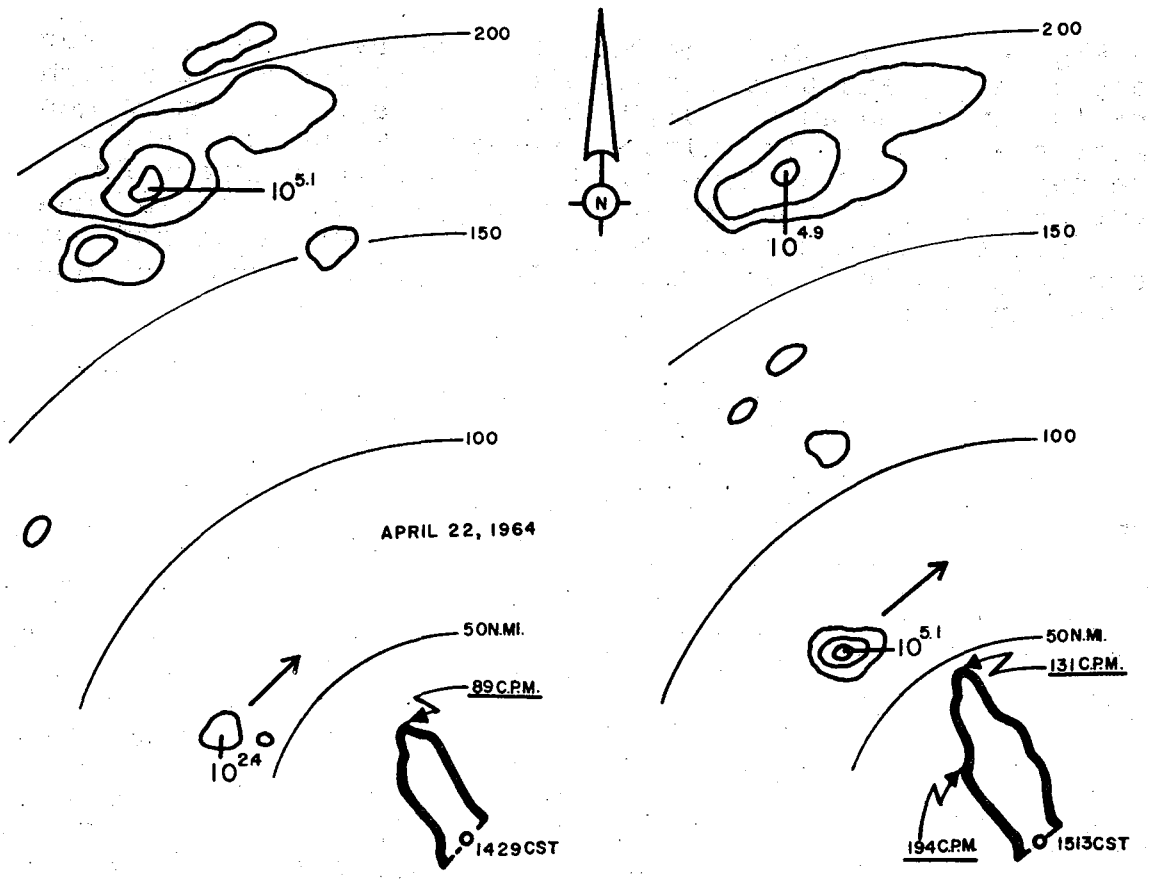

Figure 1. - Sferics data and radar echoes on April 22, 1964. The weak cell 60 mi. northwest of the NSSL WSR-57 radar at 1429 CST (left) gave practically no sferics response. At 1513 CST, the polar display gave evidence of reception from this cell, as it approached the same azimuth as the more distant storm.

denoted by the SPARSA film record at the time and in the azimuth sector corresponding to the particular severe event. In no case is a storm located between the reported event and the recording equipment, and no case of known interference is included in figure 2.

Conclusions based on figure 2 might be questioned on the basis that some data are dependent; i.e., that the sample is not a random collection from a representative population of severe weather events. We have tried to minimize this problem by including only severe events separated by 10 mi. or more. The points in figure 2 represent data collected from 32 storms on 15 different days. For various reasons, about 25 per cent of all severe storm reports were excluded from the analysis. However, it seems unlikely that the exclusion process introduced appreciable bias with respect to correlation between sferics and severe weather.

Figure 2 shows that the higher count rates do not occur at close range, and that the probability of receiving a high count is maximized at about 70-80 mi. Reception from ranges greater than 140 mi. is quite uncertain. This complicated range dependence of maximum count rate probably arises from a combination of factors related to properties of the SPARSA equipment, electromagnetic propagation between earth and ionosphere, high angle of arrival of the radiation from near discharges, and others.

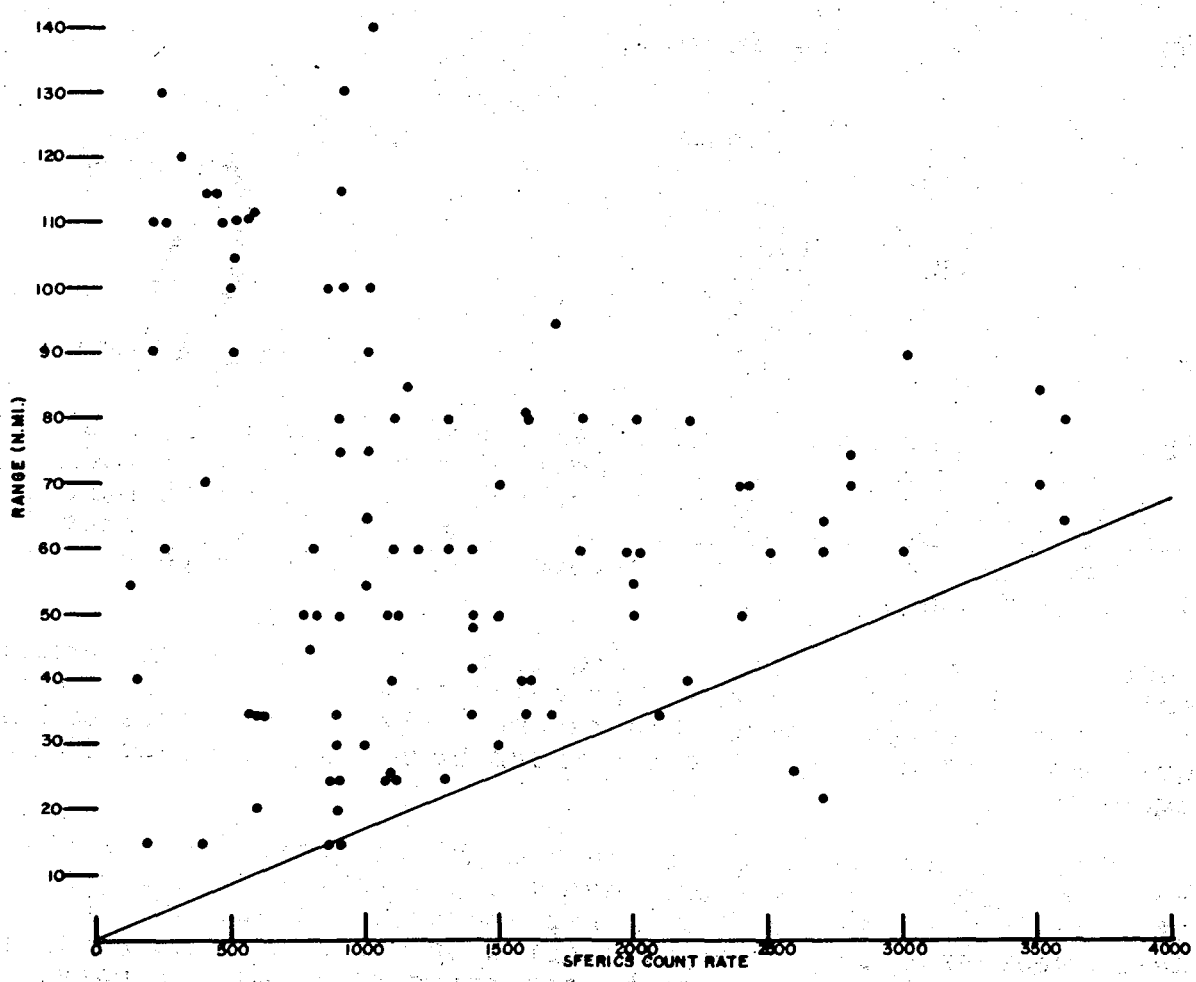

Figure 2. - SPARSA sferics count rate vs. range at the time and azimuth of severe storm events reported by cooperative observers or documented in the U. S. Weather Bureau publication Storm Data. The heavy line seems to define a count rate envelope at ranges within 70-80 mi. and is the basis for the range normalization procedure used in this study.

Dr. Keith Browning of AFCRL and Douglas Kohl of Litton Systems have discussed the use with SPARSA of sensing circuits which establish a counting threshold, set at a constant fraction (1/4) of the continuously updated average peak signal received within the same sector.[3] This is intended to provide some compensation for sferics amplitude variations with range to the source of sferics signals. Figure 2 shows that this compensation is incomplete.

Dr. Browning has proposed that the range dependence of SPARSA count for nearby sources, shown in figure 2, may be due to the increasing geometric width of each 5.6° sector as range increases, with corresponding increased probability of detecting multiple sferics sources.[4] On the other hand, the data reported here clearly manifest effects of attenuation beyond 80 mi. There is the additional consideration that some sources may be so distributed that several SPARSA sectors are simultanously influenced.

Figures 1 and 3 show sferics counts range normalized according to the equation:

$$\text{Count}_{RN} = \frac{10X\ \text{Count}}{\text{Range in miles}} \qquad (1)$$

The count rate used in normalizing is the maximum SPARSA indication for a particular storm area. The normalized maximum SPARSA counts of figure 3 are based on the same population of events plotted in figure 2, but those events removed more than two sectors from maximum sferics are omitted. We believe that storm centers are usually well defined by the cooperative observer reports, especially when storms are severe, though it is true that storm cores over unpopulated areas are unreported.

In figure 3 the data within 70 mi. show no apparent trend with range, and no high count rates occur at ranges more than 100 mi. Of course this is to be expected from application of inverse-range normalization to data like those in figure 2.

---

[3] Privately communicated. To be printed as part of a comprehensive study by AFCRL and others of the Oklahoma storms of May 26, 1963.

[4] Ibid.

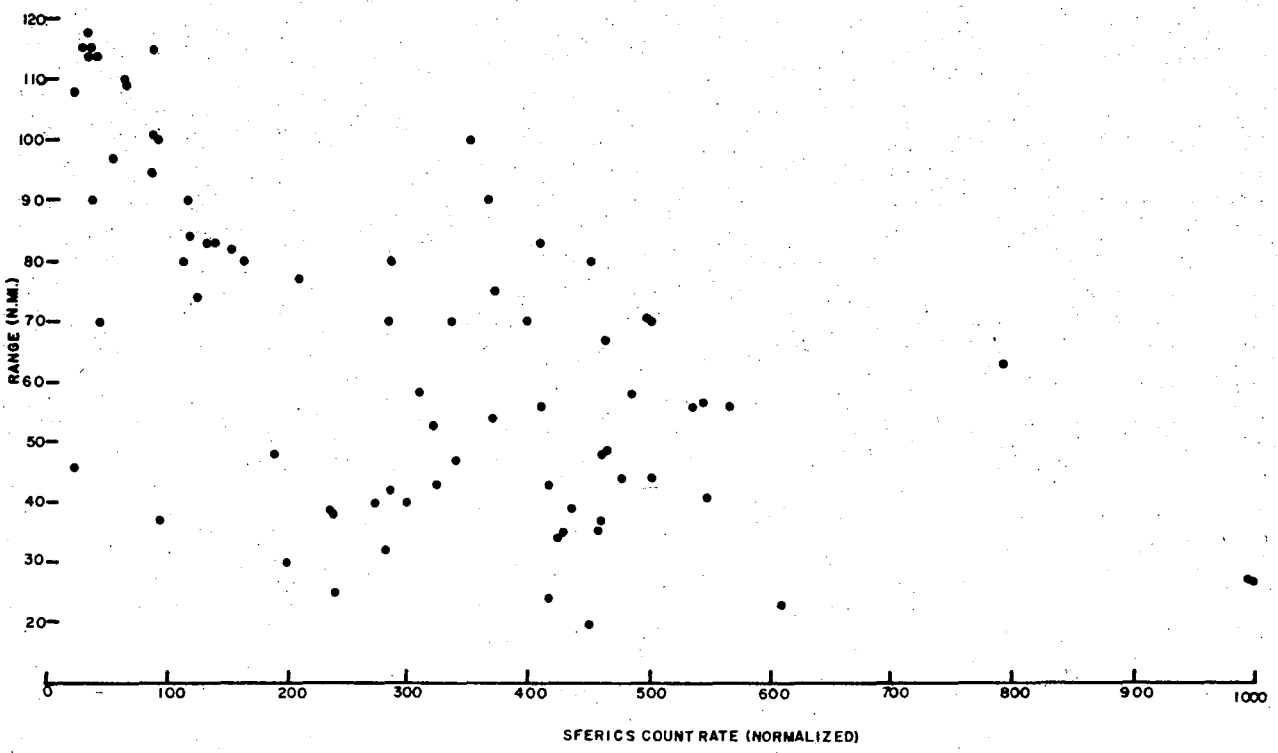

Figure 3. - SPARSA normalized count rate vs. range for the sector of maximum count associated with the storms documented in figure 2. Where the count maximum occurred more than two sectors removed from the azimuth of the reported event, the case was excluded from this figure.

In view of both empirical inadequacies and the complexity of processes associated with the reception of sferics from different kinds of electrical discharges on different occasions, we have chosen to leave further development of the range dependence of SPARSA to future investigations. However, the normalized counts shown in this report unquestionably improve the correspondence of SPARSA response to severe weather for the family of events discussed in this report, and particularly for those within about 80 mi.

The history of sferics count for a storm on April 23, 1964 is shown in figure 4. Sferics data are plotted at 8-min. intervals, corresponding to the time interval separating sequences of comprehensive radar data.

Between 1520 and 1740 CST, the distance of this storm from the recording equipment decreased from 115 to 28 n. mi., corresponding to a speed of about 40 kt. During short time periods, range changes have relatively small influence on the

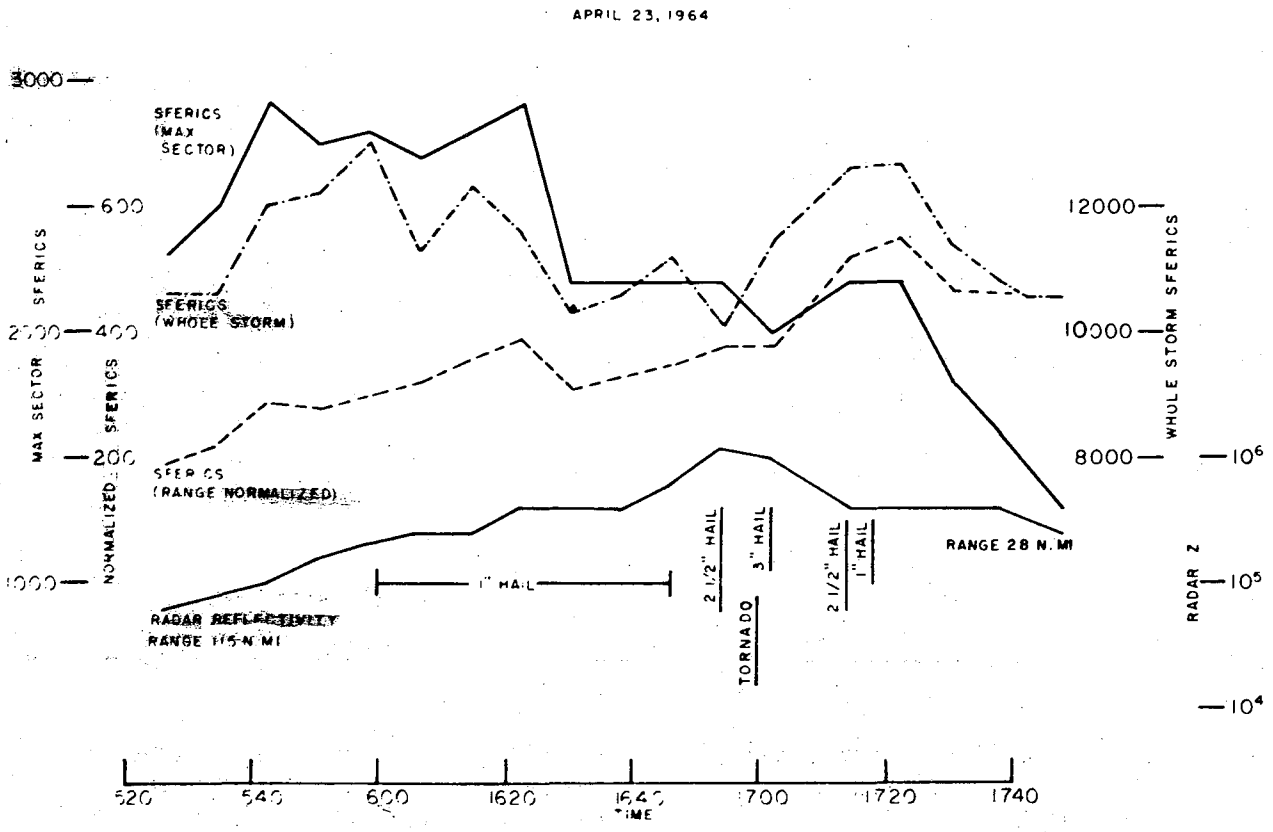

Figure 4. - Time histories of sferics count, storm core radar reflectivity, and severe events associated with a damaging storm on April 23, 1964.

count rate. We cannot know whether, on this particular occasion, the early upward trend of maximum sector sferics, and predominantly downward trend after 1620, when the storm was about 80 mi. away, reflect intrinsic trends of sferics activity or, predominantly range effects (cf. fig. 2). Figure 4 shows that the whole storm sferics count is closely related to the count in the maximum sector except when the range is short. This is typical. This figure further shows that short period sferics changes were not distributed in any obvious way about severe storm events.

The range normalized radar echo intensities[5] exhibit a fairly stable behavior. Reflectivity factors $> 10^5$ mm.^{6}/m.^{3} are associated with the hail occurrences and maximum Z's occurred at the time of maximum hail size and a tornado.

[5]Normalized according to inverse range squared.

Table 1. - Severe Storms Data with Related Sferics for the Months of April, May, and June 1964

	Tornadoes	Wind Damage	Hail 1/8 to 1/2 in.	Hail Over 1/2 to 1-1/2 in.	Hail Over 1-1/2 to 2-1/2 in.	Hail Over 2-1/2 in.	Averages of all Events
Number of Reports (Total 113)	20	20	28	28	11	6	
Radar Reflectivity, Z	$10^{5.1}$	$10^{5.5}$	$10^{5.0}$	$10^{5.3}$	$10^{5.6}$	$10^{5.7}$	$10^{5.3}$
Average Sferics Count Rate in Sector	1410 ±220	1040 ±100	1570 ±150	1280 ±160	1640 ±300	1240 ±370	1360 ± 80
Standard Deviation	958	442	798	857	952	838	846
% of Times Count Rate INCREASED during Preceding 16 min.	37	18	39	43	50	60	38
32 min.	59	35	36	69	50	72	52
% of Times Count Rate DECREASED during Preceding 16 min.	47	41	29	39	38	20	38
32 min.	32	35	48	24	40	14	34
% of Times NO CHANGE during Preceding 16 min.	16	41	32	18	13	20	24
32 min.	9	30	16	7	10	14	14
Average Count Change in 16 min. Preceding Event	- 6	-38	+32	+71	0	+42	+20
32 min.	+66	+40	0	+223	+95	+180	+97
% of Times Event Same Sector as Maximum	30	20	25	18	40	17	24
% of Times Maximum Sferics CLOCKWISE from Event	40	65	43	61	50	83	53
% of Times Maximum Sferics COUNTERCLOCKWISE from Event	30	15	32	21	10	0	23

4. STATISTICAL ANALYSES OF SEVERE STORM EVENTS

a. Unnormalized Data and Severe Weather

Table 1 is a tabulation of SPARSA data uncorrected for range for 113 severe weather events. Of these, 93 are distinct observations, and 20 reports of tornadoes combined with hail, or wind with hail are included in two columns. The frequency and severity of lightning are not considered in this tabulation.

Sferics count rates in the sectors of the events ranged from 100 per min. during the Rush Springs wind and hail storm on May 30 (range 40 mi.) to 3600 per min. during the Yukon tornado on May 1 (range 25 mi.). The grand average count rate for all events was 1355 per min. It is seen that the standard deviation of SPARSA count rates is a substantial fraction of the means for each type of event. This fact confirms the data in figure 2, viz., that variability is a noteworthy feature of sferics count rates associated with severe weather.

Table 1 also shows count rate changes during the time intervals 16 and 32 min. prior to observations of severe weather. These are relatively unaffected by distance changes, since motions are comparatively small during such a short time. However, it should be recognized that many of the storm reports from cooperative observers must represent the onset at particular points of already established storms. For the 16-min. data notice that 38 per cent of all observations were preceded by increasing sferics, 38 per cent were preceded by decreasing sferics, and no measurable change preceded 34 per cent of severe events. Within particular classifications some variations of the proportion of increases and decreases are evident; however, it is not possible to tell if these differences are due to distinctive physical processes or are purely random fluctuations.

Note that when the sferics data are compiled for 32 min. periods preceding the reports of severe storm events, a somewhat larger proportion of events is associated with SPARSA count increases. It seems likely that the electrical effects of storms usually increase when the rain, hail, and winds increase, and the differences between the 16- and 32-min. statistics reflect a combination of some regular physical associations and random processes.

The data have been examined to isolate times and places where it is quite certain that storms first developed a "severe" stage. Table 2 lists the few such cases where all equipment was working well and no interference was detected. The radar echo and SPARSA histories show that the former has a more regular correspondence to the onset of severe storms. It is well known that radar echo intensities are a semi-quantitative indicator of rainfall rate and hail size. Radar echoes from hailstorms and tornadic storms are almost invariably strong ($Z > 10^5 mm.^6/m.^3$), while SPARSA response may be weak (i.e., at a level corresponding to many non-severe events) or strong. On the average, both radar echoes and SPARSA response increase during the period when severe storm manifestations are first reported, although, as one would expect, many exceptions occur.

Of all severe weather events, 24 per cent occurred in the sector in which sferics indicated a maximum for a particular storm area. It was noted that maximum sferics count occurred at azimuths clockwise from the event 53 per cent of the time and counterclockwise only 23 per cent. This suggests a mis-alignment of equipment, but orientation was carefully checked. A great majority of the storms in this data were north and west of the observing site and the storm anvil or plumes nearly always extended toward the east or northeast.

This suggests that a strong source of 500 kc./sec. sferics is located in storm anvils, which for most of these data, would be clockwise from the storm center as viewed from the point of observation.

Table 2. - Radar-Sferics Data Related to Onset of Storm Severity

April 24, 1964, Range 120-75 n. mi.

Time (CST)	Radar Z ($mm.^6/m.^3$)	Sferics (Normalized) (Counts per min.)	Event
1516C	$10^{3.0}$	67	
24	$10^{3.6}$	67	
32	$10^{3.6}$	64	
40	$10^{4.0}$	73	
48	$10^{4.4}$	110	
56	$10^{4.4}$	105	
1604	$10^{4.0}$	120	
12	$10^{4.0}$	110	
20	$10^{4.4}$	102	
28	$10^{5.0}$	94	
36	$10^{4.5}$	88	
44	$10^{4.7}$	100	
52	$10^{4.7}$	130	
1700	$10^{5.0}$	130	1/4 in. hail
08	$10^{5.2}$	150	
16	$10^{5.2}$	140	3/4 in. hail
24	$10^{5.2}$	130	

May 1, 1964, Range 20-30 n. mi.

1422	$10^{2.4}$	-	
30	$10^{4.4}$	480	
38	$10^{5.0}$	480	
42	$10^{5.0}$	280	
50	$10^{5.0}$	340	
58	$10^{5.0}$	360	
1506	$10^{5.0}$	350	
14	$10^{5.2}$	400	
24	$10^{5.5}$	560	
32	$10^{5.5}$	560	
44	$10^{5.6}$	640	
1602	$10^{6.1}$	870	
10	$10^{6.1}$	940	
18	$10^{5.8}$	1100	
26	$10^{6.1}$	1000	Tornado
34	$10^{6.1}$	900	3 in. hail

Table 2 - Continued

Time (CST)	Radar Z ($mm.^6/m.^3$)	Sferics (Normalized) (Counts per min.)	Event
	May 10, 1964, Range 80-60 n. mi.		
1559	$10^{3.0}$	-	
1607	$10^{4.2}$	-	
11	$10^{5.2}$	-	
19	$10^{5.0}$	-	
23	$10^{5.0}$	62	
27		70	
31	$10^{5.0}$	80	
35		93	
39	$10^{5.0}$	110	
47	$10^{5.2}$	110	
55	$10^{5.2}$	130	
1703		110	3/4 in. Hail
07	$10^{5.4}$	150	
	May 30, 1964, Range 25-40 n. mi.		
1356	$10^{4.6}$	-	
1404	$10^{4.6}$	-	
12	$10^{5.0}$	-	
20	$10^{5.0}$	-	
28	$10^{5.0}$	-	
36	$10^{5.0}$	-	
44	$10^{5.2}$	-	
52	$10^{5.2}$	11	1/2 in. Hail and Damaging Wind
1508	$10^{5.6}$	24	
16	$10^{5.8}$	24	
24	$10^{5.8}$	33	
32	$10^{5.8}$	33	
40	$10^{5.6}$	70	1-1/4 in. Hail
48	$10^{5.0}$	82	
56	$10^{5.2}$	75	
1604	$10^{5.0}$	120	No further reports of severe weather
12	$10^{5.0}$	110	

Table 2 - Continued

Time (CST)	Radar Z ($mm.^6/m.^3$)	Sferics (Normalized) (Counts per min.)	Event
	June 4, 1964, Range 125-100 n. mi.		
1514	10^2	42	
21	10^3	44	
29	$10^{3.6}$	38	
37	10^4	37	1/4 in. Hail
45	$10^{5.2}$	31	Tornado
53	$10^{4.9}$	27	
	June 4, 1964, Range 40-50 n. mi.		
1703	10^2	0	
11	$10^{2.6}$	50	
19	$10^{5.2}$	50	
27	$10^{5.4}$	55	
35	$10^{5.4}$	55	
43	$10^{5.4}$	38	3/4 in. Hail

Sferics are absent in the absence of storms; however, the data of figure 2 and tables 1 and 2 suggest that unnormalized sferics may be weak or strong in the presence of severe storms and that increasing SPARSA count rate, or absolute count, are not reliable indicators of incipient or present severity.

b. Range Normalized Sferics and Severe Weather

Table 3 lists associations between sferics counts which have been range normalized in accordance with equation (1). These data are based on the sector where the count for a given storm is at a maximum, provided that the maximum count is not more than two sectors removed from that of the reported event.

These statistics are similar to those discussed in item a, above, except that there is a noticeable difference between the behavior of sferics changes prior to hail and wind storms.

The large percentage of normalized sferics-increases preceding heavy hail is worthy of further investigation, particularly in view of Browning's discussion of the May 26, 1963 storms at Oklahoma City.[6]

See Footnote 3

Table 3. - Severe Storm Data with Range Normalized Sferics for the Months of April, May, and June 1964

	Tornadoes	Wind Damage	Hail 1/8 to 1/2 in.	Hail Over 1/2 to 1-1/2 in.	Hail Over 1-1/2 to 2-1/2 in.	Hail Over 2-1/2 in.	Averages of all Events
Number of Reports (Total 73)	19	6	17	18	7	6	
Radar Reflectivity, Z	$10^{5.2}$	$10^{5.5}$	$10^{5.3}$	$10^{5.3}$	$10^{5.8}$	$10^{5.7}$	$10^{5.4}$
Sferics Count Rate in Sector	260 ±60	240 ±50	360 ±50	290 ±30	350 ±60	360 ±140	300 ±20
Standard Deviation	243	116	187	124	150	320	208
% of Times Count Rate INCREASED during Preceding 16 min.	39	33	67	41	71	83	53
32 min.	63	67	70	83	43	100	71
% of Times Count Rate DECREASED during Preceding 16 min.	39	50	33	53	29	17	39
32 min.	31	33	18	17	57	0	25
% of Times NO CHANGE in Count Rate Preceding 16 min.	22	17	0	6	0	0	8
32 min.	6	0	12	0	0	0	4
Average Count Change in Preceding 16 min.	+ 4	+ 4	+18	+13	+44	+24	+15
32 min.	+32	+ 5	+32	+33	+21	+86	+26

c. SPARSA and Lightning

SPARSA indications of lightning have been investigated by comparing cooperative observer reports of lightning during storms with normalized SPARSA data for the same time and azimuth sector. Table 4 shows that average SPARSA response was least for observers reports of "no lightning" and increased regularly to the greatest average value when both cloud-to-cloud and cloud-to-ground lightning were reported. It is interesting that SPARSA responds significantly at sectors where "no lightning" is reported.

Such observer reports do not necessarily mean that lightning is absent in the storm area. During daylight, particularly, lightning can be obscured by rain and low clouds and thunder may not be audible in the presence of heavy rain and strong winds. It does seem likely, however, that "no lightning" reports are associated with less extensive and intensive lightning than the others. It is also probable that some sferics arise from electrical activity which is neither visible nor audible.

Table 4. - Lightning-Sferics Data

Observer Report	Number of Cases (Total = 107)	Average Normalized SPARSA Count and Estimated Standard Error of Mean
No Lightning	28	235 ±25
Lightning at a Distance	8	275 ±60
Cloud-to-Ground Only or Cloud-to-Ground and Overhead	21	295 ±60
Cloud-to-Cloud Only or Cloud-to-Cloud and Overhead	37	325 ±20
Cloud-to-Cloud and Cloud-to-Ground	13	335 ±65

d. Aircraft Turbulence and Sferics

During the aircraft program, a total of 53 in-storm flights was made for which aircraft and SPARSA data can be compared. Figure 5 is a plot of normalized sferics vs. turbulence based on pilot comments[7]; the correlation coefficient is +0.52. Note that most turbulence was only light to moderate, since radar was used on an operational basis to avoid flights in weather severe enough (hail large enough) to damage the aircraft. Note also that turbulence in the severe category was registered three times with little or no SPARSA response.

[7]It is very difficult to devise an objective criterion for defining aircraft-experienced turbulence, since its occurrence is highly erratic. The standard deviation of derived gusts has been related to pilot comments over comparable intervals of time; this shows that the pilots' discrimination is essentially linear. See P. 15.

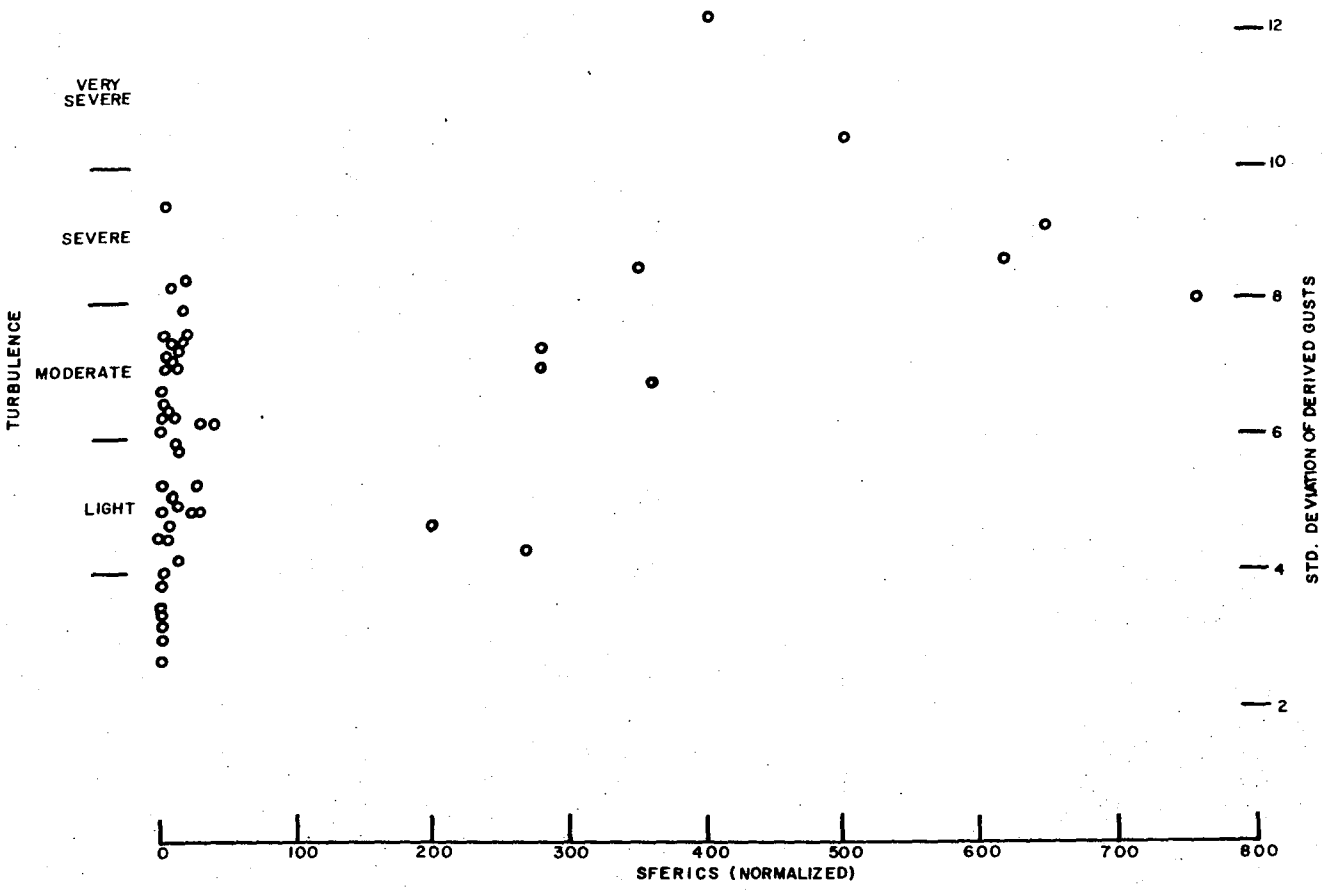

Figure 5

An example of sferics-turbulence relationship is given by the May 27 data, illustrated in figure 6. A line of intense echoes developed northeast of Norman during the afternoon, while a widespread area of somewhat weaker echoes continued at a range of 75 to 150 n. mi. SPARSA indicated a much larger count rate from the area to the southeast. Aircraft penetrations of the line of cells was followed immediately by flight through the stratified area. In the intense line at 1611 CST, where SPARSA indicated the low rate of 25 counts per min. (cpm), the pilot reported mostly moderate turbulence with "a little bit of heavy." He did not mention lightning. At 1642 CST, in the area of weaker radar echo, but higher sferics count (72 cpm, normalized) he reported only light turbulence, but considerable lightning.

This with other examples suggests that the SPARSA response is indicative of electrical activity, but that neither SPARSA nor electrical activity is regularly identified with other severe manifestations of storms.

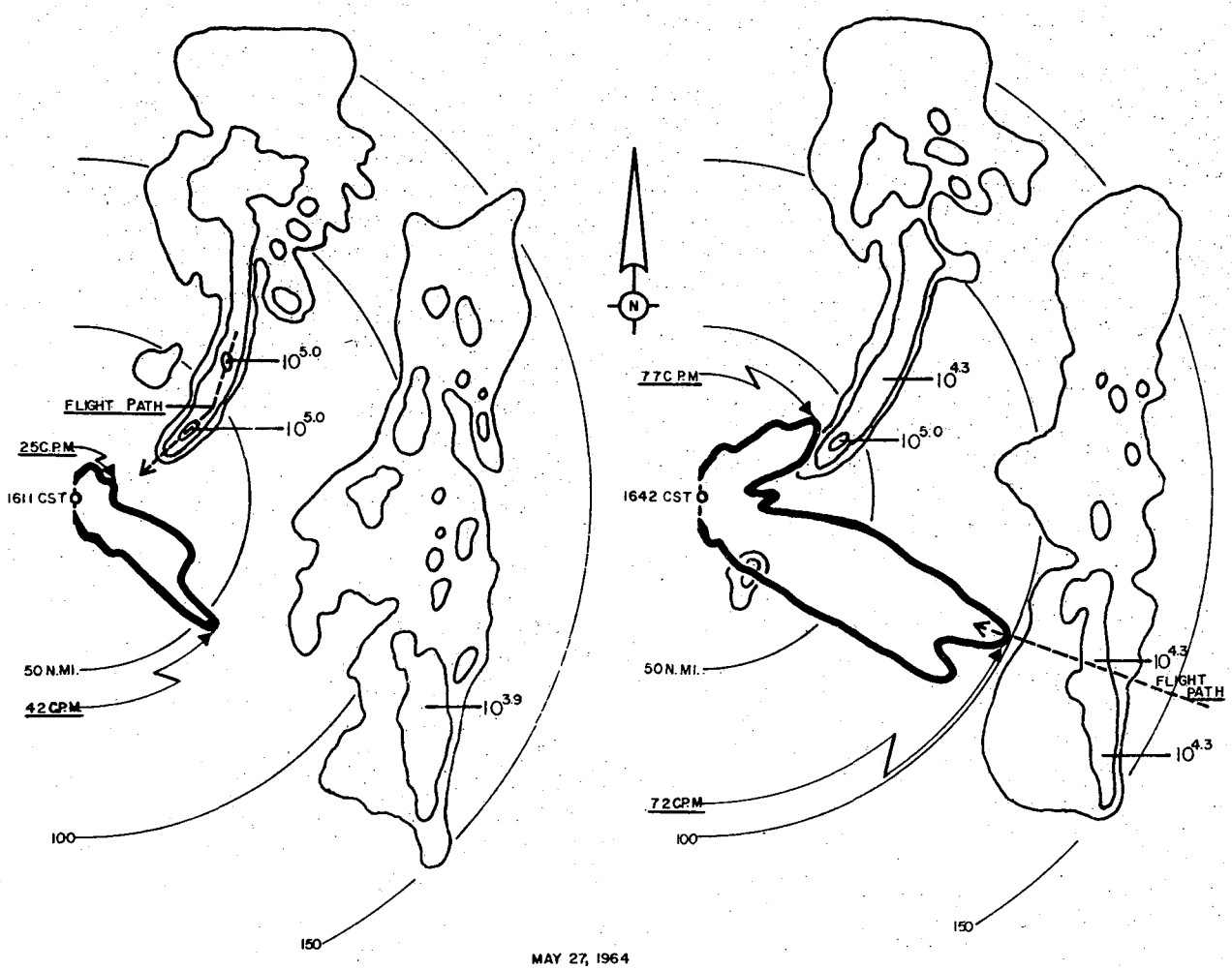

Figure 6.

5. DAILY SUMMARIES

The following items summarize various features of severe events on different days. In the figures, sferics are indicated by the heavy tracing of the polar diagram and the count rate is proportional to the amount of deflection from the center. The deflection is shown at either high or low SPARSA sensitivity and the numerals labeling particular azimuths refer to sferics normalized to 10 mi. range. It is interesting to compare these to the average normalized count rate of 300 cpm for all severe weather events studied. The radar echoes from the 10-cm. WSR-57 radar are displayed in light solid contour lines and the range shown by radar or severe storm reports is the basis for sferics normalization.

April 22, 1964

This storm is illustrated by figure 1. It was attended by severe hail, damaging wind, and a major tornado along a path 60 to 75 mi. northwest of Norman, between 1600 and 1800 CST. The storm was first detected by radar before 1400 CST in its developing stage at azimuth 295° and range 65 n. mi. There were no detectable sferics from the storm until 1445 CST, although there were extensive sferics from weather in other directions. At 1513 CST, the storm neared a sector where moderate sferics were being received from a more distant storm. From then until 1600 CST, when a tornado and large hail began, the data do not permit us to distinguish between the sferics received from these storms. After 1600 CST, the sferics count rate was high (400-500 cpm) and the direction of the severe storm was accurately indicated.

April 23, 1964

A severe storm developed in west-central Texas and at 1300 CST it was 175 n. mi. southwest of the Norman radar, which showed reflectivity factor $Z = 10^5 mm.^6/m^3$. Sferics were very weak at this time but increased as the storm moved nearer and indicated the storm direction quite well. By 1622 CST (fig. 7) sferics had increased to 387 cpm while extensive 1-in. diameter hail was being produced (see also fig. 4). After a temporary decrease, sferics later increased to a maximum of 600 cpm at 1725 CST. During this period of increasing sferics, giant hail fell and a tornado was reported. The radar reflectivity factor exceeded the high value of $10^6 mm.^6/m.^3$ during this time.

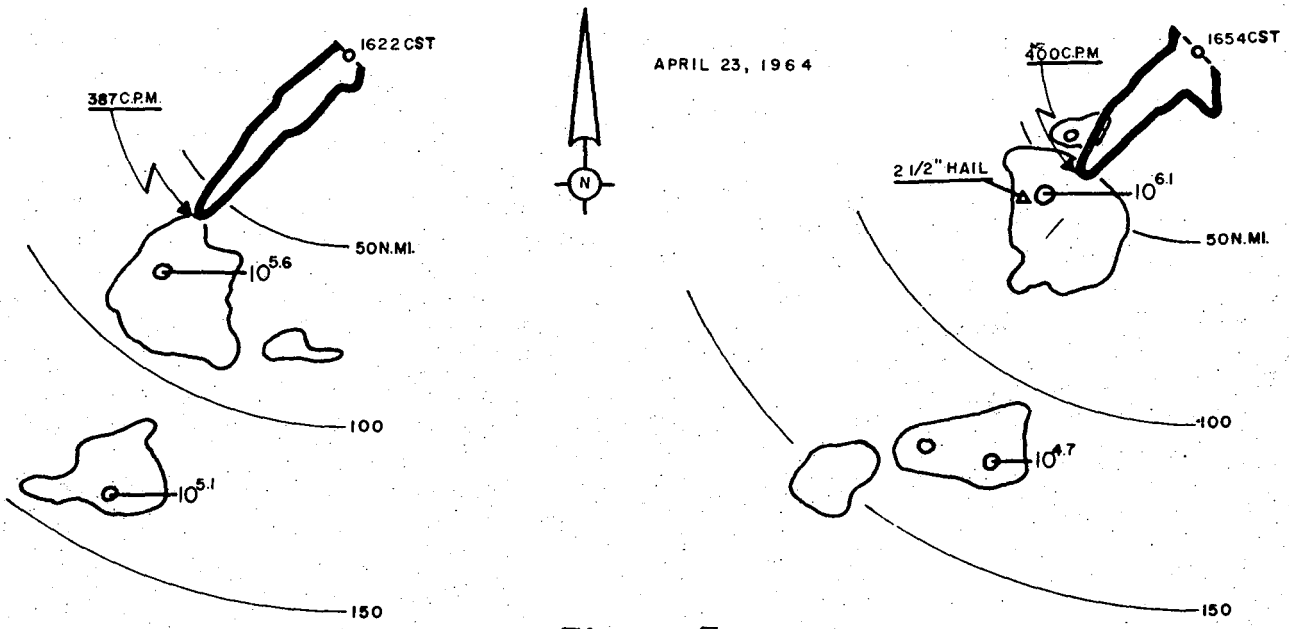

Figure 7

April 24, 1964

A thunderstorm area ("A" in fig. 8) was at an azimuth of 220° and 110 n. mi. from Norman, had a radar Z of 10^5 and a sferics count rate of 75 cpm at 1530 CST. A new area of development (storm "B") began on the north side of the original storm, broke away and moved more rapidly north-northeastward. Sferics from Storm "A" had increased to 240 cpm by 1620 CST, then fluctuated above and below that value until 1800 CST, after which they decreased. One report of hail damage was received from storm "A".

Sferics from storm "B" were up to 125 cpm at the time of the first hail report at 1700 CST. They then fluctuated between 100 and 160 (average for this size hail, 291 cpm) for the next 2 hr., during which time 5 reports indicated hail of 3/4 in. fell from the storm.

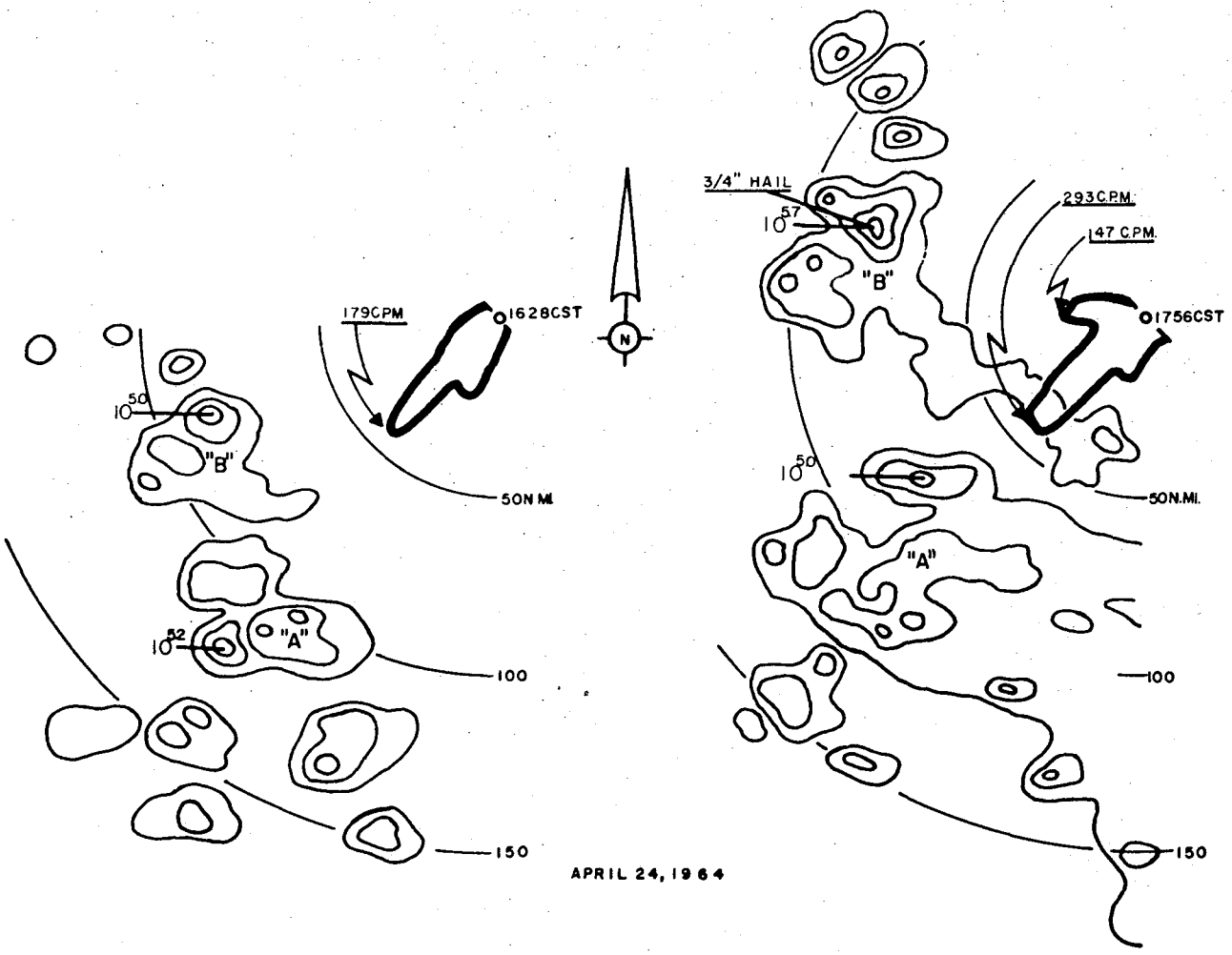

Figure 8

May 1, 1964

This day was characterized by very strong sferics, stronger than average by a factor of 2 to 3. Severe storm "A" (fig. 9), 50 to 100 n. mi. north-northwest, produced 430 cpm as early as 1400 CST, when radar Z was 10^5. Heavy fall of hail as large as 3/4 in. was reported around 1430 CST. A maximum of 850 cpm was reached at 1500 CST, decreasing slowly thereafter. Numerous reports of hail during the next 2 hr. were received from the area. The severe tornado and hailstorm "B" began developing around 1400 CST and reached radar $Z = 10^5$ by 1440 CST with moderate to strong sferics. Both sferics and radar reflectivity increased during the next 2 hr., reaching 1100 cpm and Z in excess of 10^6. During the late portion of this period, giant hail fell and a major tornado occurred. Sferics and radar reflectivity continued very high and additional hail falls were reported for several hours.

The low actual counts from storm "B" during its early stages assume significance in light of the radar indication of relatively short range to this storm.

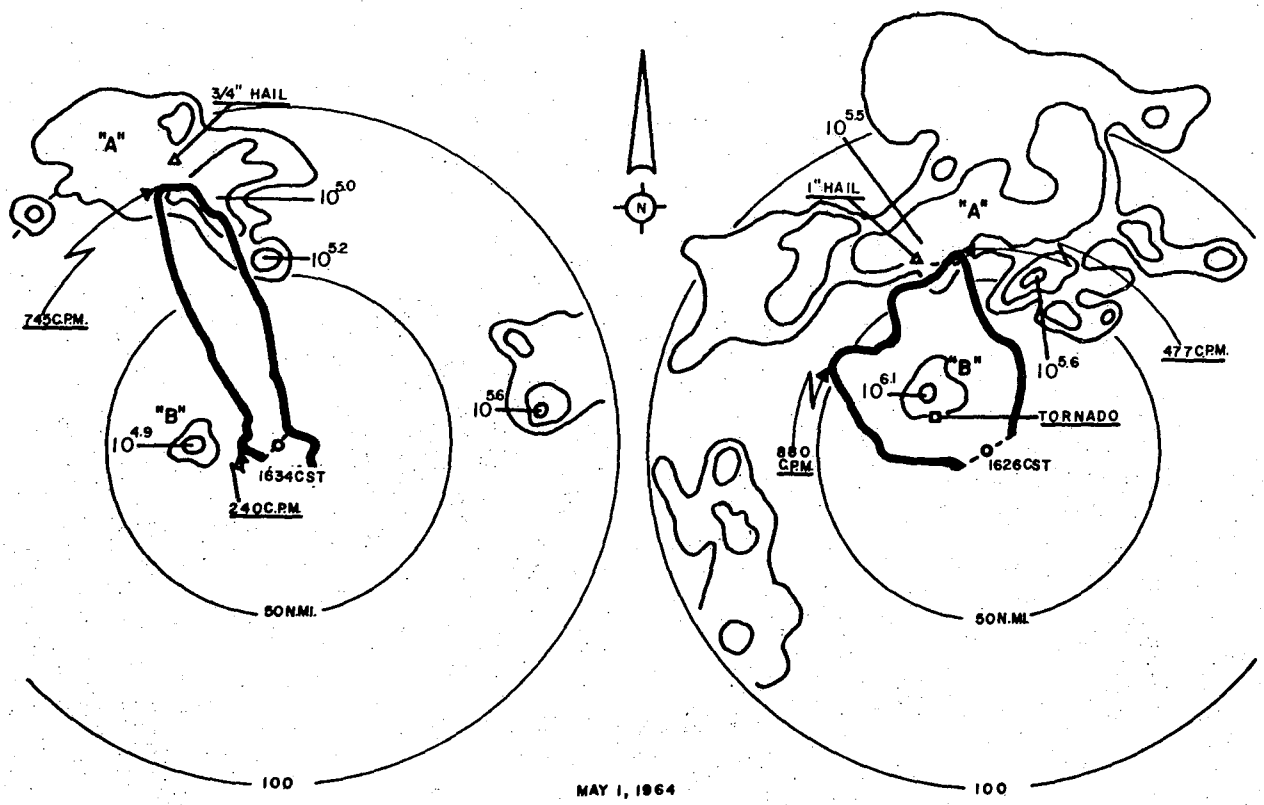

Figure 9

May 5, 1964

This was a day of very severe weather at a range of 100 n. mi., accompanied by very weak sferics. Storms to the northwest had a radar reflectivity factor Z of 10^5 by 1615 CST, while the sferics normalized rate was 18 cpm (200 cpm absolute count). In figure 10 the sferics are displayed at high sensitivity of the equipment, because of the low count rate. Large hail, 2 in. in diameter was reported at 1715 CST and the first tornado and 3-1/2 in. hail at 1725 CST, at which time sferics had increased to 34 cpm, about 1/10th the average for this event. A second tornado occurred at 1800 CST when the count was up to 43 cpm. At 1830 CST the third tornado occurred, accompanied by 3 in. hail and sferics of 64 cpm. The count rate was 45 when another tornado occurred at 2100 CST and 80 during others at 2225 and 2315 CST.

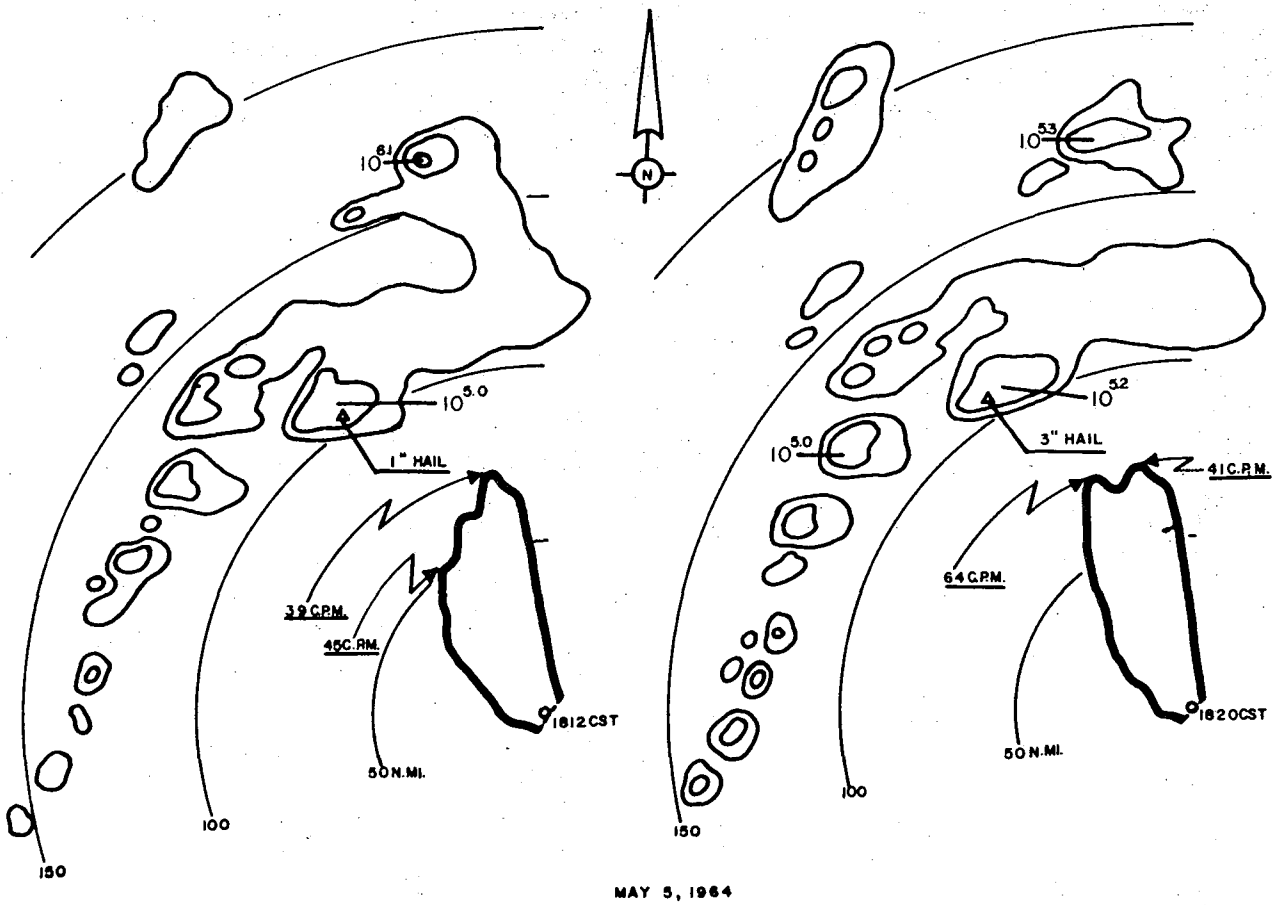

Figure 10

May 7, 1964

A thunderstorm complex at 1620 CST was located at 230° and range of 120 n. mi. when the reflectivity was in excess of 10^5 and sferics 120 cpm. The sferics maximum indication was toward the east (10° counterclockwise) of the radar storm center. At 1700 CST, it was reported that hail 2 and 3 in. in diameter occurred in western portions of the storm, or 20° to 25° clockwise from the maximum sferics indication, which had then risen to 340 cpm. Later, at 1825 CST small hail was reported from a small storm ($Z = 10^{4.6}$), from which no significant sferics were received. This storm was 60° clockwise from the sferics maximum identified with four reports of heavy rain accompanied by lightning.

May 8, 1964

An extensive area of thunderstorms southeast at a range of 80 to 150 n. mi. (fig. 11) produced moderate sferics during the morning and midday hours. The sferics were accompanied by significant rates of increase, which nearly coincided with increases in radar reflectivity. The maximum sferics of 225 cpm, near the average for severe weather, coincided with a maximum Z of $10^{4.2}$. No severe weather was reported with this storm.

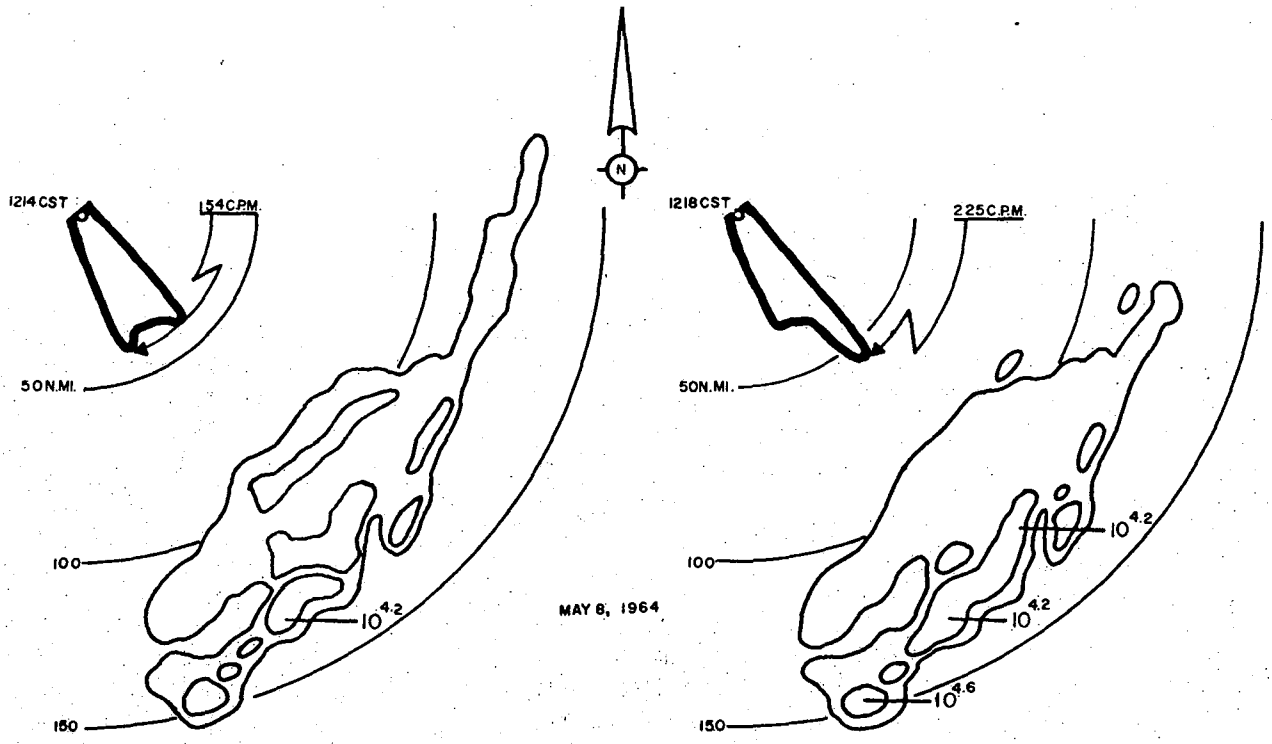

Figure 11

May 9, 1964

A very severe storm (fig. 12) located at 250° and a range of 100 n. mi. at 1800 CST, later caused the disintegration of an Air Force C-124 aircraft at about 1903 CST [3]. Maximum sferics were indicated to be about 20° clockwise of the most severe storm, but a significant increase was shown in the sector involved prior to 1900 CST.

Sector 47: (Az. 258°)	Time (CST)	Sferics (cpm)	Radar "Z"
	1821	100	$10^{5.2}$
	1845	220	$10^{5.6}$

Thus, the sferics count in this sector more than doubled in 24 min.

In another sector 45° clockwise, or 50 mi. northeast of the major storm, there was another area where sferics increased greatly:

Sector 55: (Az. 304°)	Time (CST)	Sferics (cpm)	Radar "Z"
	1754	150	$10^{4.6}$
	1817	320	$10^{4.6}$

A 23-min. increase of 170 cpm, or +110 per cent. However, no severe wind or hail was reported from this sector.

For the next 2 hr., the storm continued very severe, and sferics ranged from 300 to 500 cpm with good indications of direction.

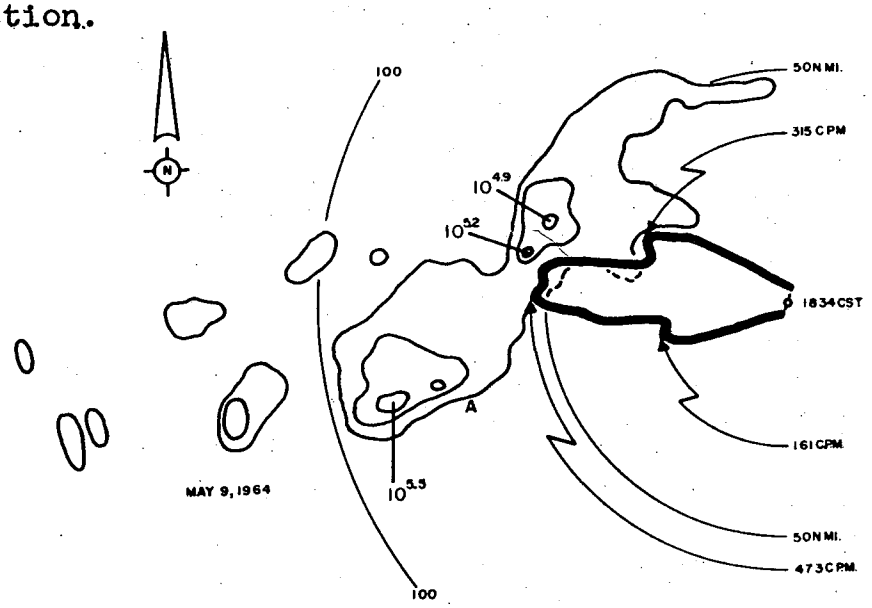

Figure 12

May 10, 1964

There were two periods of sferics and weather activity on this day, one maximum at mid-morning (fig. 13) and the other in the late afternoon (fig. 14). SPARSA response during the morning was very strong, reaching a normalized rate of 600 cpm shortly after 1000 CST. At this time, the storm arc was 50 to 75 n. mi. distant. Since sferics increased as the storm moved toward the receiving site, the normalized count rate showed great increases, as much as 140 per cent within 30 min. This morning period was characterized by heavy rain, but no severe weather was reported even though SPARSA response was twice the average value for severe events, and showed large changes.

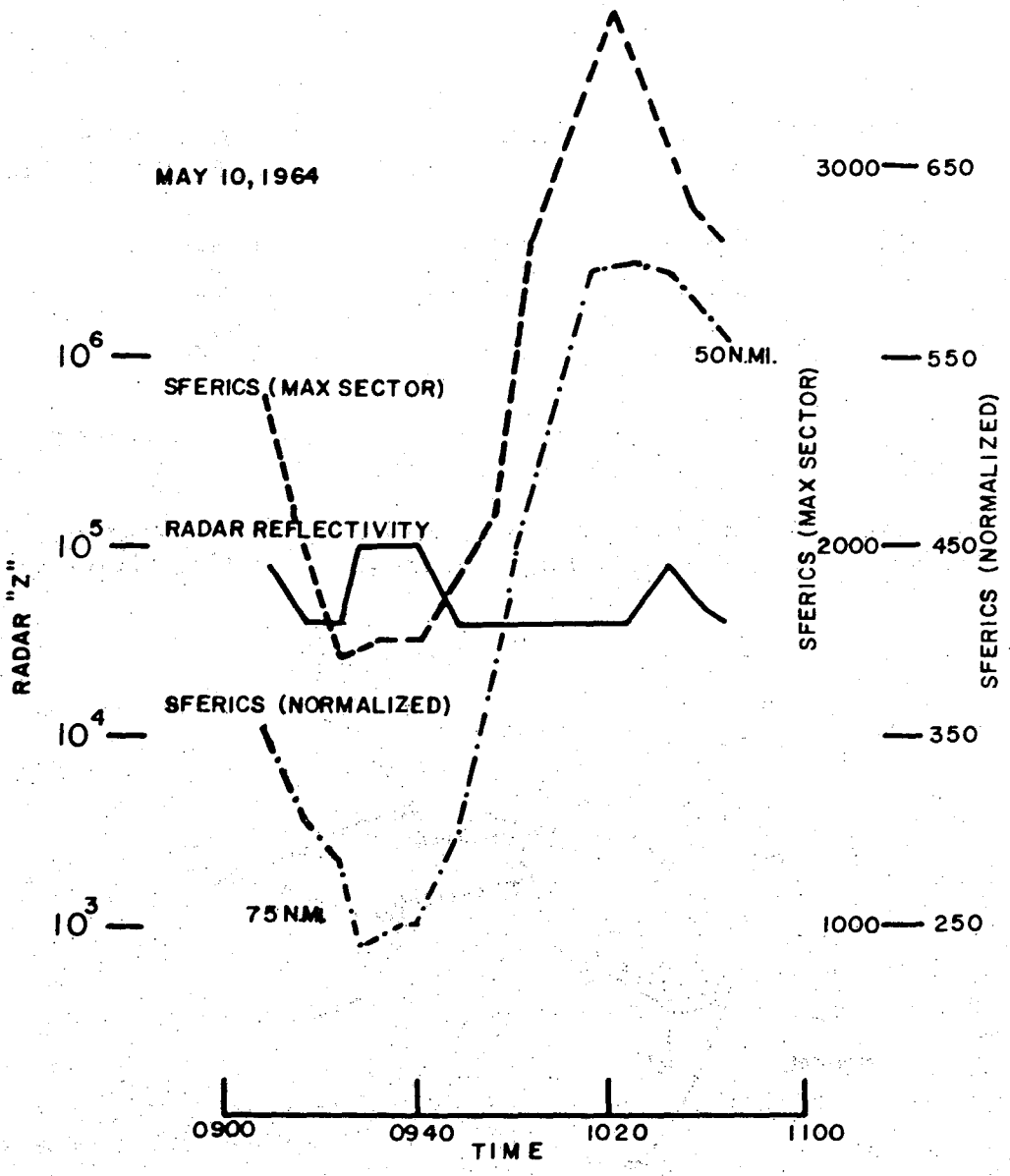

Figure 13

During the afternoon (fig. 14) there were many severe weather events reported and the radar reflectivity was as high as 10^6. Absolute sferics were less than for the morning period but after normalization attained very high values during the period of severe weather. In figure 14, the broken traces for normalized sferics indicate the passage of successive areas into the ground pattern of the radar; the great rate of increase is almost entirely due to the normalization procedure, whose applicability is, of course, subject to serious question.

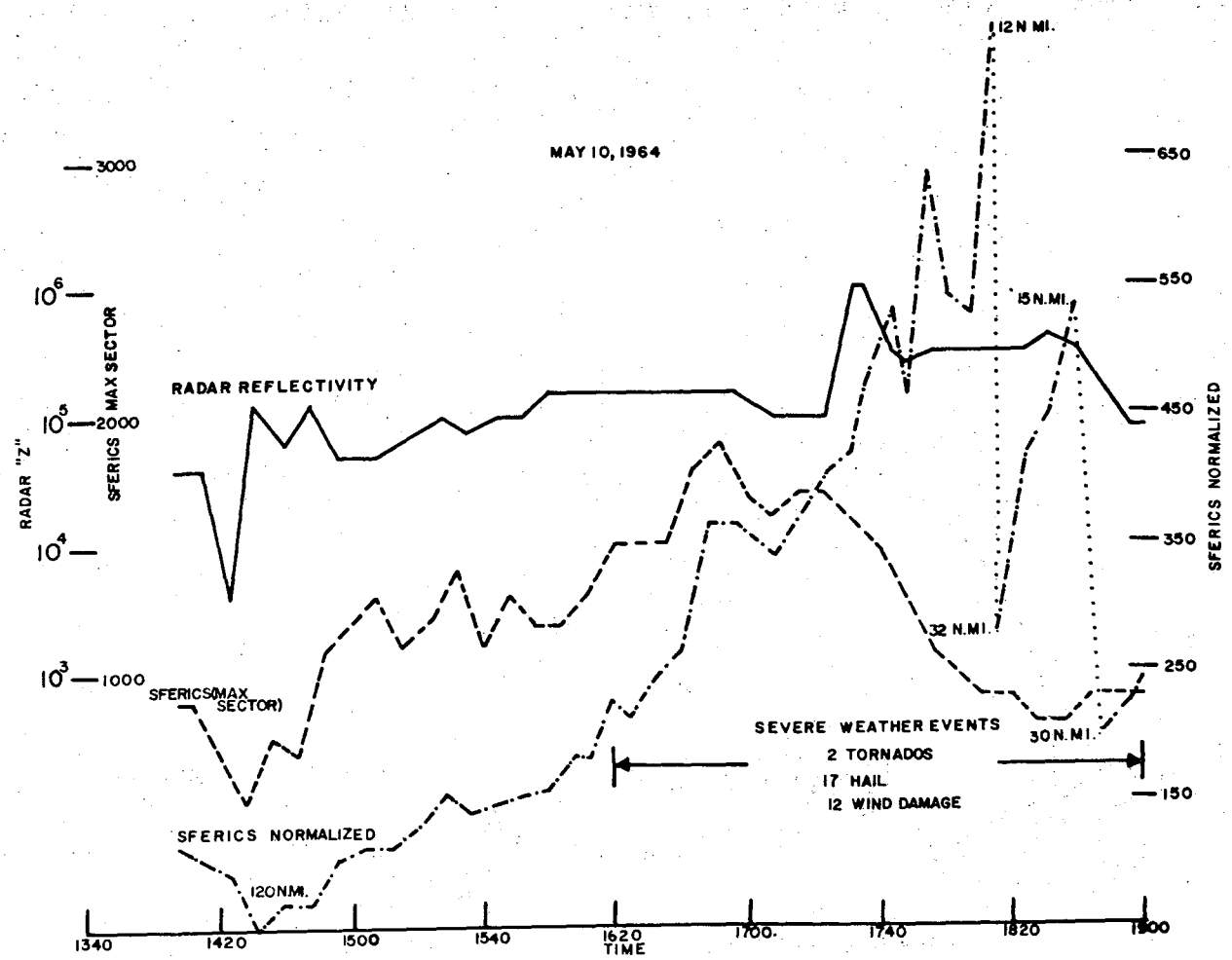

Figure 14

May 27, 1964

Two separate storms produced tornadoes around midday at ranges of 60 and 65 n. mi. They were accompanied by sferics of 16 and 50 cpm respectively, which compare with the average count rate for tornadoes of 261 cpm.

May 28, 1964

This was a day with an isolated thunderstorm area moving east-southeastward (fig. 15) with no severe weather reported although radar reflectivity reached $10^{5.2}$, and sferics 180 cpm. It is a typical example of the disagreement in direction frequently indicated between radar and sferics. In the figure, the broken line indicates the limits of the upper portion of the storm as seen by radar with the antenna elevated. It appears the sferics may be related to the areal coverage of the sferics sectors by the storm in three dimensions.

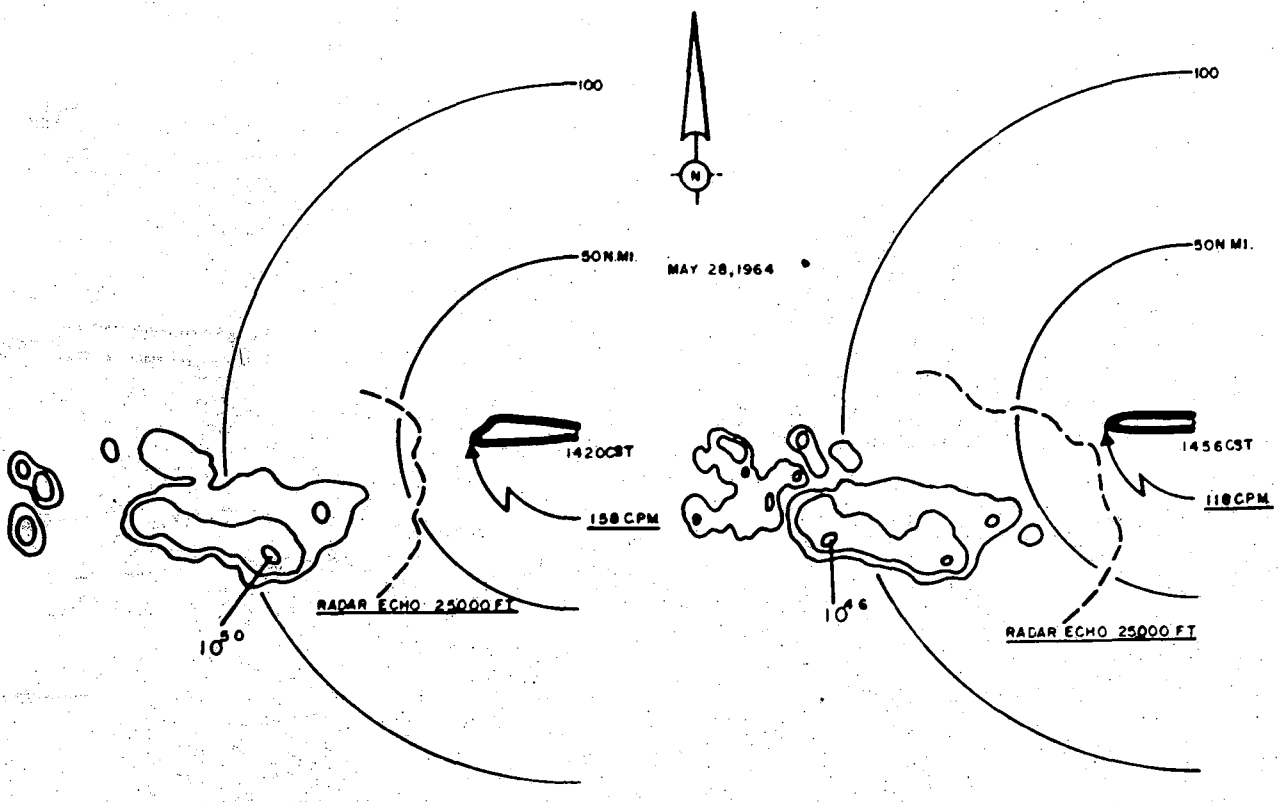

Figure 15

May 29, 1964

The entire day was characterized by heavy cloud cover and extensive areas of thundershowers. During early morning hours the precipitation areas (fig. 16) were toward the south and accompanied by maximum reflectivity factors of $10^{4.6}$ and normalized sferics of 260 cpm at 0056 CST. At 0152 CST, sferics were at the rate of 280 cpm and radar echoes nearest Norman had decreased to $Z = 10^{3.8}$. Another period of high activity occurred shortly before noon in the west and southwest when reflectivity reached 10^{5} and sferics exceeded 200 cpm. There is no evidence of severe weather of any kind on this day, although reports were received from 16 special observers advising of rainfall amounts and related lightning.

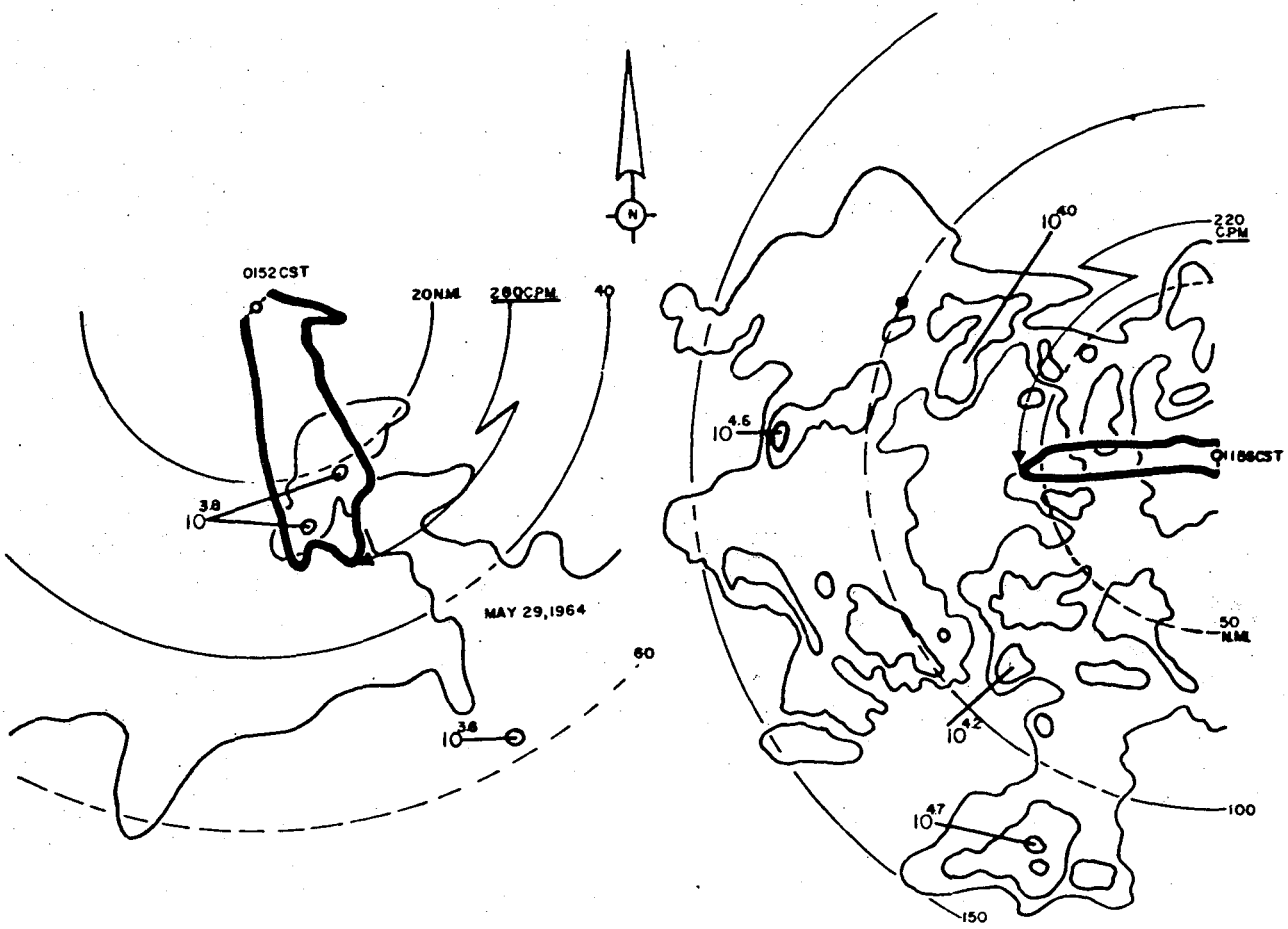

Figure 16

May 30, 1964

This was another day of heavy cloudiness and extensive thundershowers. Sferics were characteristically light throughout the day. During the morning, they were mostly in the 40 to 80 cpm range and correlated well with radar both in direction and intensity. About mid-afternoon a single storm became severe (fig. 17), produced large hail and damaging wind, and the radar reflectivity factor reached $10^{5.8}$. The reflectivity factor had increased to 10^{5} in the storm about 40 min. before sferics were detected in that direction (fig. 18). Sferics began occurring about 10 min. before the first hail was reported. At the time heavy hail of 1-1/4 in. diameter was falling, sferics had increased to 80 cpm, and later reached a maximum of 120 cpm, about 1/3 the average for hail.

The sferics indication toward the west is probably not due to weather phenomena, since it persisted for several hours with little change.

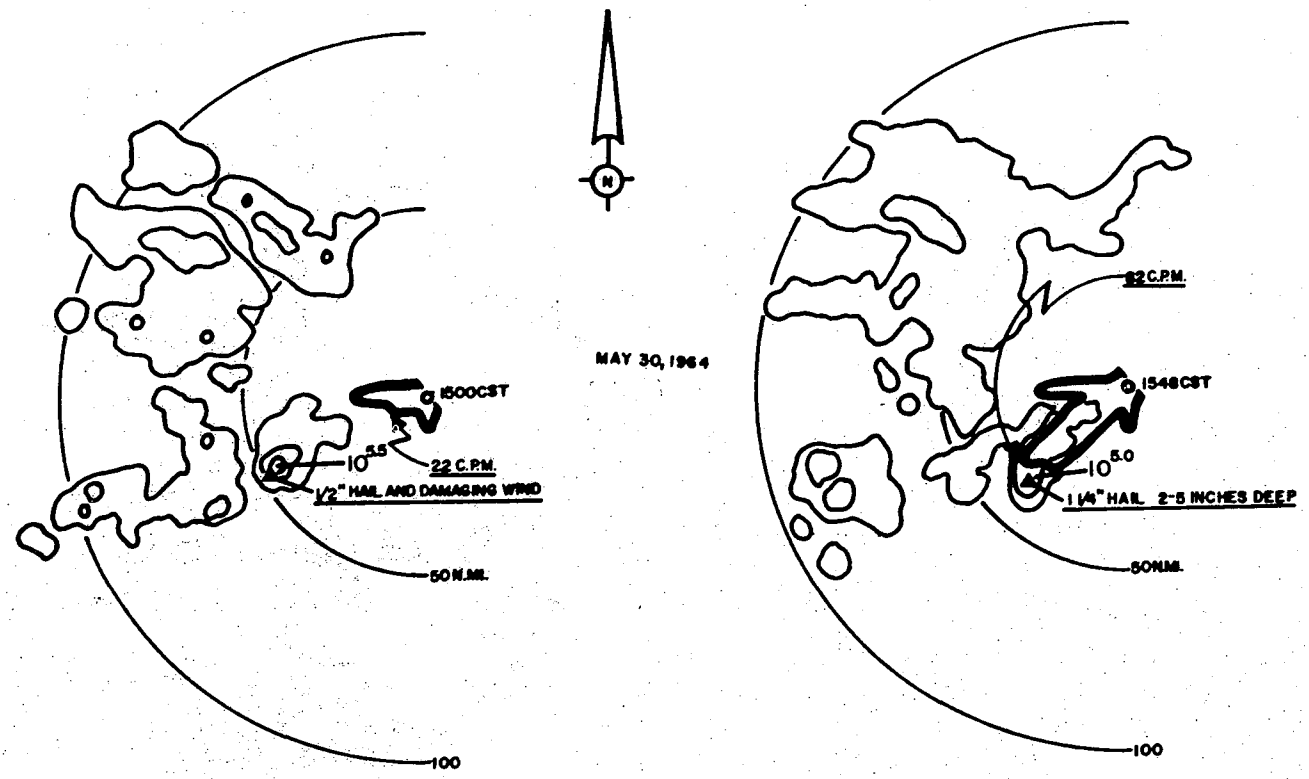

Figure 17

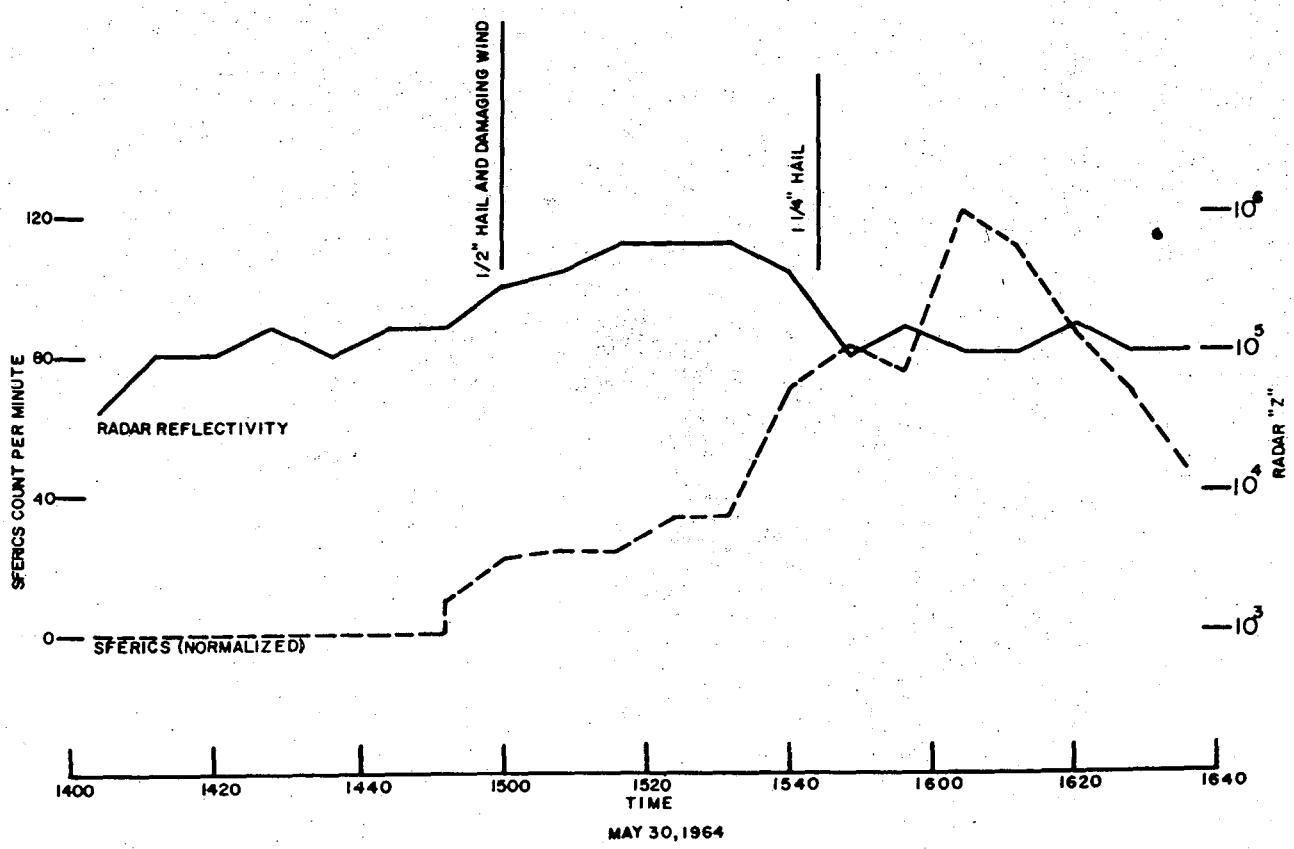

Figure 18

June 4, 1964

A developing storm at a range of 100 n. mi. was producing sferics at the rate of 50 cpm when the related radar echo reflectivity was $10^{3.2}$. During the next 25 min. the radar reflectivity increased to $10^{5.3}$ and a tornado with hail was reported. During the same period, sferics decreased to 30 cpm at 1545 CST. A second tornado was reported at 1630 CST with sferics of 25 cpm.

Later, at 1740 CST, a strong thunderstorm at 300° and only 40 n. mi. distant developed to a maximum reflectivity factor of $10^{5.6}$ (fig. 19). This storm produced hail 3/4 in. in diameter. Sferics were very weak and almost completely masked by indications from other storm areas. The observer, in reporting the hail, added the remark that the storm was accompanied by "very little lightning."

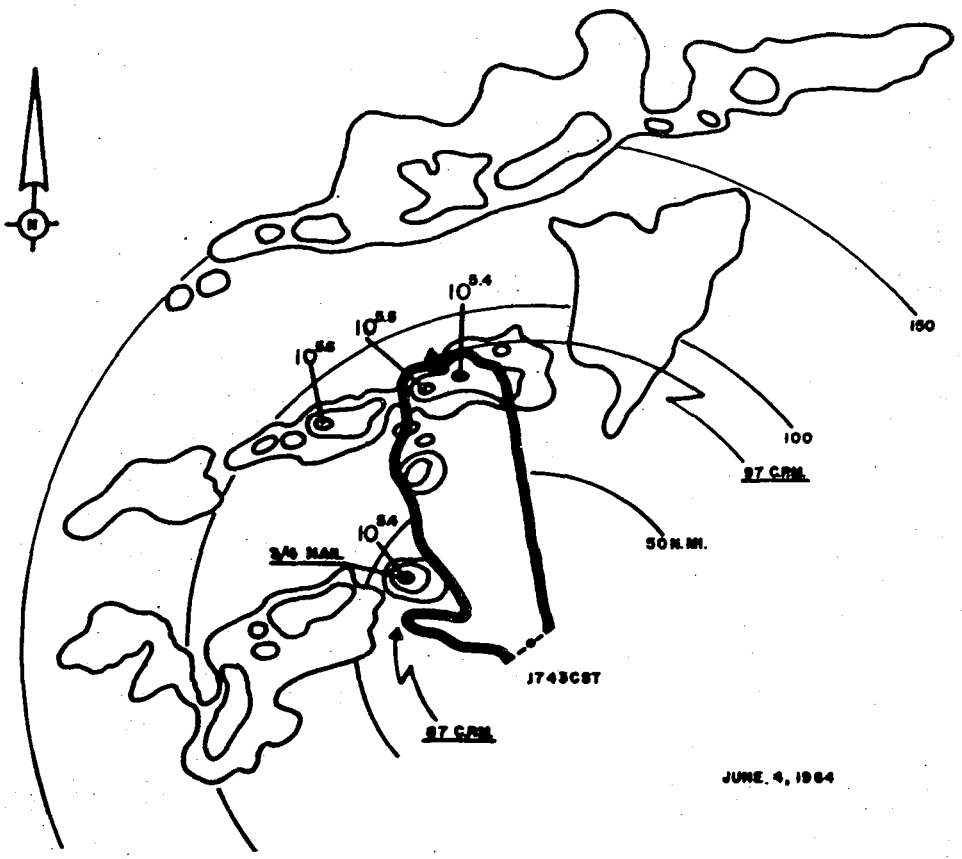

June 10-11, 1964

Moderate to heavy thunderstorms developed at a range of 170 to 200 n. mi. to the west and northwest during the early afternoon and continued, moving northeastward. No severe weather was reported but radar reflectivity approached 10^5 and normalized sferics reached 170 cpm (unnormalized count 3000). Direction indications of SPARSA were good and storm movement was well followed. A second line began developing around 2000 CST about 100 n. mi. west of the first. As the first line moved to the northeast, significant sferics continued in the direction of 355°, between the two echo lines in figure 20. This figure shows the outline of all echoes detectable from the Norman radar in solid lines, including a search with antenna elevated . The broken lines indicate the boundaries of radar information as obtained by other stations of the radar network. No conclusive explanation of the sferics in the sector shown (No. 64) can be offered although it seems possible that phenomena of night-time propagation and downwind advection of sferics centers may have played a role. There was no indication of radiations from other than meteorological sources.

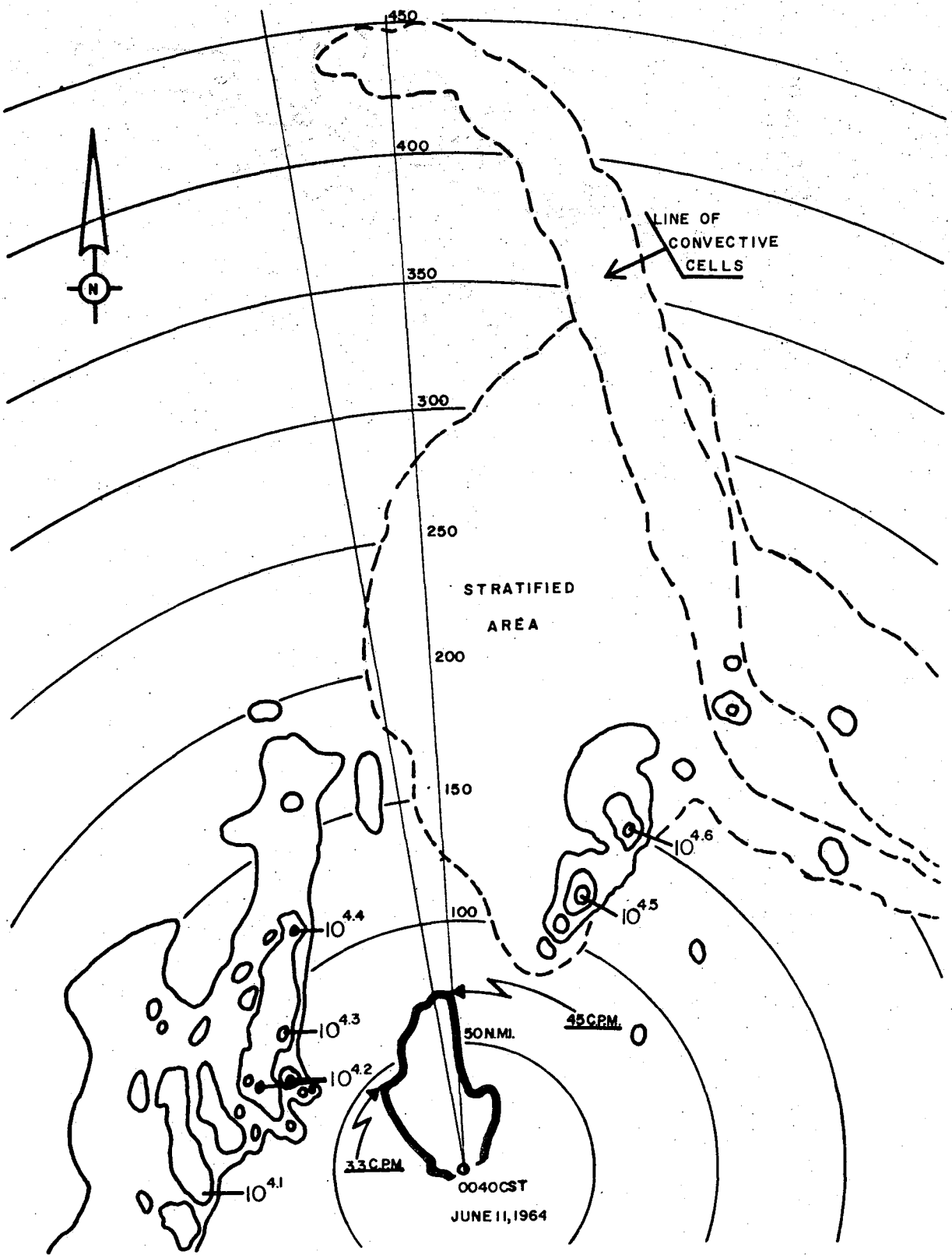
450
400
350
300
250
200
150
100
N
LINE OF
CONVECTIVE
CELLS
STRATIFIED
AREA
$10^{4.6}$
$10^{4.5}$
$10^{4.4}$
$10^{4.3}$
$10^{4.2}$
$10^{4.1}$
50 N.MI.
45 C.P.M.
33 C.P.M.
0040 CST
JUNE 11, 1964

Figure 20

6. SUMMARY AND CONCLUSIONS

SPARSA response to damaging wind and hail events is variable. Although SPARSA shows little or no response when thunderstorms are absent, prominent response may or may not occur when such severe storms are present. Similarly, count rate trends are not sufficiently regular to provide reliable bases for operational short-period prediction of the onset of severe wind and hail events, or for discrimination of such severe events when they occur within a larger family. Similarly, the data of this study indicate that SPARSA does not discriminate appreciably between situations posing hazards of turbulence and hail to aircraft flight and those associated with lightning alone.

A significant characteristic of hailstorms may be increasing sferics activity and SPARSA count rate during the storms' developing phases. However, additional study of this is required.

The development of strong radar echo intensities typically parallels the development of other storm manifestations. Because range discrimination is an inherent radar feature, and the range dependence of radar weather echoes is comparatively well understood, radar is much to be preferred for identification and short range prediction of severe events. On the other hand, SPARSA shows a parameter of the azimuthal distribution of electrical activity, concerning which the ordinary radar indicates very little.

Since the data examined here is inadequate to establish all the above findings with high reliability, it is plausible that a future study would lead to somewhat different conclusions.

This study, as an evaluation, was premature. Above all, it demonstrates the need for a fundamental approach to sferics-radar-weather relationships, employing carefully sited equipment whose operation is clearly understood, and appropriate considerations of radiation theory and atmospheric effects on propagation. The variability of electrical activity with respect to the other manifestations of severe storms constitutes a compelling reason for vigorous efforts in this subject area.

REFERENCES

1. Miller, J. and D. A. Kohl, "Further Study of the Relationship between 500 kc Sferics and Severe Storms," Proposal 2103 from Applied Science Division, Litton Industries, to U. S. Weather Bureau, 1963, 12 pp.

2. Kohl, D. A. and J. E. Miller, "500 kc/sec. Sferics Analysis of Severe Weather Events," Monthly Weather Review, vol. 91, No. 5, May 1963, pp. 207-214.

3. Anonymous, 1964. "Thunderstorms Equal Tragedy," MATS Flyer, vol. 11, No. 10, pp. 9-12.

LOCATING AND TRACKING AREAS OF LIGHTNING

Gilbert D. Kinzer, Byron B. Phillips, and William E. Cobb[1]

ABSTRACT

The amplitudes of component frequencies greater than 10 kilocycles per second in the Fourier spectral representation of electric signals from lightning are inversely proportional to range beyond about 25 n. mi. On this basis, a system for locating effective positions of lightning flashes from measurements at two or more receiving stations is being developed to operate over a range extending from 40 to 200 n. mi.

1. SOME REASONS WHY IT IS DESIRABLE TO LOCATE AND TRACK AREAS OF LIGHTNING

A successful search for associations between electrical effects and such features as precipitation and air motions promises a new insight into the physical processes of thunderstorms. Lightning is an attractive effect to choose for such a search because it is prominent and it terminates in charge accumulation centers about which additional knowledge may be obtained. Precipitation patterns are attractive features to examine because of the possibility that precipitation and electrification are somehow related. The ideal search would be made in space, but a preliminary search in the projection of space upon the earth's surface is worthwhile. Areas of lightning can be found by measuring the horizontal range and azimuth of lightning strokes. Radar can simultaneously furnish maps of rainfall areas. The search will be for elements of association between these two sets of areas.

The Civil Aeronautics Board recently announced that the probable cause of the crash of a passenger-carrying airplane on December 8, 1963, was the ignition, probably by lightning, of a mixture of fuel vapor and air inside a wing tank. As a result of this accident, airline operators and the Federal Aviation Agency are asking if lightning areas can be recognized in the thunderstorm displays furnished by radar. The answer may possibly be provided by the search for association between areas of lightning and areas of precipitation as outlined above.

---

[1]When this note was written, authors were associated with the Physical Sciences Laboratory, USWB. Dr.Kinzer's present affiliation is with NSSL, and Messrs. Phillips and Cobb are associated with the Atmospheric Physics and Chemistry Laboratory.

Electronic switching and control systems, particularly those having digital operation, are increasingly used in aircraft and spacecraft and are components of a growing number of electronic applications elsewhere. The electromagnetic signals generated by nearby lightning often penetrate ordinary shielding and, being similar to normal control pulses, induce malfunctions. Those who must depend upon error-free operation of electronic switching and control systems are concerned and would like to have instruments that will locate and track areas of lightning and provide a warning if the areas move toward specific installations or positions.

2. DEFINITION OF AREAS OF LIGHTNING

The position given by a measurement of range and azimuth of a source of electromagnetic signals is related to the dimensions and orientation of the source. These vary widely and blur the meaning of position when the source is lightning. Still, areas outlined by plotting such positions must represent definite zones of lightning activity. The limited number of cases examined thus far indicate that areas outlined by a 10-min. accumulation of such positions define a useful concept of a lightning area whose movement can be followed by updating the accumulation every 5 min.

Areas defined this way were determined every half hour during storms that occurred south of Norman, Okla. on May 22, 1964. Sample radar photographs of the storms are shown in figure 1, and the lightning areas in relation to the radar echoes are shown in figures 2 to 5. The measuring instruments were located at the sites marked Griffith and Baker. The azimuth was measured at Baker and magnetic signal strengths observed at both sites were combined with their positions to obtain the range from Baker by assuming that the signal strength varies inversely with the distance from the source.

3. INTERPRETATIONS OF LIGHTNING SIGNALS

A formal treatment of the signals produced by lightning may be developed in several ways. One that is easily visualized begins by considering the effect of the earth, assuming the latter to be a perfect semi-infinite conductor having a plane surface. The effect is accounted for by assuming that every electric charge in the air above is accompanied by a mirror image of opposite polarity below the earth's surface. The charge and its image form a vertical dipole, as illustrated

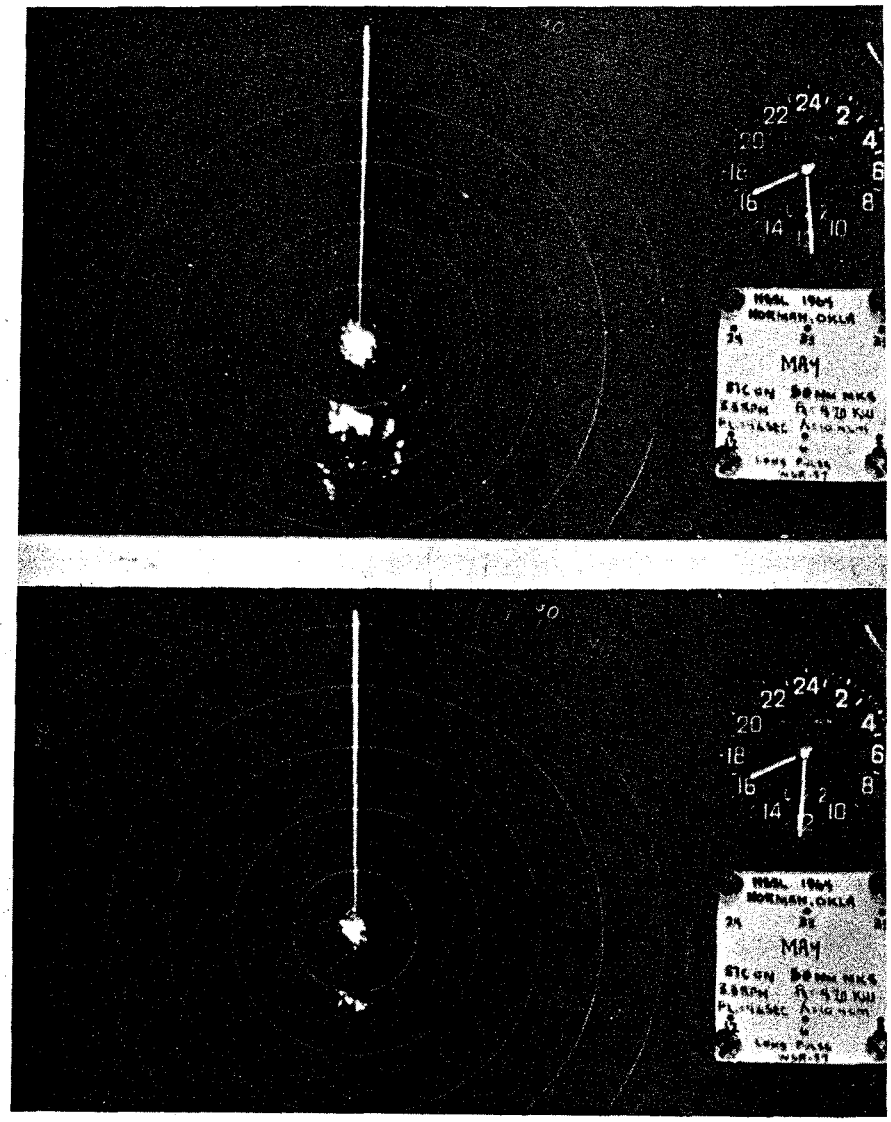

Figure 1. - PPI photographs, WSR-57 radar at Norman, Okla., May 22, 1964, 1630 CST. The upper photograph was made with the receiver gain at maximum, the lower with gain reduced 24 db. Range marks are at intervals of 50 n. mi.

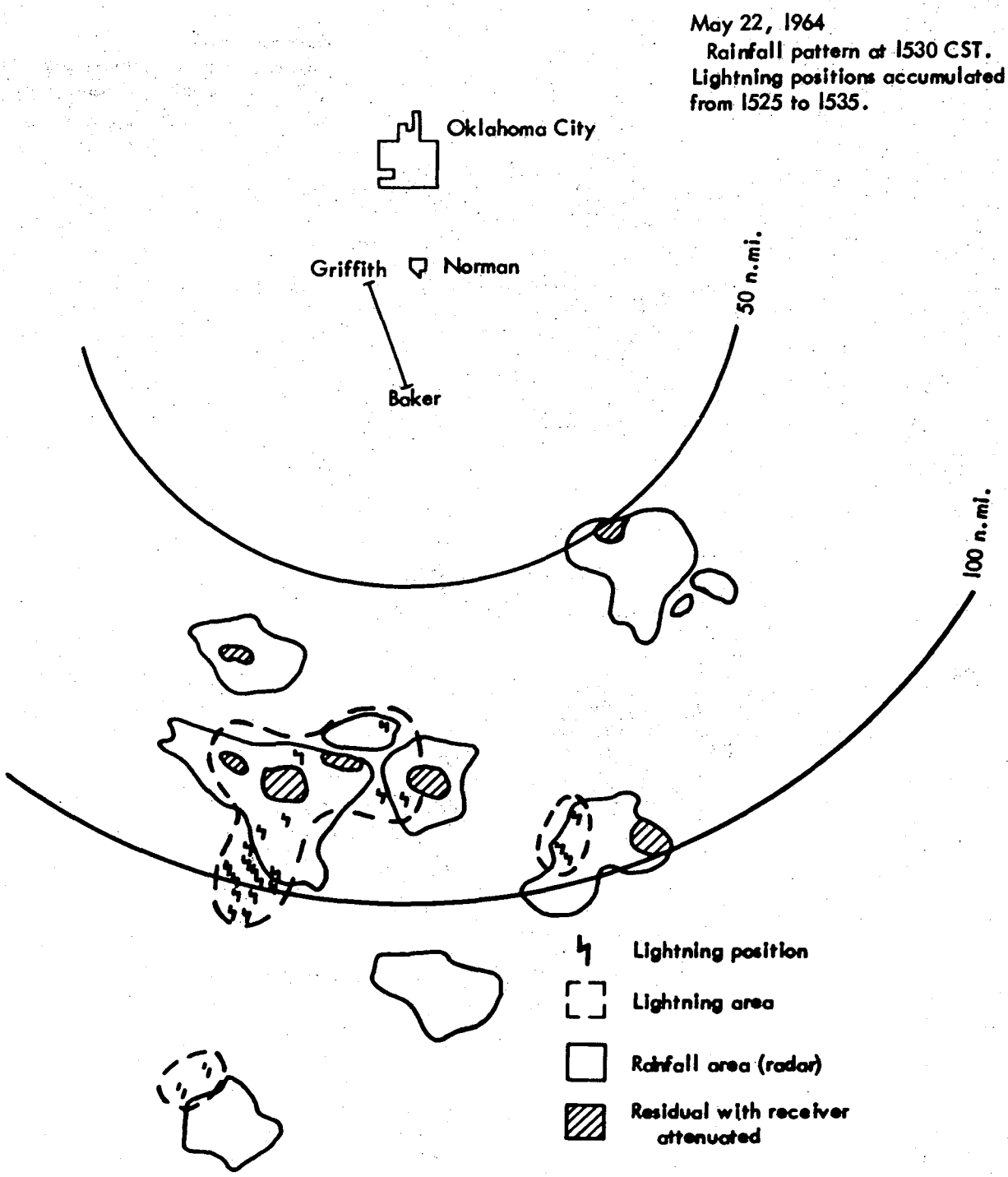

Figure 2. - Superimposed areas of lightning and rainfall; the shaded areas are residuals when the gain of the radar receiver is reduced 24 db. Time of radar echoes is 1530 CST on May 22, 1964; lightning positions are accumulated from 1525 to 1535 CST.

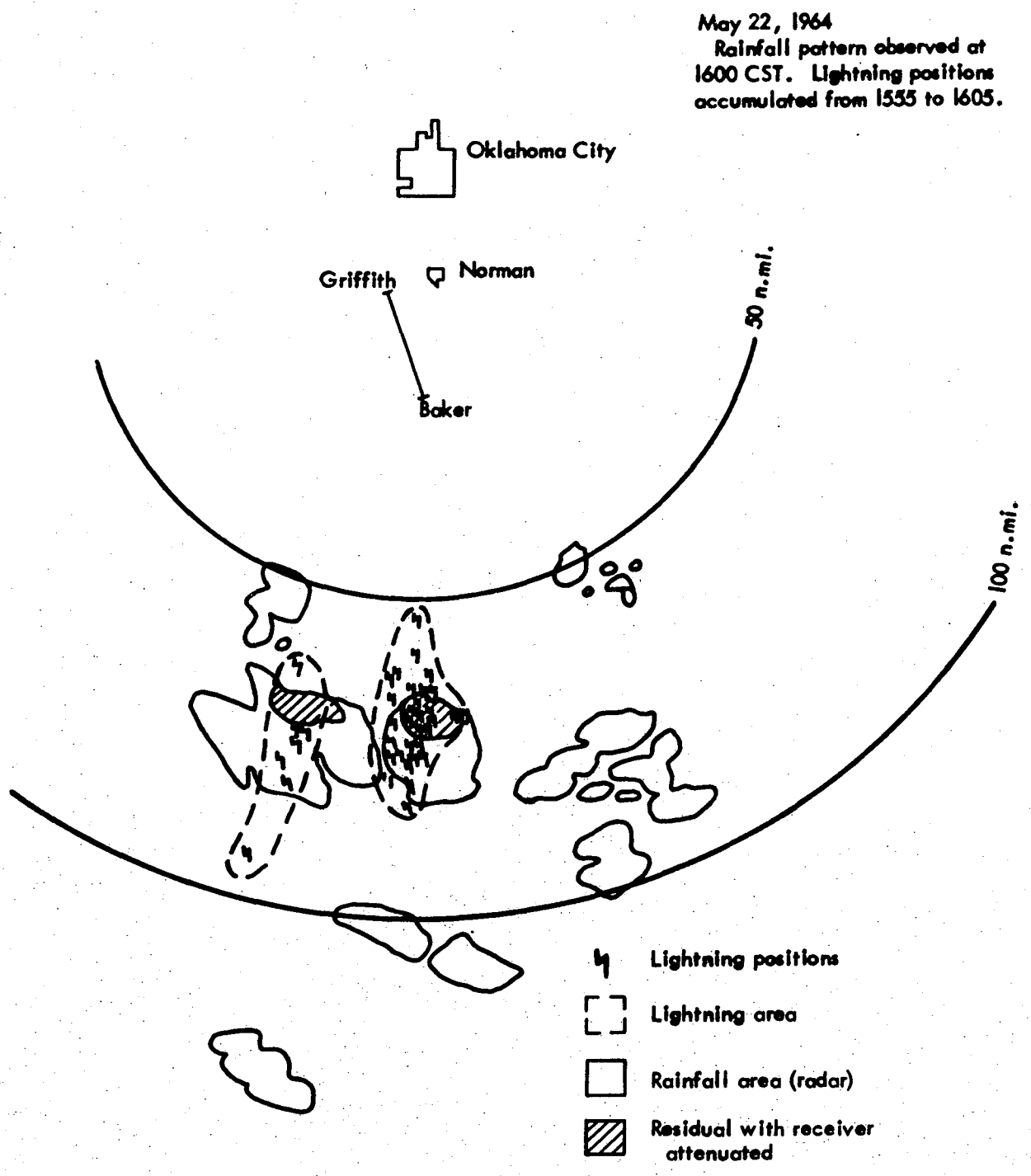

Figure 3. - Similar to figure 2. Time of radar echoes is 1600 CST and lightning positions are accumulated from 1555 to 1605 CST.

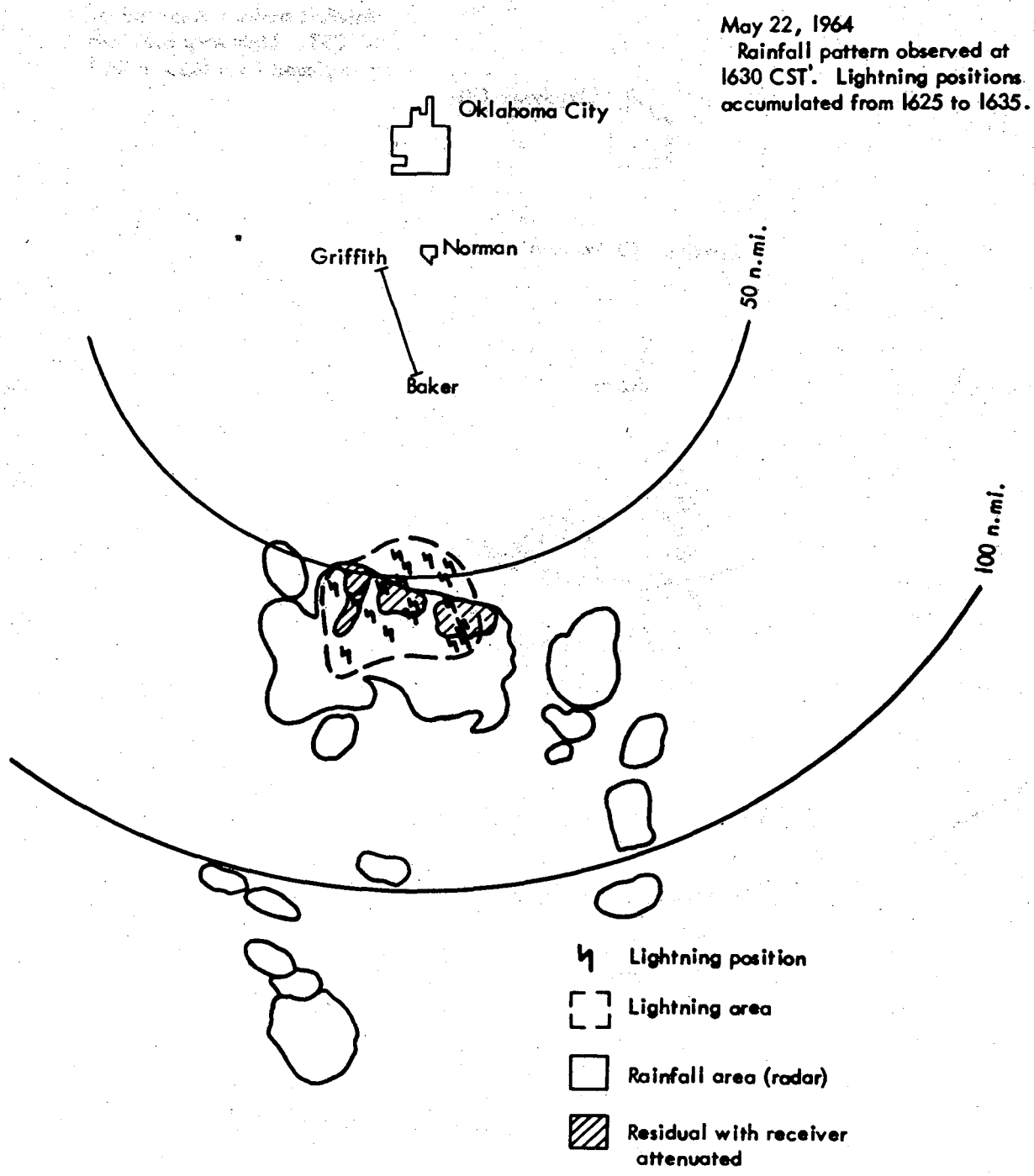

Figure 4. - Similar to figure 2. Time of radar echoes is 1630 CST and lightning positions are accumulated from 1625 to 1635 CST.

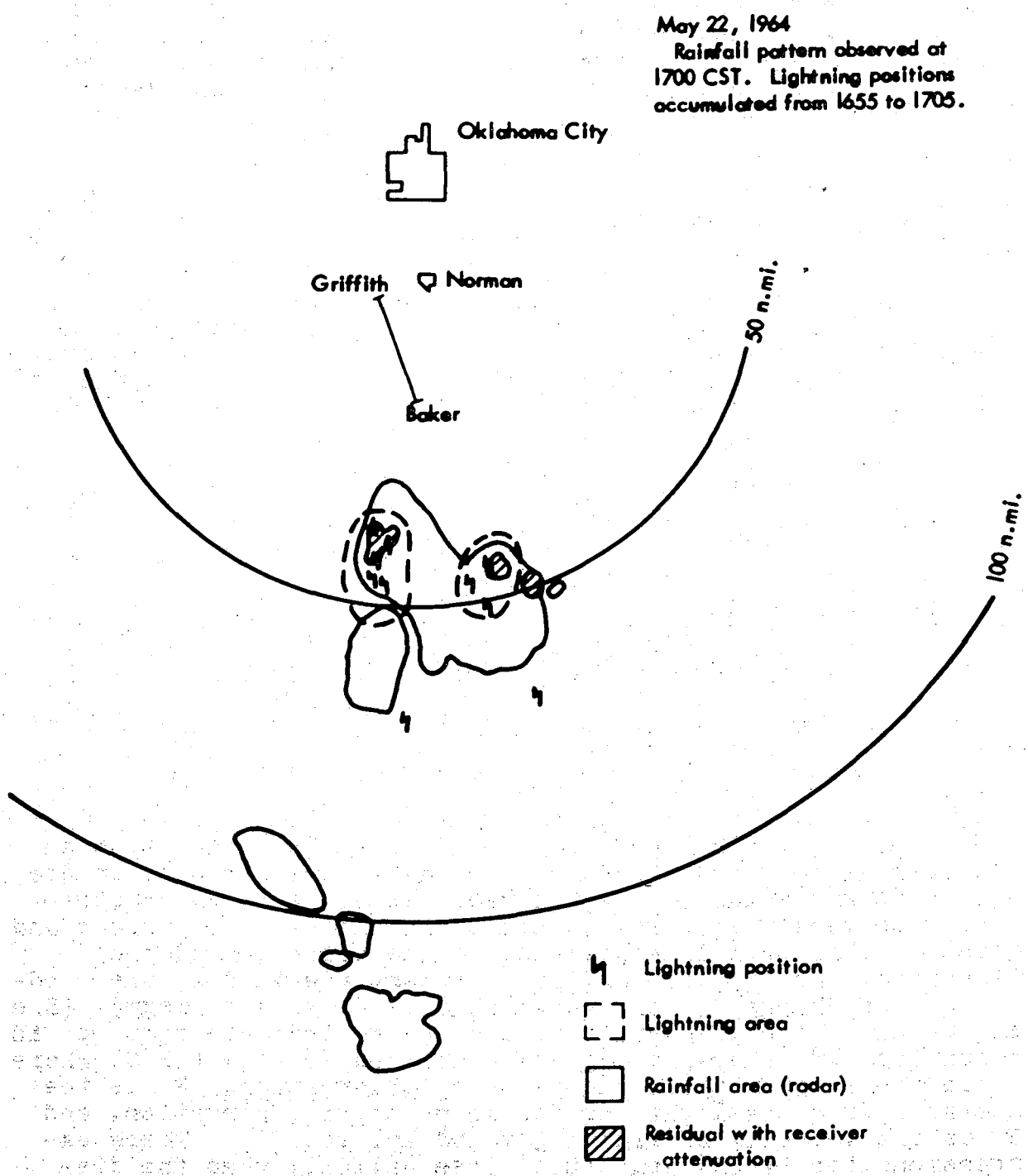

Figure 5. - Similar to figure 2. Time of radar echoes is 1700 CST and lightning positions are accumulated from 1655 to 1705 CST.

in figure 6a. An accumulation of space charge represents a cluster of dipoles whose composite may be regarded as a single dipole when observed from a distance that is large compared to the average separation of charges and images. (See fig. 6b.) Distant lightning, in effect, erases dipoles of this kind.

Lightning between the earth and a cloud removes dipoles having common polarities but intercloud and intracloud lightning removes dipoles of opposing polarities, as shown in fig. 6c.

The signals generated at the earth's surface by distant lightning (neglecting sky reflections) are equivalent to the resultant obtained by superimposing the separate signals produced by the erasure of the separate dipoles. Each dipole erasure will produce a signal having the form [1], [2], [3]:

$$E(t,R) = \frac{[p]}{R^3} + \frac{1}{CR^2}\frac{d[p]}{dt} + \frac{1}{C^2R}\frac{d^2[p]}{dt^2} \qquad (1)$$

and

$$H(t,R) = \frac{1}{CR^2}\frac{d[p]}{dt} + \frac{1}{C^2R}\frac{d^2[p]}{dt^2} \qquad (2)$$

where $E(t,R)$ is the magnitude of the electric signal with a representative vector that is vertical at the earth's surface, $H(t,R)$ is the magnitude of the magnetic signal with a representative vector that is horizontal at the earth's surface and perpendicular to a line pointing in the direction of the lightning, and $[p]$ is the dipole moment (defined as the product of the charge q and the distance h to its image). (See figure 6a.) The brackets surrounding p indicate that p is a function of delayed time, t^*, defined as $t^* = t - R/C$, where t is the local time at the point of observation, R is the distance from the lightning to the point of observation, and C is the velocity of light (3×10^5 km. sec.$^{-1}$). These expressions for $E(t,R)$ and $H(t,R)$ lose validity when the distance R is so small that the ratio of R to $(R^2 + h^2/4)^{1/2}$ differs appreciably from unity. This ratio is about 0.925 when charge centers are at altitudes of 10 n. mi. and the distance R is 25 n. mi.

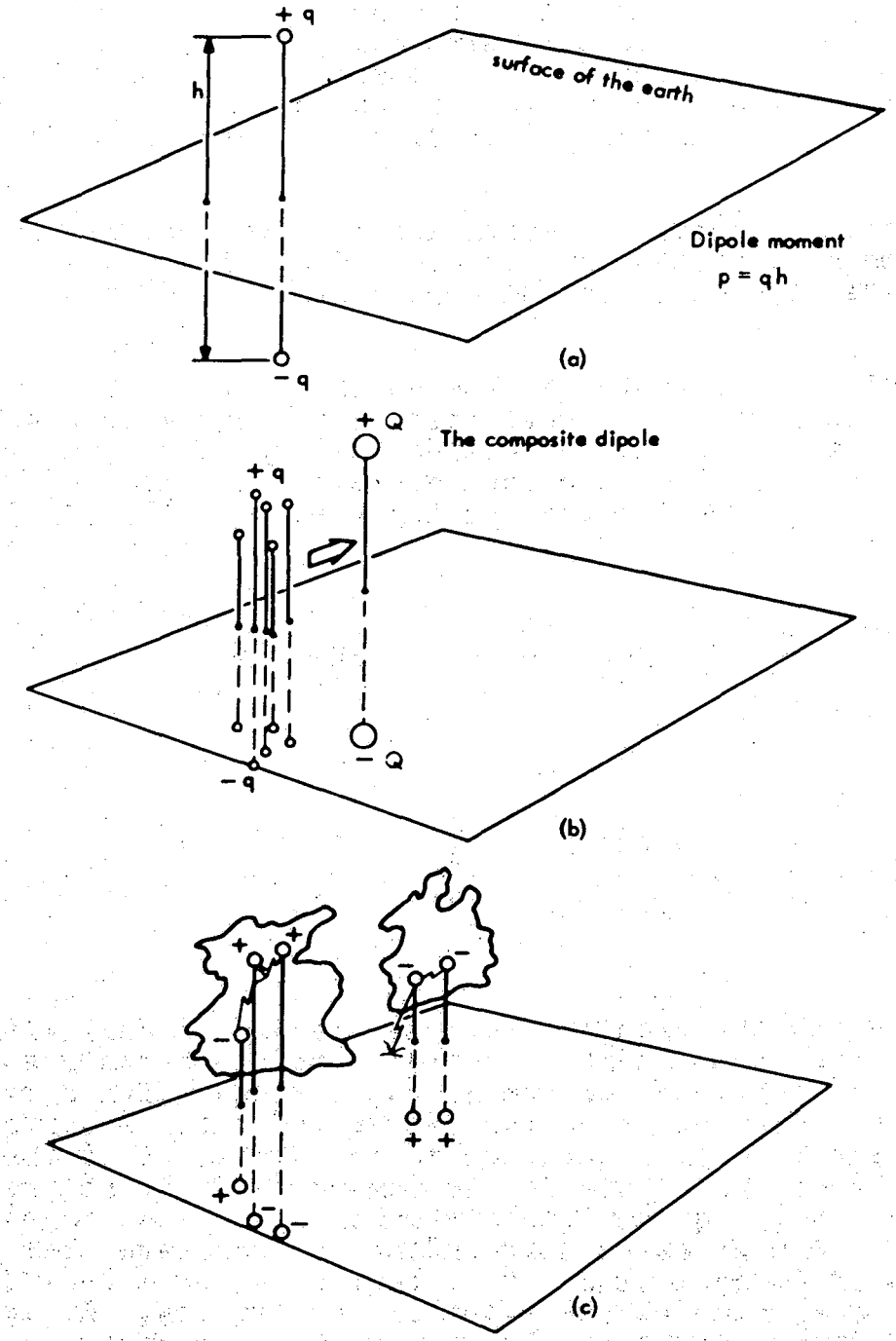

Figure 6. - Dipole representations of electrical charges in thunderstorms; (a) a vertical dipole of moment p = qh, equivalent in its effect to the charge in space and the induced charge on the surface of the earth; (b) a composite dipole replacing an accumulation of individual dipoles; (c) typical dipole patterns existing just prior to their erasure by lightning.

The decrease in the strength of lightning signals with increasing distance from the flash is the same as that given by equations (1) and (2) for dipole signals. This is because the time variations of linear combinations of distant dipoles produce the same effects as distant lightning. The last term on the right side of both equations dominates the other terms by at least one order of magnitude when the Fourier transform of the lightning signal (the spectral density of the pulse) is small at frequencies below 10 kc. sec.$^{-1}$ and the distance R is greater than about 50 km. or 25 n. mi. This domination under these conditions implies that the signal strength varies inversely with the distance from the flash. The observed amplitudes of lightning signals depend upon time in a widely varying and unpredictable manner, and their Fourier transforms have not been adequately surveyed. Further study and field experience are needed in order to establish the minimum range for which the inverse first power of the distance determines signal strength. The fair agreement between areas of lightning and areas of rainfall found in the 1964 measurements does suggest, however, that this minimum distance may be less than 25 n. mi.

4. MEASUREMENTS AND TESTS PLANNED FOR APRIL AND MAY 1965

The work on locating and following areas of lightning has been exploratory thus far. Improved instrumental calibrations, an attempt to use the electric rather than the magnetic signal strength for determining range and azimuth, and a shift from photographic to magnetic tape data recording are planned in the forthcoming work at the National Severe Storms Laboratory.

Extensive field tests will be conducted during the first two weeks to establish the minimum distance from lightning at which the signal strength begins to diminish inversely with the first power of the distance.

A limited amount of data processing is to be carried on concurrently with the measurements in order to check the performance of the instruments.

REFERENCES

1. J. D. Jackson, Classical Electrodynamics, John Wiley & Sons, New York, 1962, pp. 268-272.

2. J. A. Stratton, Electromagnetic Theory, McGraw-Hill, New York, 1941, pp. 434-437.

3. W. L. Taylor, "Lightning Characteristics as Derived from Sferics," in Problems of Atmospheric and Space Electricity, S.C. Coroniti, Ed., Elsevier Publishing Co., 1965, pp. 388-404.

NSSL RADAR-HYDROLOGY PROGRAM

Jack L. Teague

ABSTRACT

Radar observations on four days with intense convective rains have been compared with the data of 175 recording rain gages spread over an 1100 mi² area within 55 n.mi. of the radar.

Use of the relationship $Z = 200R^{1.6}$ to estimate the radar echoes' rainfall equivalent produces a substantial overestimate of the mean areal rainfall in one case, a substantial underestimate in another, and fair correspondence in two. The differences may be due to variations in the Z-R relationship, to an unmonitored variability in radar performance, and to other factors. It seems likely that applications of radar data to operational hydrology will require use of some rain gage data to calibrate the radar.

It is concluded tentatively that rainfall rates on the WSR-57 radome of 1 in./hr. do not measurably attenuate the radar signal.

1. INTRODUCTION

Radar gives great promise as a means for measuring precipitation but properties of precipitation echoes have not been adequately investigated. Coordinated observations of rainfall by rain gages and radar are necessary, and large amounts of data must be processed by high-speed computers to assess the feasibility of using radar to provide accurate rainfall data for flood forecasting, water resources management, and studies of the water budget of precipitating weather systems.

The radar-hydrology analysis program at the National Severe Storms Laboratory (NSSL) began in 1964. During spring and summer, rain gage and radar data were collected and processing techniques were developed.

The empirical relation between the radar reflectivity factor Z and precipitation rate R has been studied by many with all investigators reporting equations of the form $Z = aR^b$, where a and b are constants. Some of the a's and b's have been listed by Battan ([1] Table 7.]). Battan suggests that a different relationship be used for different rain types and different geographical locations. This is supported in a paper by Atlas and Chmela [2]. Wilson [3] notes that values of a and b are often stable within storms, but that significant variations occur from storm to storm.

2. 1964 DATA SOURCES AND PROCESSING

A. Hydrologic Data

Four sources of rainfall data are routinely available for the NSSL hydrology program:

1. USWB stick gage (8-in. nonrecording gage) network for climatology;
2. USWB recording gage network for regular synoptic reporting;
3. NSSL mesonetwork (see p.131 in this report);
4. Agricultural Research Service (ARS) network.

These networks comprise a total of 494 rain gages within a radar range of 100 n.mi. Table 1 summarizes the characteristics of the data. Only the last two sources are immediately useful to NSSL. The ARS maintain, within 55 n.mi. of NSSL, a network of 175 rain gages located over an area of 1100 $mi.^2$ as shown in figure 2 of Sanders' paper on p. 134. The rain gage spacing is approximately the same as the radar grid used for digitizing, 2.5 mi. on a side.

The 1964 rain gage data from the Agricultural Research Service network were entered on IBM punch cards by ARS personnel using a Benson-Lehner chart reader. A card is punched at each change of slope of the trace showing accumulated rainfall, so that all apparent fluctuations of rainfall rate are recorded.

Table 1. - Rainfall Data Summary

Source	Reporting System	Approx. No. of Stations	Time Resolution	No. of Sq. Miles per Gage	Format of Data as Received	Delay in Receipt of Data
1. USWB	Climatological Data	220	Daily	140	Publication	6 months
2. USWB	Climatological Data	50	Hourly	600	Publication	6 months
3. NSSL	Original Gage Charts	50	± 1 minute	150	Original Gage Charts	Few days
4. ARS	IBM Punch Cards	175	± 1 minute	6	IBM Punch Cards	Few days

A 1620 computer program written by ARS has been used to process the rainfall data cards. This program lists the intensities and time interval between readings as shown in figure 1. It also computes rainfall amount and average intensities in successive 15-min. and 60-min. periods. Considerable control of quality is afforded by isochrone analysis and examination of rainfall totals in the first computer tabulations. After such checks, the corrected rainfall data are processed by computer a second time.

The same procedure used for reducing the ARS data has been applied to the NSSL rain gage data.

B. Radar Data

The radar data for this study have been collected by PPI photography and processed by the semi-automatic radar data assembly program discussed in detail in the paper starting on p.111. In most cases radar data sequences at 15-min. intervals have been semi-automatically digitized in squares 2.5 n.mi. on a side.

The basic computer product is the digitized display of the echo intensity distribution. A second computer program converts the echo intensity at each location to equivalent rainfall rates, using the equation:

$$Z = aR^b = \frac{\overline{Pr}}{Pt\ C}$$

or

$$R = \frac{\overline{Pr}}{Pt\ C\ a}^{1/b}$$

where $\overline{Pr}$ is the average range-normalized power received by the radar, C combines radar and refractive-index parameters, and a and b are semi-empirical constants which may vary from storm to storm. While $\overline{Pr}$, Pt and C are measured radar parameters, the values of a and b are somewhat dependent on unknown factors, and can be varied in the computer program. However, the values of a and b applied with the 1964 data are 200 and 1.6, respectively, corresponding to the use of many investigators.

This computer program multiplies precipitation rate equivalents of echo intensities by half the time interval from preceding to following observations. Thus, the instantaneous radar observations are usually extrapolated over 15 min. in this study. Computed rainfall totals are accumulated and the hourly and storm totals are categorized and printed as illustrated in figure 2. At locations where rain gage data are available, the precise computed totals are listed for comparison.

1	2	3	4	5	6	7	8	9	10
085	05	28	64	2300	0000.0	00.00	0000.0	00.00	00.000
085	05	28	64	2305	0005.0	00.04	0005.0	00.04	00.480
085	05	28	64	2316	0016.0	00.06	0011.0	00.02	00.109
086	05	28	64	2310	0000.0	00.00	0000.0	00.00	00.000
086	05	28	64	2315	0005.0	00.01	0005.0	00.01	00.120
086	05	28	64	2318	0008.0	00.05	0003.0	00.04	00.800
086	05	28	64	2324	0014.0	00.21	0006.0	00.16	01.600
086	05	28	64	2329	0019.0	00.22	0005.0	00.01	00.120
087	05	28	64	2310	0000.0	00.00	0000.0	00.00	00.000
087	05	28	64	2319	0009.0	00.06	0009.0	00.06	00.400
087	05	28	64	2323	0013.0	00.12	0004.0	00.06	00.900
087	05	28	64	2327	0017.0	00.19	0004.0	00.07	01.050
087	05	28	64	2332	0022.0	00.21	0005.0	00.02	00.240

Explanation of column numbers

1 - Rain gage number
2 - Month
3 - Day
4 - Year
5 - Greenwich Meridian Time
6 - Minutes since the first reading
7 - Gage reading in inches and hundredths
8 - Minutes since the previous reading
9 - Difference in gage from previous reading
10 - Average rainfall rate in inches/hour between readings

Figure 1. - Example of computer listing of rain gage data.

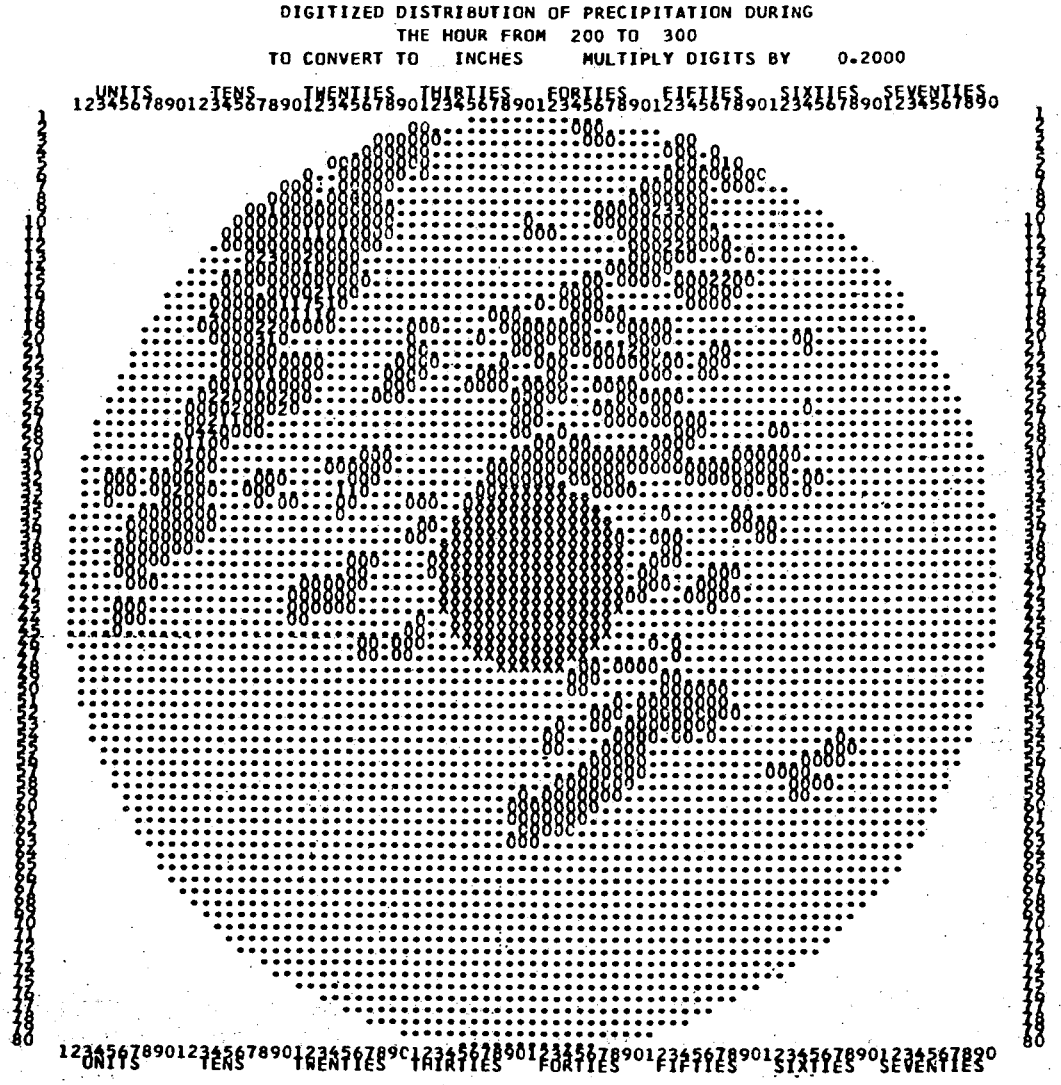

THE TIMES FOR SEQUENCE 7 ARE FROM 208 TO 208 MAXIMUM GAIN = A
THE TIMES FOR SEQUENCE 8 ARE FROM 218 TO 218 MAXIMUM GAIN = 9
THE TIMES FOR SEQUENCE 9 ARE FROM 227 TO 227 MAXIMUM GAIN = 8
THE TIMES FOR SEQUENCE 10 ARE FROM 232 TO 232 MAXIMUM GAIN = 8
THE TIMES FOR SEQUENCE 11 ARE FROM 249 TO 249 MAXIMUM GAIN = 8
THE TIMES FOR SEQUENCE 12 ARE FROM 258 TO 258 MAXIMUM GAIN = 7

PRECIPITATION TOTALS AT RAIN GAUGE
STATION DURING THE HOUR FROM
200 TO 300

STATION I	STATION J	PRECIPITATION INCHES
23	32	ZERO
24	36	0.006
24	37	0.006
25	36	ZERO
25	37	ZERO
26	12	0.074
26	13	0.168
27	12	0.192
27	13	0.542
29	12	0.295
29	13	0.017
27	20	ZERO

Figure 2. - Output of computer program which converts radar data to precipitation totals.

3. 1964 DATA ANALYSIS

A. Radar-Rain Gage Data Comparison

Radar data for four storm days (April 3, April 23, May 9, and May 10) have been processed, using $Z = 200R^{1.6}$ for hourly and storm precipitation totals, and compared to ARS's 175 rain gages.

Scatter diagrams illustrating the comparison between rain gages and radar storm totals for the four days are shown in figures 3, 5, 7, and 9 and related isohyetal maps are given by figures 4, 6, 8, and 10. As expected, only a rough correspondence between rain gage and radar data is evident in the scatter diagrams. The radar data is itself uncertain by about ± 3 db. as related in the paper starting on p.122. Furthermore, the radar data represent the average reflectivity over about 6 $mi.^2$ while the standard 8-in. rain gage measures precipitation over about 10^{-8} $mi.^2$ The rainfall sampled by the radar beam above the ground has a variable drop size distribution, it may not fill the radar beam uniformly, and it may be moved horizontally by the wind and partially evaporate before it arrives at the ground where the rain gage measures it. Most of these factors are especially important when the rain varies much over a short distance.

Table 2. - Comparison between radar and rain gage estimates of the mean storm rainfall for the ARS area.

Storm (1964)	No. of Rain Gages	Mean Areal Rainfall		Radar Average $Z = 200R^{1.6}$
		Rain Gage Main Rainfall	68% Confidence Limits for Areal Mean Rainfall	
Apr 3	69	.29	.29 ± .04	.32
Apr 23	81	.21	.20 ± .02	.47
May 9	143	.92	.92 ± .08	.39
May 10	138	1.09	1.09 ± .04	.87

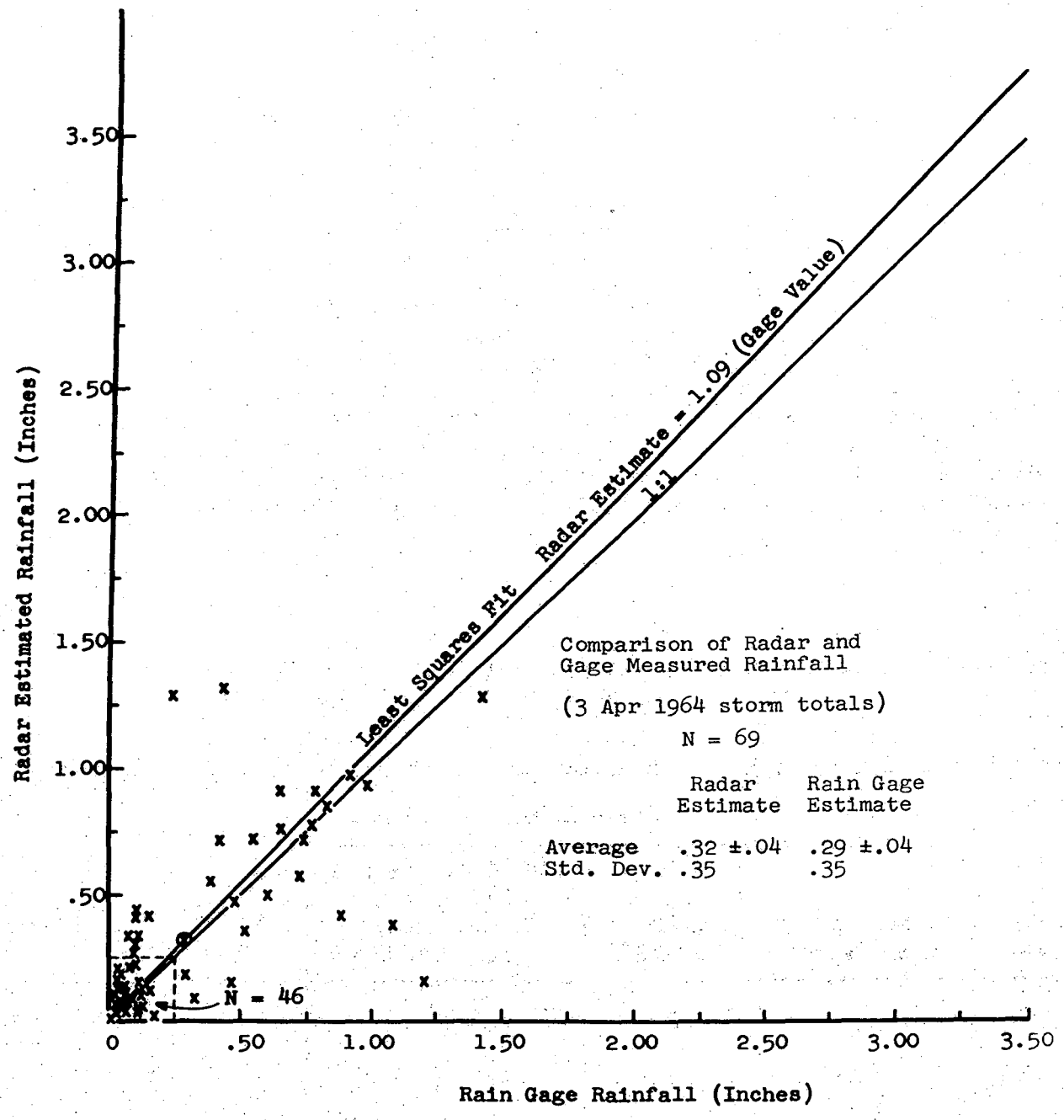

Figure 3. - Comparison of radar- and gage-measured storm total rainfall (4/3/64).

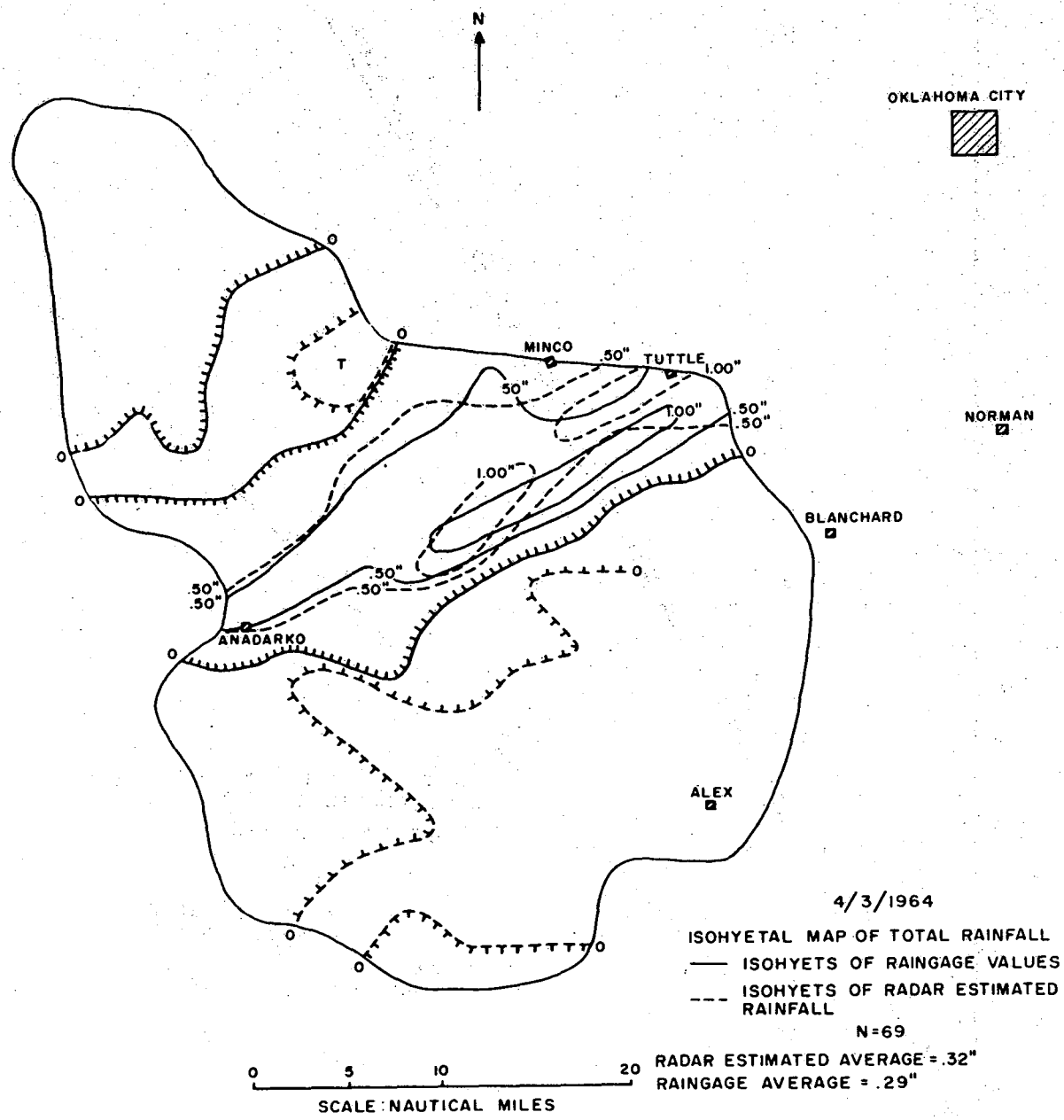

Figure 4. - Isohyetal map of rain gage- and radar-estimated total rainfall (4/3/64).

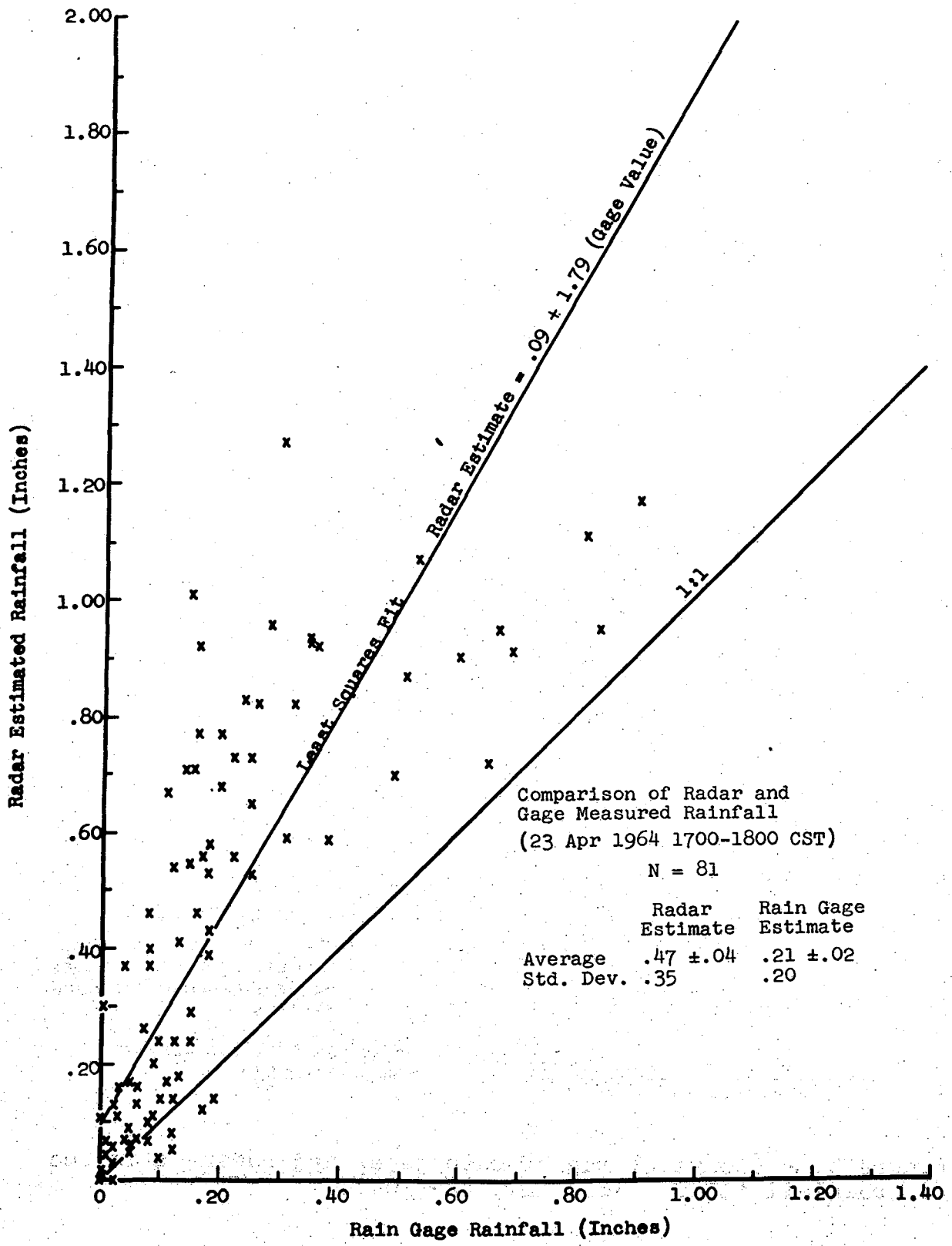

Figure 5. - Comparison of radar- and gage-measured rainfall (1700 - 1800 CST, 4/23/64).

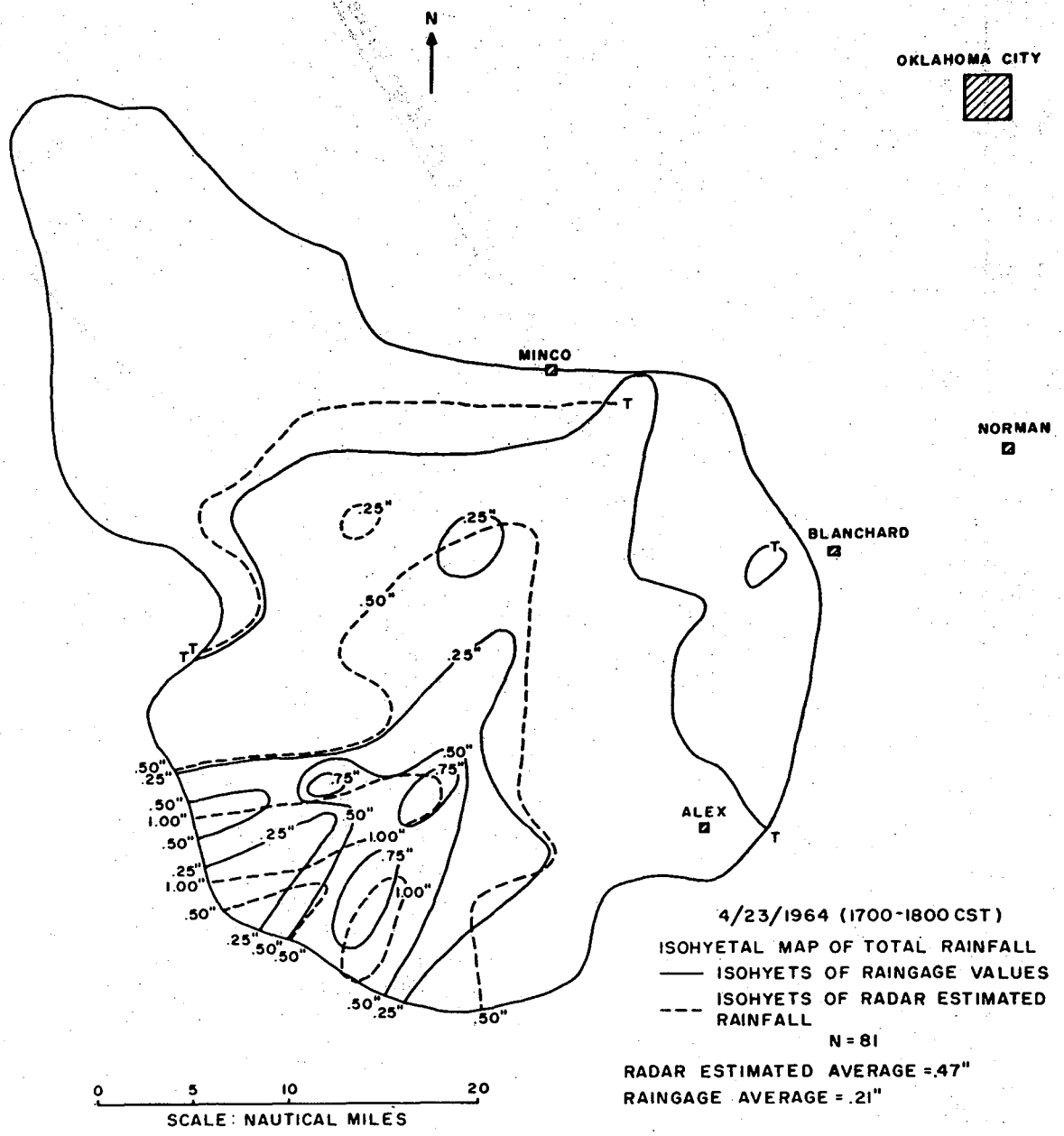

Figure 6. - Isohyetal map of rain gage- and radar-estimated rainfall (1700 - 1800 CST, 4/23/64).

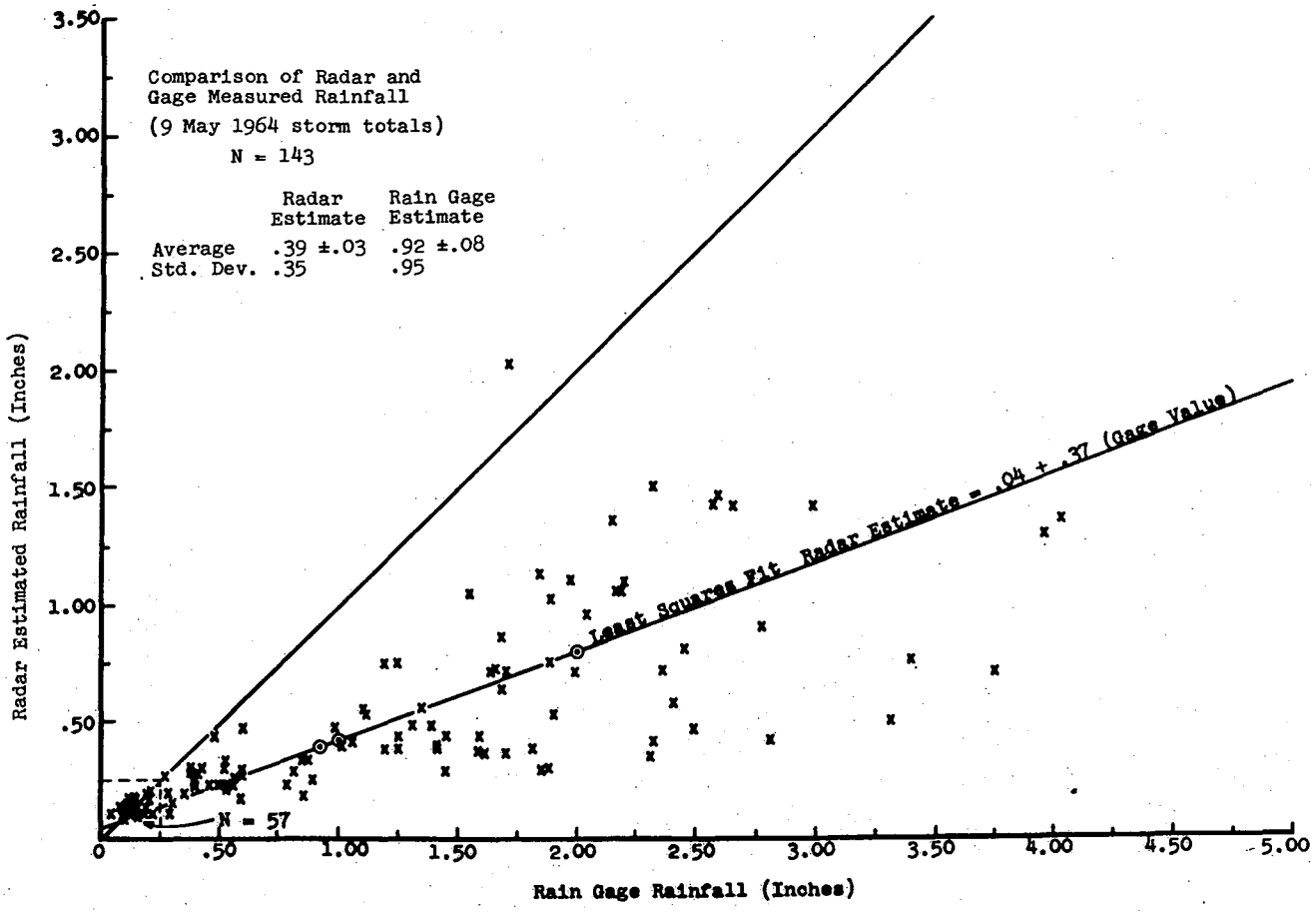

Figure 7. - Comparison of radar- and gage-measured storm total rainfall (5/9/64).

The average best fit line in the scatter diagrams is located at the mean position of the least squares regression lines of radar rainfall on rain gage amounts on radar rainfall. The 1:1 line is simply an equal-value line.

Examination of Table 2 indicates that only one of the four radar estimates based on $Z = 200\ R^{1.6}$ are within the 68 percent confidence limits of the areal mean rainfall. Of the four cases listed, the radar areal estimate is too high by the factor 2.2 in one case and too low by the factor 2.4 in another.

The isohyetal maps illustrated in figures 4, 6, 8, and 10 show that some of the scatter in the corresponding even-numbered figures would be removed by a moderate deformation and relative translation of the rain gage- or radar-estimated patterns. Some of the remaining pattern differences may be attributed to extrapolation of instantaneous radar-based estimates over the interval between radar data. Of course, differences of average value remain, but it appears that some rain gage measurements, if the

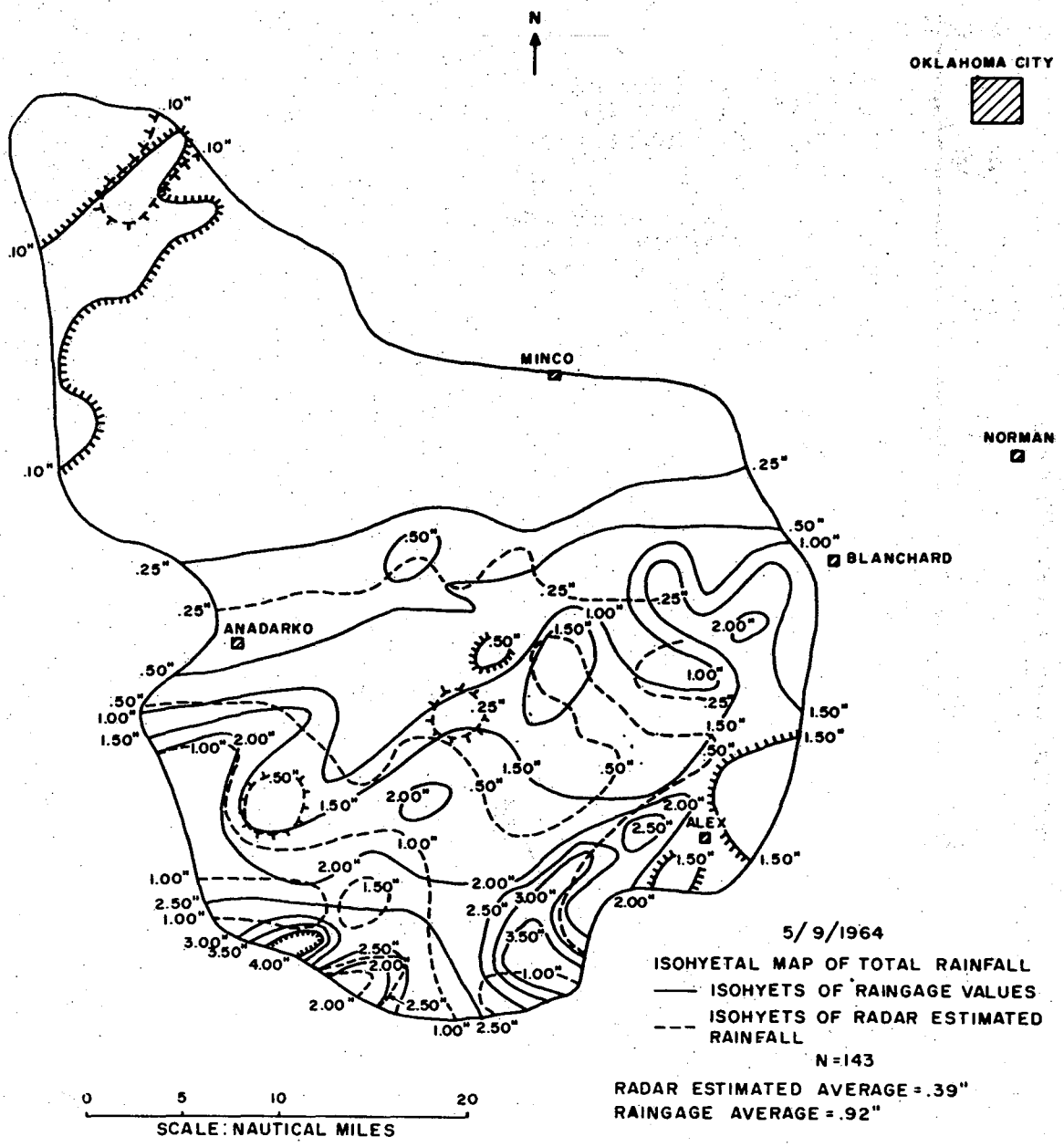

Figure 8. - Isohyetal map of rain gage- and radar-estimated rainfall (5/9/64).

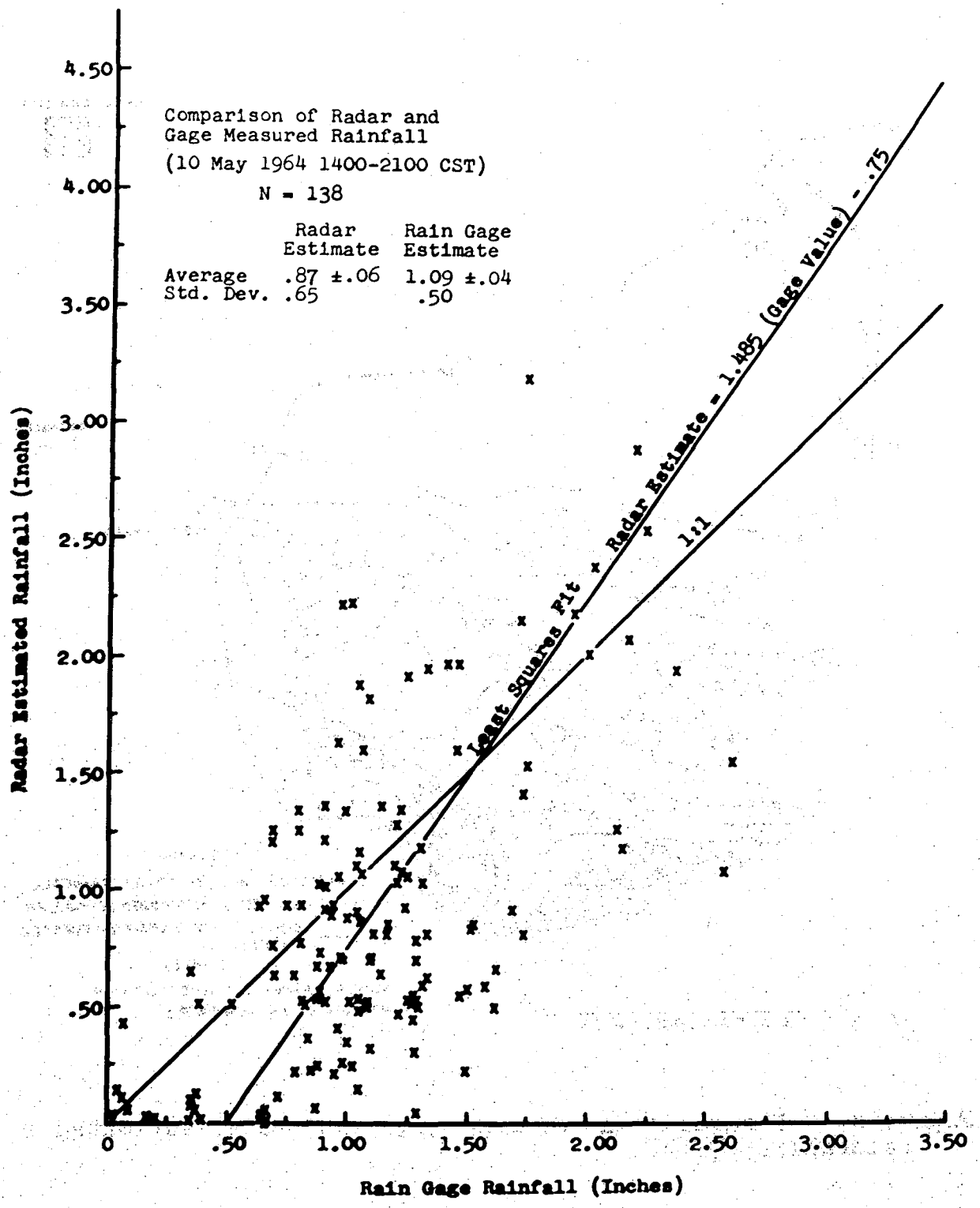

Figure 9. - Comparison of radar- and gage-measured rainfall (1400-2100 CST, 5/10/64).

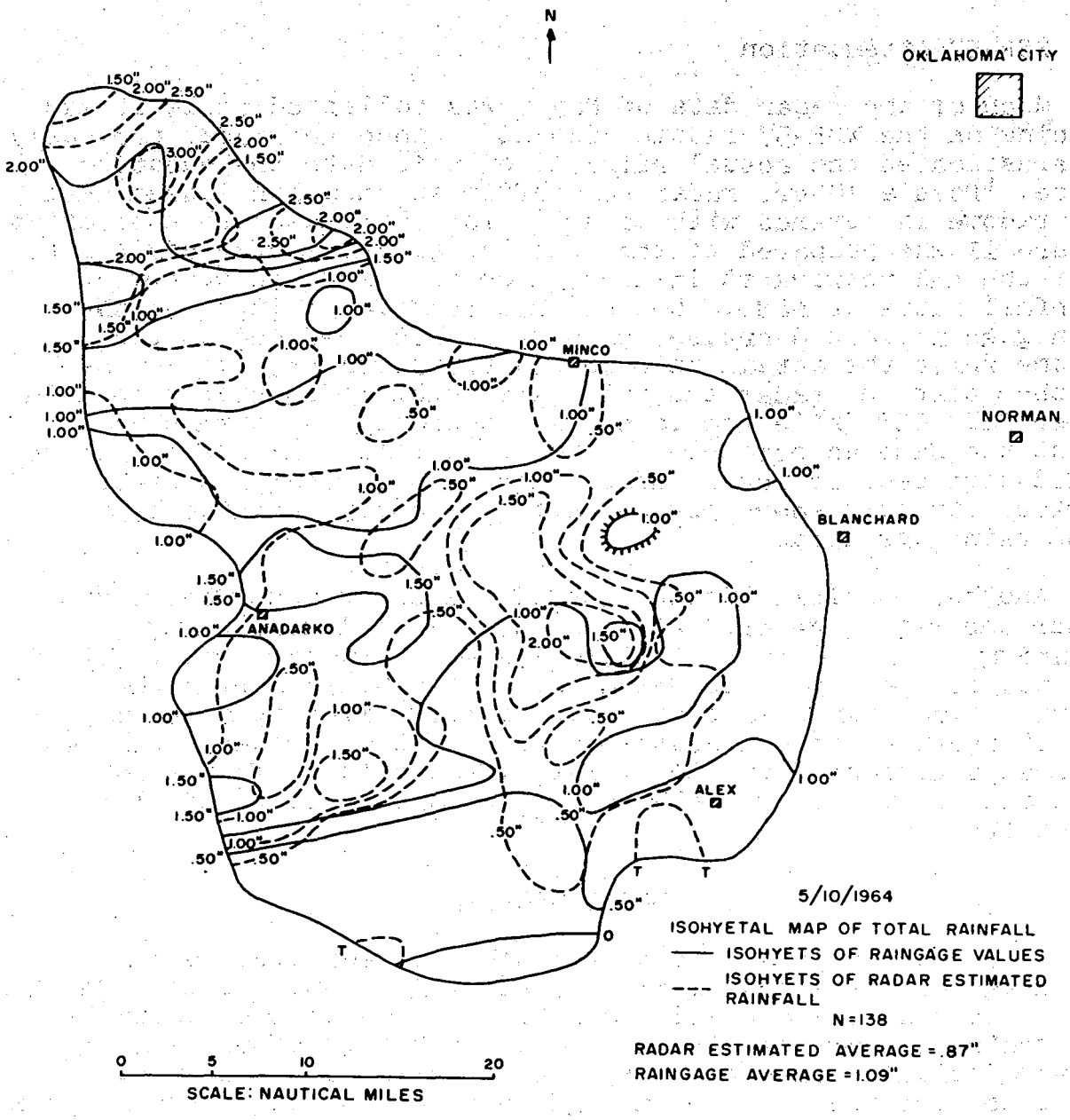

Figure 10. - Isohyetal map of rain gage- and radar-estimated rainfall (1400 - 2100 CST, 5/10/64).

rain gages are to be believed, could be used to calibrate the radar and to obtain estimates of rainfall averaged over a (watershed) area which are more timely than those provided by rain gages alone and more accurate than those provided by either a rain gage network of conventional density or the radar alone.

B. WSR-57 Attenuation

Much of the radar data of May 9 was collected while it was raining on the WSR-57 radome at NSSL. Since the radar seriously underestimated the actual rainfall on this date the question arose, "Does a 10-cm. radar set suffer attenuation losses when its radome is covered with water?" To help answer this question, figure 11 was prepared to show the actual average rainfall rate over the ARS network at 15-min. intervals, and the observed rainfall rates at NSSL. Notice that echo intensity over the rain gage network decreased when it started raining on the radome while the actual rain intensity increased, but notice further that the radar and rain gage intensities nearly coincide after 2200 CST while the rainfall intensities at Norman are about the same as before. We note that this analysis cannot be conclusive because the rainfall rate at the radar had great variability over short periods not accurately depicted by the NSSL rain gage data.

Another possible explanation of the discrepancy between radar and rain gage estimates on May 9 is illustrated by figure 12. This suggests that different raindrop distributions existed over the ARS network at different times during the storm. Also, for this particular storm, figure 13 shows that the difference between quantized rain gage and radar estimates increases linearly with the rainfall intensity. This also indicates that the Z-R relationship changes with rainfall intensity.

4. ADDITIONAL STUDIES

Substantial systematic differences between the radar and rain gage estimates of total rainfall vary among storms. This indicates that the overall radar calibration is substantially uncertain, and/or that the Z-R relationship or other radar meteorological parameters vary significantly among storms. In any case, the use of some rain gages to calibrate the radar data seems indicated, and we are pressed to explore every reasonable means for standardizing radar performance within the narrowest practical limits. We expect improved calibrations and data collections to result from use of radar-echo integrating and quantizing circuits now being developed [4]. We are hopeful that computer-measured statistical properties of reflectivity distributions can be used to define an "expected correspondence" between rain gage and radar data in particular situations, and provide a rational definition of the amount of rain gage data

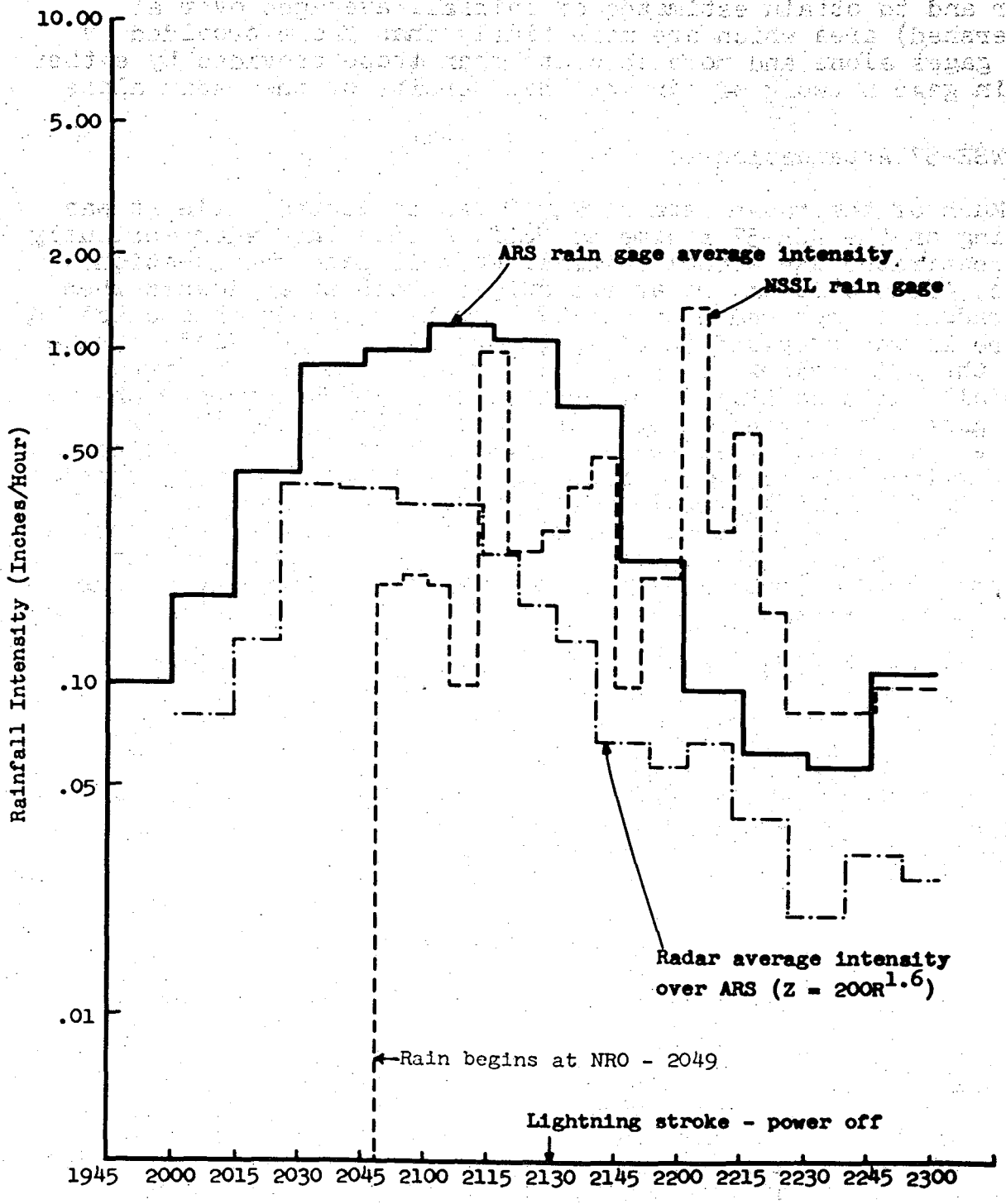

Figure 11. - Histogram of rainfall intensities over ARS rain gage network, at NSSL, and radar estimates over ARS network (5/9/64).

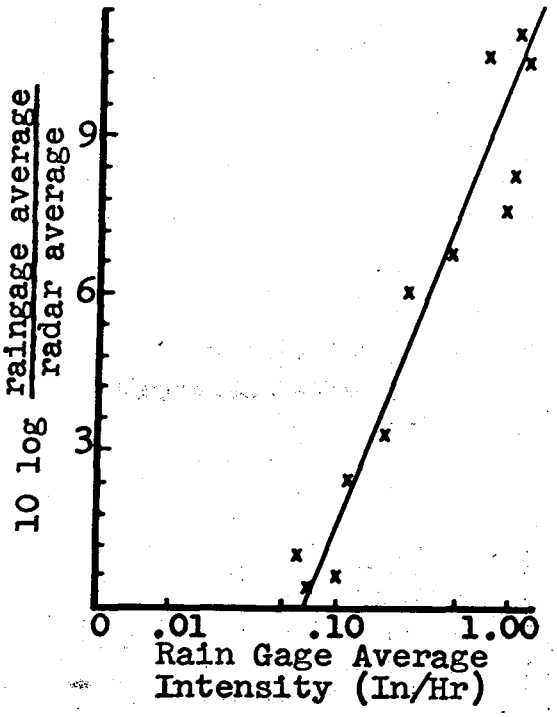

Figure 12.- Average hourly rainfall rates based on gage-measured 15-min. totals and as defined by the echo intensity with $R=(.005Z)^{.625}$mm/hr.

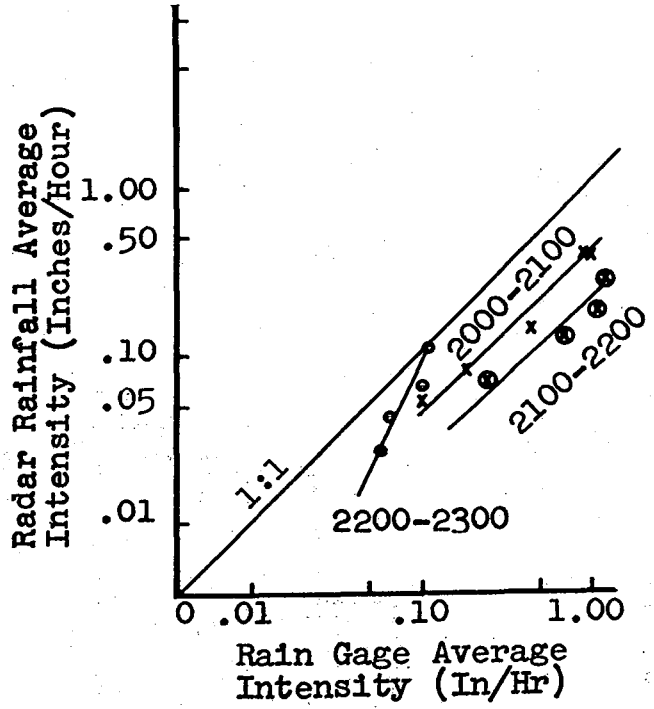

Figure 13.- The amount by which the averaged echo intensity underestimated the gage-measured rainfall predicted by $Z=200R^{1.6}$.

needed to calibrate the comprehensive radar-rainfall information to specified accuracy. Use of rain gages and radar data in combination is being examined now in a program involving NSSL and the River Forecast Center at Fort Worth, Texas.

REFERENCES

1. L. J. Battan, Radar Meteorology, The University of Chicago Press, 1959.

2. D. Atlas and A. C. Chmela, "Physical-Synoptic Variations of Raindrop Size Parameters" Proceedings Sixth Weather Conference, American Meteorological Society, Boston, Mass., 1957, pp. 21-30.

3. J. W. Wilson, "Evaluation of Precipitation Measurements with the WSR-57 Weather Radar," Journal of Applied Meteorology, vol. 3, No. 2, April 1964, pp. 164-174.

4. R. M. Lhermitte and E. Kessler, "A Weather Radar Signal Integrator," Proceedings, Conference on Cloud Physics, Tokyo and Sapporo, Japan, 1965, pp. 301-308.

COMPUTER PROGRAM FOR CALCULATING AVERAGE LENGTHS OF WEATHER-RADAR ECHOES AND PATTERN BANDEDNESS

Edwin Kessler

ABSTRACT

A computer program estimates the average length of echoes and a measure of pattern bandedness in digitized PPI displays from exponential-function approximations to the pattern autocorrelation coefficients. Average echo lengths estimated by the computer are correlated to actual lengths in 39 cases with a coefficient of 0.9. However, the distributions of echo lengths do not cluster closely about the exponential function implied by the theoretical basis of the computer program.

1. INTRODUCTION

The transports of heat, momentum, and moisture occur in eddies of various scales. These transports in microscale and macroscale have been studied extensively ([1,2] for example) but the mesoscale eddies have been comparatively neglected.

It seems that radar may become a powerful tool for investigating mesoscale transport phenomena. The size of the cells in which rising motion occurs should be indicated approximately by the echo sizes, since the echoes are due to precipitation which forms in rising air. The magnitude of rising motion is closely related to precipitation rate; the latter is indicated by the echo intensities. Newell, for example, [3] has considered the implications of cell width-to-depth ratios as defined by echo sizes for characterizing the eddy transports of heat and moisture.

The computer processing of digitized radar data provides an opportunity to survey a large number of radar records. In particular, programs have been developed to compute certain statistical properties of radar echoes [4,5]. The author believes that such statistical properties will become an important index of the scale, intensity, and other characteristics of mesoscale meteorological processes.

2. COMPUTER PROGRAM FOR DETERMINING ECHO SIZES

If weather radar echoes and spaces between were equally probable (i.e., if the echo coverage were 50 percent) and were distributed as the random wave with Poisson-distributed crossings so often treated in communications theory, the autocorrelation function ρ of radar patterns would be an exponential

$$\rho = \exp\left(-\frac{2S}{\bar{L}}\right), \tag{1}$$

where S is the lag distance and $\bar{L}$ is the average length of the echoes or spaces in the direction of S ([6] p. 61). Thus, if ρ is an exponential function, the average length is

$$\bar{L} = 2\int_0^\infty \rho \, d\, S \tag{2}$$

and this equation has been used as a definition even when ρ is only roughly approximated by the form (1).

The usual case in which the average lengths of echoes and spaces are unequal (i.e., the echo coverage is different from 50 percent) has been considered by Cole [7]. Cole suggests that average lengths L_E and L_{NE} of echoes and spaces, respectively, be determined by use of equations

$$L_E = \frac{\bar{L}}{2(1-P)}$$

$$L_{NE} = \frac{\bar{L}}{2P} \tag{3}$$

where P is the fractional area covered by echoes and $\bar{L}$ is defined by an exponential function approximation to the actual autocorrelation function, as discussed in [4]. Note that when $P = 0.5$, L_E, L_{NE}, and $\bar{L}$ are all equal.

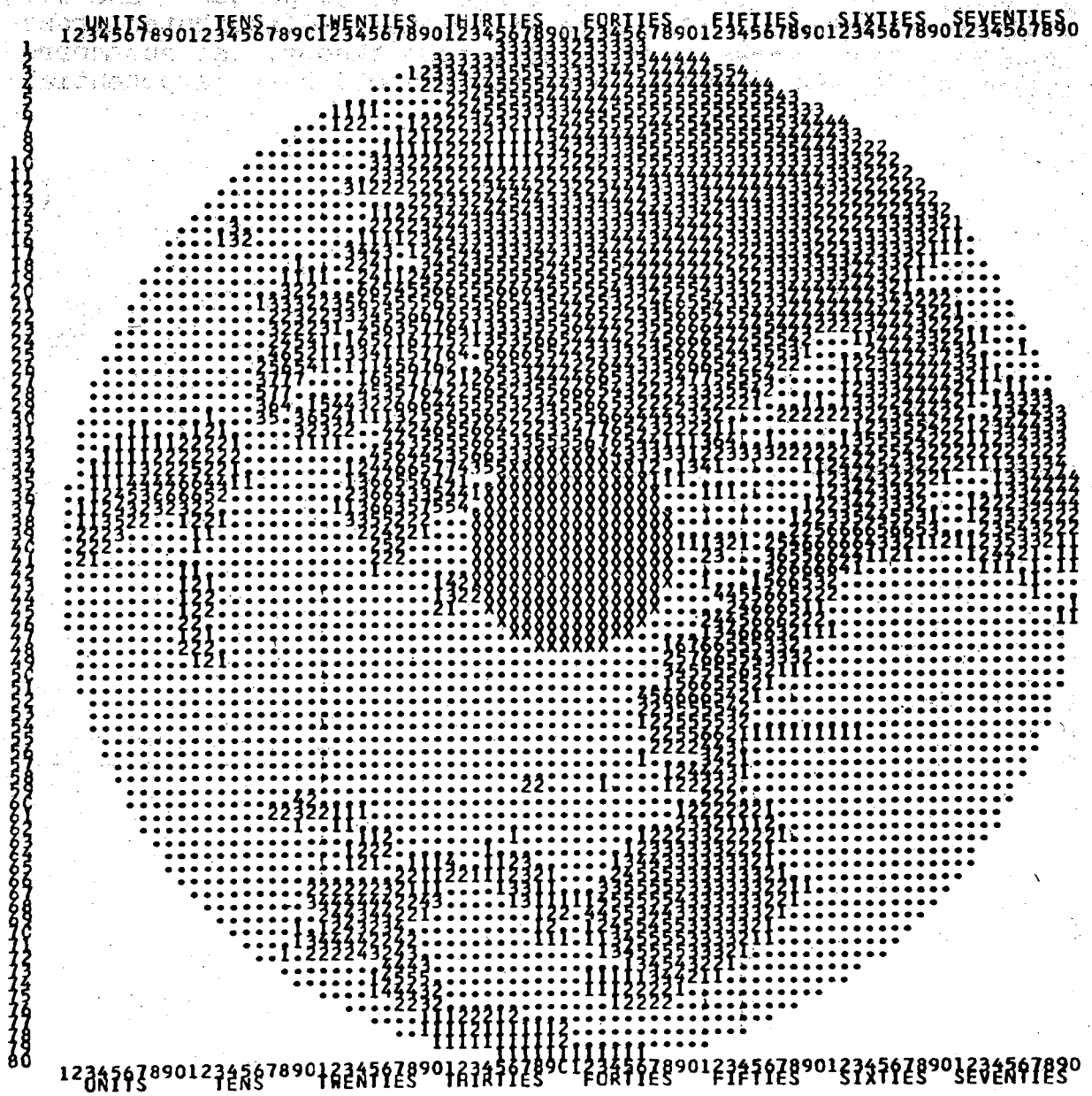

Figure 1. - Digitized version of the WSR-57 PPI display on May 10, 1964, 1500-1502 CST. The echo coverage is 49 percent. Integers correspond to 6 db steps of echo intensity. The photographed PPI display at high receiver sensitivity is shown in the lower right of figure 7.

The computer program processes digitized radar echo patterns like that shown in figure 1, for autocorrelation coefficients in a 5 x 5 lag array as shown in figure 2. Since the elementary grid units are 2-1/2 mi. square, the maximum lag represented in the correlation array is only $6.25\sqrt{2}$ mi. or about 9 mi. In computing the autocorrelation coefficients, all intensity integers greater than an assigned value are treated as 1's; periods are treated as zeros; and no pairs are considered of which one or both members are terrain echo (X), or are located outside the circular area portrayed in figure 1.

SEQUENCE 6. TIMES FROM 1500 TO 1502 EST
AUTOCORRELATIONS AT VARIOUS LAGS
ALL ECHOES ABOVE OR EQUAL TO 1 TREATED ALIKE

J LAG / I LAG	-2	-1	0	1	2
-2	0.60	0.65	0.68	0.69	0.65
-1	0.66	0.74	0.80	0.77	0.69
0	0.72	0.85	1.00	0.85	0.72
1	0.69	0.77	0.80	0.74	0.66
2	0.65	0.69	0.68	0.65	0.60

Figure 2. - Autocorrelation coefficients calculated from the pattern shown in figure 1.

The computer determines a quadratic surface

$$f(x,y) = \rho = Ax^2 + Bxy + Cy^2 + M, \qquad (4)$$

where the coefficients are calculated to provide a least squares fit to the correlation coefficients with center point excluded. This surface is a dome whose intersections with planes parallel

to the ρ axis are parabolas, as illustrated in figure 3, and whose intersections with planes parallel to the x-y plane[1] form a family of ellipses. A tower with exponential walls and elliptical cross section is defined by a family of curves like equation (1) which assumes the magnitude 1 at the origin (lag = zero) and intersects the parabolic dome along the ellipse where f(x,y) is the average correlation coefficient in the 5x5 array. This also is illustrated in figure 3. The lengths are determined directly from the exponential function in accordance with equation (1) or (2). In the example shown in figures 2 and 3, $2/\bar{L} = .1835$ and $\bar{L} \approx 11$ grid mesh units in the direction of the y axis.

Regardless, then, of the actual character of the autocorrelation function of a pattern, the computer finds an exponential approximation. The exponential function is an approximate measure of the average scale of pattern elements. A measure of linear bandedness in the pattern is estimated by the ellipticity, the ratio of average lengths across and along bands. The computer solves for and prints the lengths in the directions along and across bands, i.e., along the axes of the autocorrelation ellipse. The results of computations concerning lengths and bandedness in this example are tabulated in figure 4.

3. EMPIRICAL TEST OF THE COMPUTER PROGRAM

We ask how accurate are the estimates of average length given by the computer program described above and how well does the distribution of echo lengths L approximate the distribution $P(L) = \exp(-L/\bar{L})$, associated with the random wave hypothesis described in section 1.[2]

The data input format permits a tabulator to list echo lengths in the east-west direction. The lengths of spaces between echoes have not been tabulated because, with Oklahoma data, their average is usually a large fraction of the diameter of the PPI display, and the computer program is not expected to yield representative results in such cases. In the cases of weather echoes which intersect edges of the circular display or the boundary of terrain echoes, those edges or boundaries are counted as echo edges.

---

[1] Matrix notation was used in the computer program (note figure 2). Increasing x eastward corresponds to increasing j; increasing y northward corresponds to decreasing i.

[2] This member of the Poisson Distribution family has unit average and defines the fraction of lengths L in a unit length range.

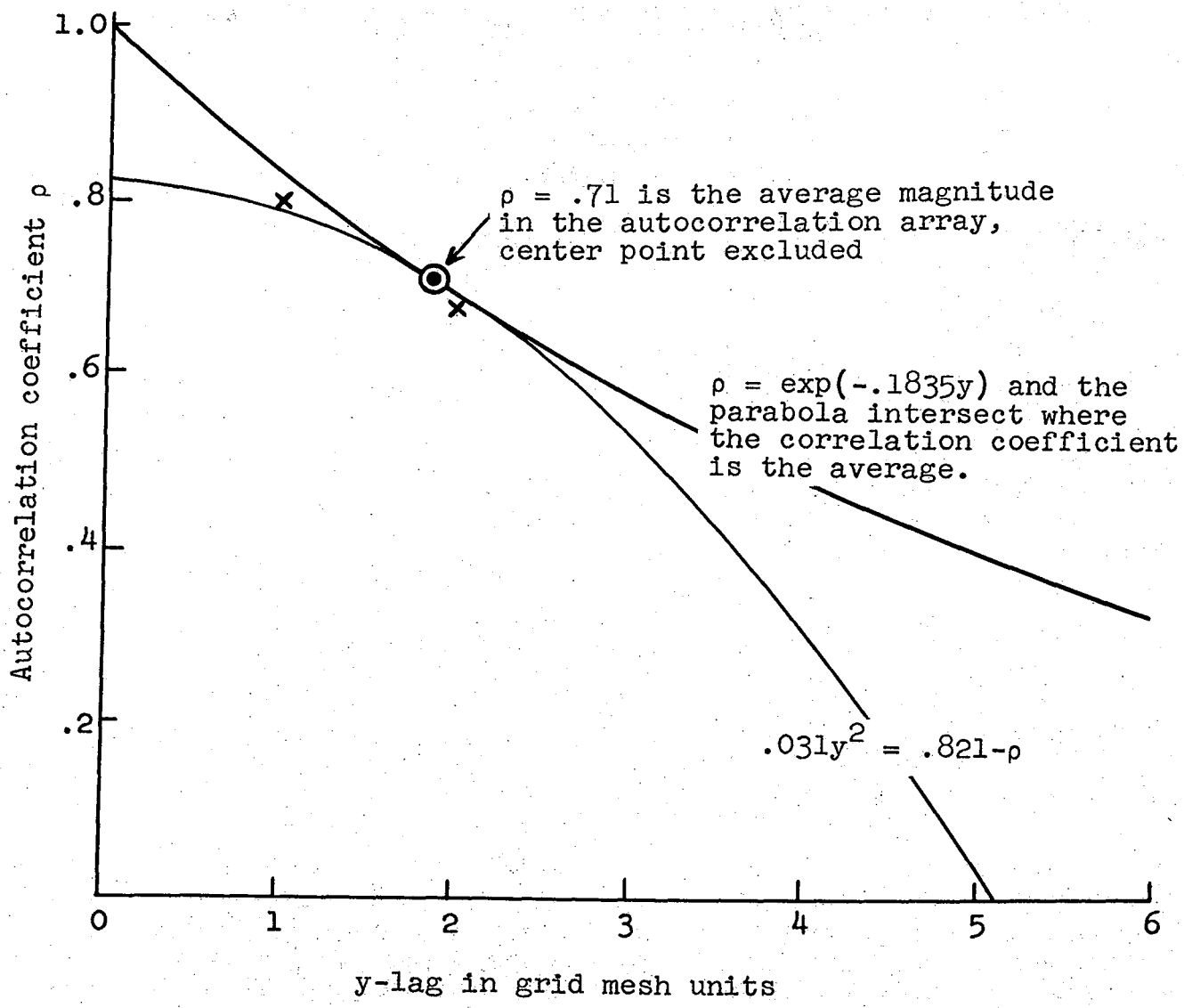

Figure 3. - Illustration of the computation of average lengths. Crosses mark the actual correlation coefficients in the y-direction through the center of the correlation array in figure 2. The smoothed (elliptical) locus of the average coefficient in the array (excluding the center point) is provided by a least-squares fitting quadratic surface. The intersection of this surface with the y-ρ plane is a parabola, as shown by the light line. The average echo lengths are defined by the exponential section which intersects, in the x-y plane, the alliptical locus of the average correlation coefficient and the origin at ρ = 1.

THE AVERAGE AUTOCORRELATION COEFFICIENT EXCLUDING THE CENTER POINT IS R = 0.71

THE COEFFICIENTS OF THE QUADRATIC SURFACE WHICH BEST APPROXIMATES THE AUTOCORRELATION DISTRIBUTIONS ARE

A = -0.02300160
B = -0.00777641
C = -0.03102647
M = 0.82068200

THE ANGLE CLOCKWISE FROM NORTH OF THE MAJOR AXIS IS 67.95 DEGREES
THE LENGTH OF THE SEMI-MAJOR AXIS IS 2.29 GRID MESH UNITS
THE LENGTH OF THE SEMI-MINOR AXIS IS 1.86 GRID MESH UNITS
THE ELLIPTICITY IS 0.81
THE ECCENTRICITY IS 0.59
THE CHARACTERISTIC LENGTH
ALONG BANDS IS 33.20 MILES
ACROSS BANDS IS 26.92 MILES
AVERAGE IS 30.06 MILES
THE ECHO LENGTH
ALONG BANDS IS 33.04 MILES
ACROSS BANDS IS 26.78 MILES
AVERAGE IS 29.91 MILES
THE ECHO-FREE LENGTH
ALONG BANDS IS 33.37 MILES
ACROSS BANDS IS 27.05 MILES
AVERAGE IS 30.21 MILES

Figure 4. - Coefficients of the surface $f(x,y)$ defined by equation (4) in the text, fitted by a method of least squares to the autocorrelation coefficients shown in figure 2, excluding the center point. The echo lengths are derived from the exponential sections which have the value 1 at zero lag and intersect $f(x,y)$ where $f(x,y) = \bar{\rho}$, the average correlation coefficient in the array. The orientation of bands is just the orientation of the major axes of the ellipses $f(x,y) =$ constant.

Thirty-nine digitized PPI displays like figure 1, distributed over 8 days and in no case less than 1 hr. apart in time, have been chosen for study. The average measured east-west length L_{E-W} is normalized to the estimated length along the bands by the equation:

$$\bar{L}_{EST} = L_{E-W} \sqrt{\frac{\cos^2\theta}{e^2} + \sin^2\theta} \qquad (5)$$

where θ is the computer-determined orientation of the major axis of the bands, measured clockwise from north, and e is the computer-determined ratio of lengths across bands to lengths

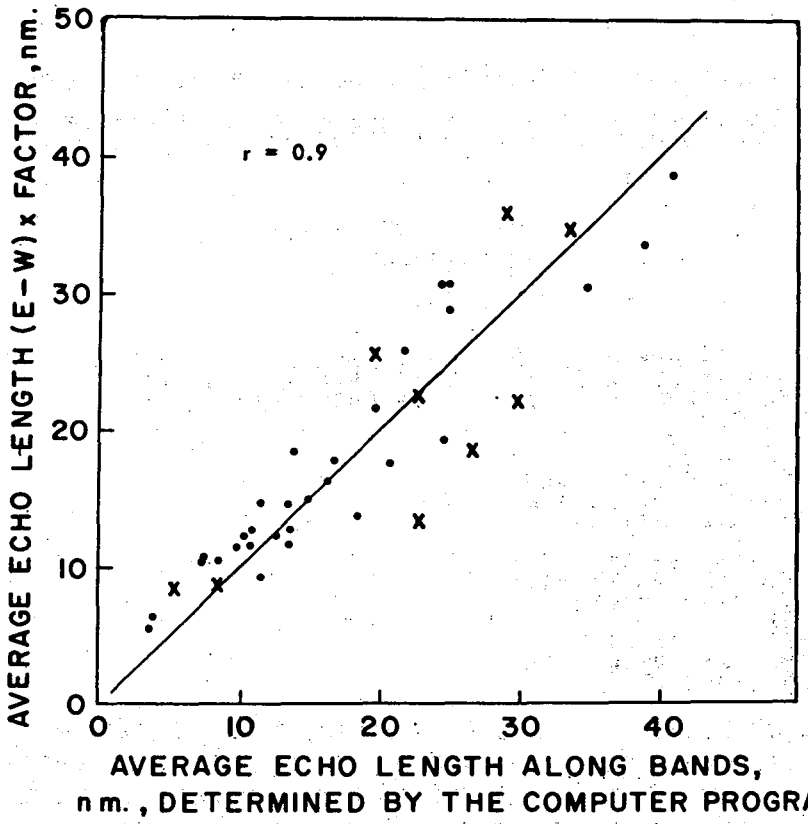

Figure 5. - Echo lengths along bands determined by the computer program, on the abscissa, are compared with actual average echo lengths in the east-west direction, normalized by use of equation (5) to the direction of bands. Each of the 39 points in the diagram is based on a digitized PPI display at one moment. Points correspond to 8 different days and no two are closer than 1 hr. in time. X's represent data selected for detailed examination in figures 6 and 7.

along bands, i.e., the ellipticity listed in figure 4.[3] Figure 5 shows how the lengths $\bar{L}_{EST}$ determined by actual measurement and adjusted in accordance with equation (5) compare with those given by the computer's indirect approach. The agreement is good enough to suggest that the computer program has interest for application in theoretical studies and operational routines when objective techniques are desirable.[4]

[3] L_{E-W} is the distance from the center of an ellipse to its edge along the line at an angle $90^\circ-\theta$ to the orientation of the major axis, when the semi-major axis is L_{EST}.

[4] Note that the scatter of data in figure 5 is unchanged if the measured E-W lengths are compared with the computer-determined lengths normalized to the E-W direction.

In order to discover whether the larger departures from the locus of perfect fit shown in figure 5 occur with obvious features of the PPI patterns, frequency distributions of the measured lengths have been prepared for the points marked by X in figure 5. The frequency distributions with corresponding PPI photographs are shown in figures 6 and 7. The author sees no hint of an association between features of the PPI patterns in the photographs and the frequency distributions, and positive and negative deviations of actual average lengths from the computer estimates.

Figure 6 illustrates that the observed distributions of echo lengths vary widely and do not cluster closely about the exponential distribution associated with the random wave hypothesis. Although we know that the real autocorrelation functions are approximately fitted by exponentials, it seems remarkable that the good estimates shown by figure 5 can be derived by an analysis of 24 autocorrelation coefficients at lags of only 9 mi. and less.

4. CONCLUSIONS

The relatively simple analysis of radar echo pattern autocorrelation coefficients employed in the NSSL program provides meaningful definitions of average echo length and of banded structures, but theoretical foundations for this statistical processing require further examination.

REFERENCES

1. Priestley, C. H. B., Turbulent Transfer in the Lower Atmosphere, The University of Chicago Press, 1959, 130 pp.

2. Starr, Victor P., "Studies of the Atmospheric General Circulation, IV," Final Report by Dept. of Meteorology, MIT, on Contract AF19(604)6108, 1963, 315 pp.

3. Newell, R. E., "Some Radar Observations of Tropospheric Cellular Convection," Research Report No. 33, Contract AF19(604)2291, Dept. of Meteorology, MIT, Cambridge, Mass., 1959.

4. Kessler, E., and J. A. Russo, Jr., "Statistical Properties of Radar Echoes," in Proceedings 10th Weather Radar Conf., Washington, D. C., 1963, pp. 25-33.

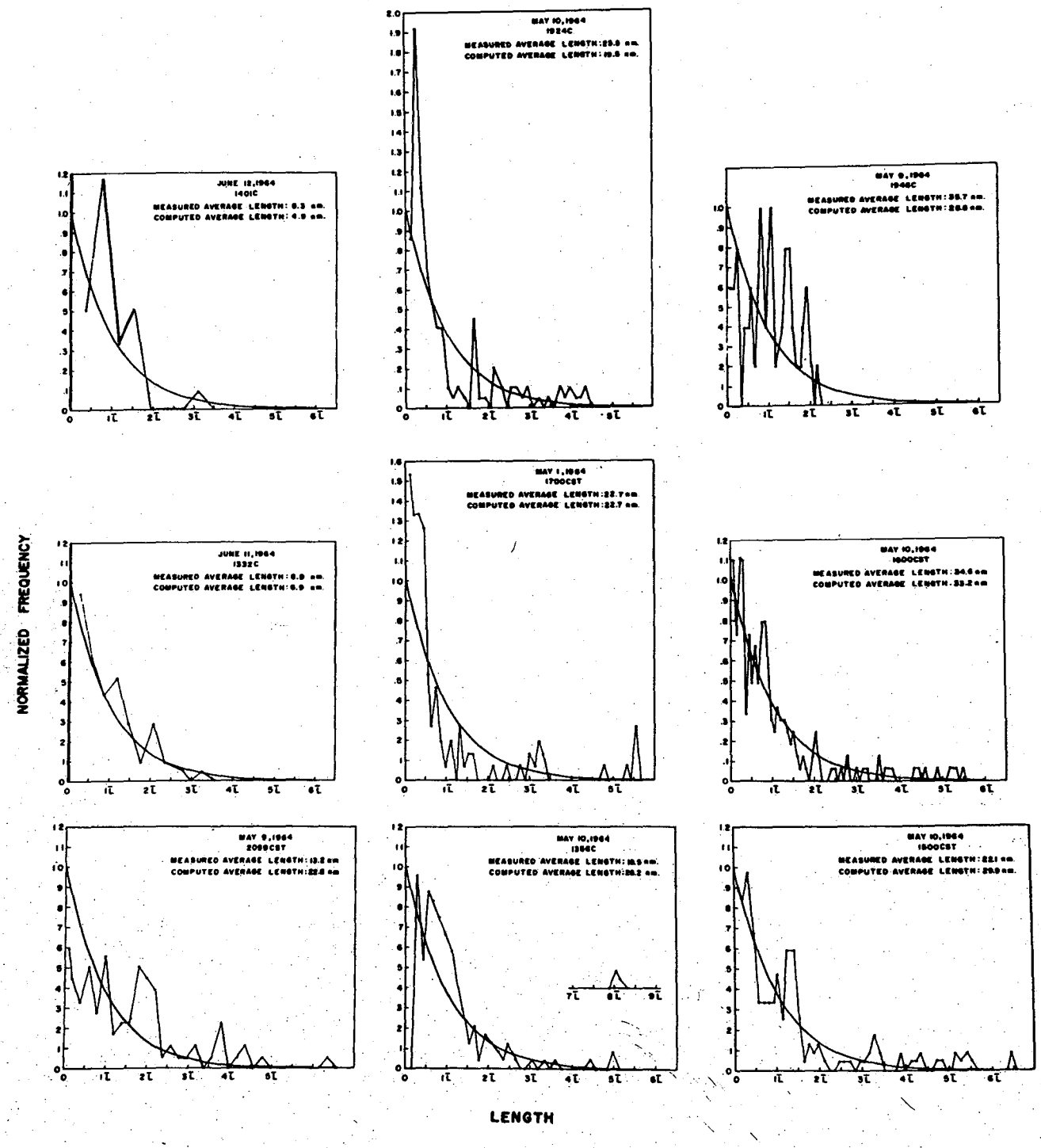

Figure 6. - Frequency distributions of lengths for X-data in figure 5 determined from digitized displays like figure 1. The top row corresponds to points above the line in figure 5, in the same order. Similarly, the middle and lower rows correspond to points on and below the line in figure 5. The heavy line is the locus of exp (-L/$\bar{L}$).

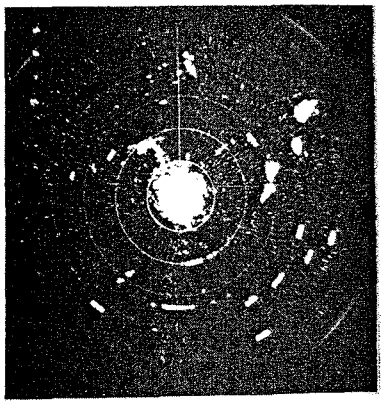

June 12, 1964; 1401 CST

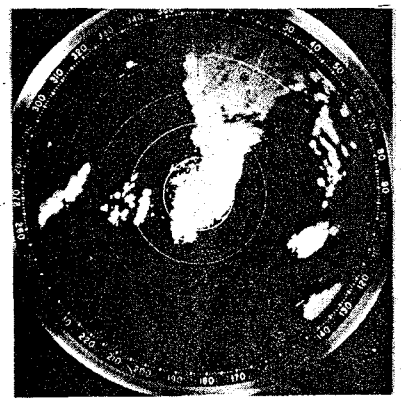

May 10, 1964; 1924 CST

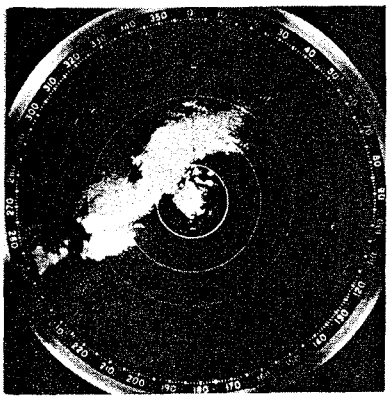

May 9, 1964; 1946 CST

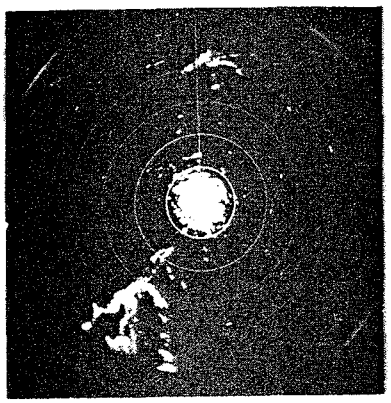

June 11, 1964; 1332 CST

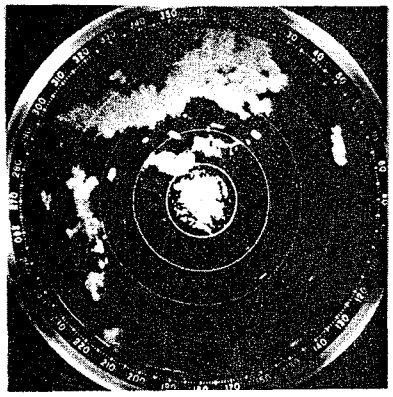

May 1, 1964; 1700 CST

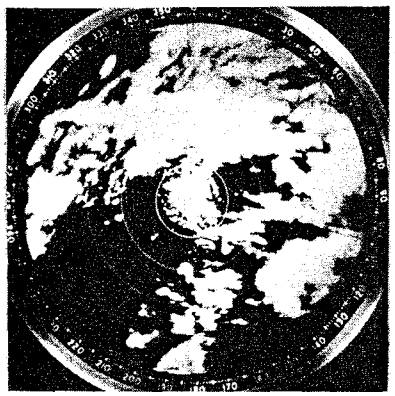

May 10, 1964; 1600 CST

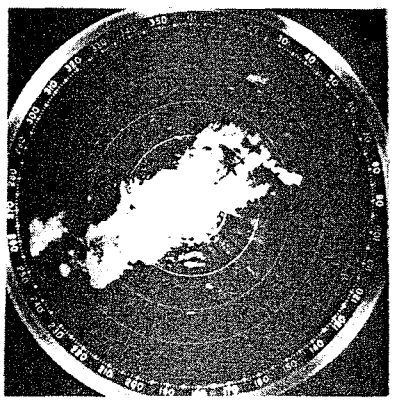

May 9, 1964; 2059 CST

May 10, 1964; 1356 CST

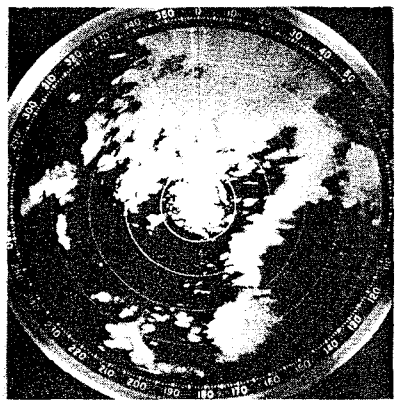

May 10, 1964; 1500 CST

Figure 7. - PPI photographs corresponding to the frequency distributions shown in figure 5. Echoes due to airplanes, interference, and other spurious sources are mostly eliminated during manual digitizing and are not treated in the computation of lengths. The photograph in lower right is one of the series at steps of the receiver gain used to produce figure 1.

5. Kessler, E. and J. A. Russo, Jr., "A Program for the Assembly and Display of Radar Echo Distributions," Journal of Applied Meteorology, Vol. 2, No. 5, 1963, pp. 582-593.

6. Davenport, W. B., Jr. and W. L. Root, An Introduction to the Theory of Random Signals and Noise, McGraw-Hill Book Co., New York, 1958, 393 pp.

7. Cole, J. W., "Statistics Related to Shape and Scale of Pattern Elements," Final Report on Contract Cwb-10709 by Travelers Research Center, Hartford, Conn., 1964, pp. 34-40.

DATA PROCESSING AT NSSL IN 1964

Kathryn C. Gray and Kenneth E. Wilk

1. INTRODUCTION

The data collection program of NSSL during spring and summer 1964 produced a large volume of radar scope photographs and mesonetwork records. In July of that year, a data processing program was begun with the following objectives: (1) to develop procedures and techniques suitable for rapid transfer of film and strip chart records to digital formats; (2) to digitize selected radar scope photographs made over a period of 150 hours and process the data by computer; (3) to evaluate the data processing techniques. This paper summarizes the 1964 data processing project.

It should be noted that some processing programs had been developed elsewhere in USWB and their continued refinement formed a part of the NSSL endeavor. Also, Travelers Research Center had developed radar data handling programs under contracts with the FAA and Weather Bureau and these programs were modified to meet NSSL requirements. Other processing programs were developed ab initio.

2. RADAR DATA DIGITIZATION

During the fall of 1963, NSSL (then the Weather Radar Laboratory, USWB) provided scientists at Travelers Research Center (TRC) with WSR-57 radar film records of an 8-hour storm for computer processing. Studies of these data confirmed the usefulness of the TRC computer programs for routine radar data processing at NSSL.

The experience gained by TRC in processing and analyzing radar data was also considered in developing the NSSL radar photography program. Sequences of radar photographs at steps of the receiver sensitivity and antenna elevation angle contain comprehensive three-dimensional data. The time interval between adjacent sequences, and the number of displays in each sequence varies with the maximum intensity and height of the echoes at the time of collection. This is discussed in the article by Dooley and Clark elsewhere in this report.

Routine radar data reduction at NSSL started in April 1964. Tracing, manual coding, and key punch digitizing described in [1] were used for the test run. This introduced radar data processing to NSSL staff and provided bases for tailoring procedures to fit NSSL conditions and for conducting time and cost analyses of the techniques employed.

The PPI photographs made during the 1964 spring operational season were catalogued, edited, and reviewed for application to studies of atmospheric turbulence and electricity, rainfall, and the dynamics and morphology of mesoscale weather systems. Approximately 150 hours on 16 storm days were selected for digitizing (see table 1) and the time interval between sequences was chosen in accord with requirements of the proposed studies. For example, turbulence and precipitation studies require comprehensive data at intervals at least as short as 15 minutes, while climatological studies can be based on hourly data. The time between sequences ranges from 7 minutes to 1 hour.

Table 1. - 1964 Data Processing

Date 1964	Data	Time CST Begin	Time CST End	No. of Seq. in Storm	Digit. Freq. in Min.	Number of Sequences: Traced & Digitized	Card Check Program 3748-02	Assembly Program 3763-02	Precip. Program 3712	Stat. Prop. 3713
April										
3	NRO WSR-57	0832	2338	35	30	35	35	35	35	35
3	NRO WSR-57 & Mesonetwork	0832	1812	52	15	26	--	52	--	52
4	NRO WSR-57	0001	2258	24	60	24	24	24	--	--
12	NRO WSR-57	--	--	1	--	1	--	1	--	--
23	NRO WSR-57	1601	1824	25	7	25	--	25	25	25
26	NRO WSR-57	--	--	1	--	1	1	1	--	--
May										
1	NRO WSR-57	1423	1730	9	20	9	9	9	9	9
9	NRO WSR-57	1629	2356	44	10	44	44	44	44	44
10	NRO WSR-57	1356	2105	31	15	31	31	31	31	31
14	NRO WSR-57	1024	1139	10	7	10	10	--	--	--
15	NRO WSR-57	1301	1319	2	15	2	2	--	--	--
21	NRO WSR-57	1518	1650	14	15	14	14	--	--	--
22	NRO WSR-57	1243	1800	29	15	29	29	--	--	--
29	NRO WSR-57	0000	2305	64	7-30	34	--	15	15	15
30	NRO WSR-57	0007	2102	44	15	--	--	--	--	--
June										
4	NRO WSR-57	1005	1420	11	30	11	11	--	--	--
5	NRO WSR-57	1354	1628	15	13	15	15	15	15	15
11	NRO WSR-57	1332	1710	25	10	25	25	25	25	25
12	NRO WSR-57	1257	1815	27	13	27	27	27	27	27
Oct										
12	NRO WSR-57, MPS-4	0815	1818	10	60	10	10	--	--	--
Nov										
3	OKC,NRO WSR-57	1232	1235	2	--	2	2	2	--	2
14-15	OKC WSR-57	0050	1251	43	45	43	--	43	43	43
	148 hrs, 22 min			518		413	289	349	269	323

Semi-automatic digitizing began in mid-June. By July 1, 276 radar-weather patterns, representing 18 sequences and 3-1/2 hours of the storm of May 10, had been traced and intensities registered on approximately 16,000 punched cards. By January 30, 1965, a total of 418 radar sequences representing 15 storm days and 119 hours of radar observations had been processed using the TRC computer programs.

The routine preparation of photographic radar data for computer processing proceeds as follows: A film reader is used to project vertically the photographically recorded radar pattern onto a 12-inch square 80x80 grid for image tracing. A pad of tracing paper is placed under the grid with carbon paper inserted beneath the first sheet. Thus, the first scope tracing on the grid is carbon registered on the back of the first tracing. Such a traced carbon image serves as an alignment guide for each following echo display, and insures that contours of high intensity are always enclosed by contours of lower intensity. The high velocity of echoes often results in significant displacement of echoes during the 2-minute period required for attenuation steps. Contour discrepancies produced by this displacement are easily checked with this tracing method.

The step-attenuation recording system requires careful checks of the minimum detectable signal. The total loss between receiver output and the traced image averages 6 db. In order to evaluate subjective factors in tracing, tests were conducted in which duplicate tracings were prepared by different persons; the correlation coefficient between patterns was 0.86, which agrees with similar test results reported by TRC personnel.

The echo tracings are placed on a Benson-Lehner Oscar Model K trace reader, with connected IBM 026 card punch for automatic reading as shown in figure 1. Grid positions are read to the nearest tenth of a square (0.25 mile) and the Oscar patch panel is wired to punch the grid positions in whole numbers.

After the echo pattern is aligned over the positioned grid mounted on the Oscar K, one row address (ii) is read at a time, by automatically punching the column addresses (jj) where echo data begin and end. All beginning and ending jj addresses for a particular ii address containing echo data are read into one punched card which is automatically punched also with storm date, antenna tilt angle, and attenuation code. On one storm day, a "color code" identification was also punched into the cards. Echoes were assigned separate code numbers in order to isolate particular echoes for computer processing. The punch card format is illustrated by figure 2.

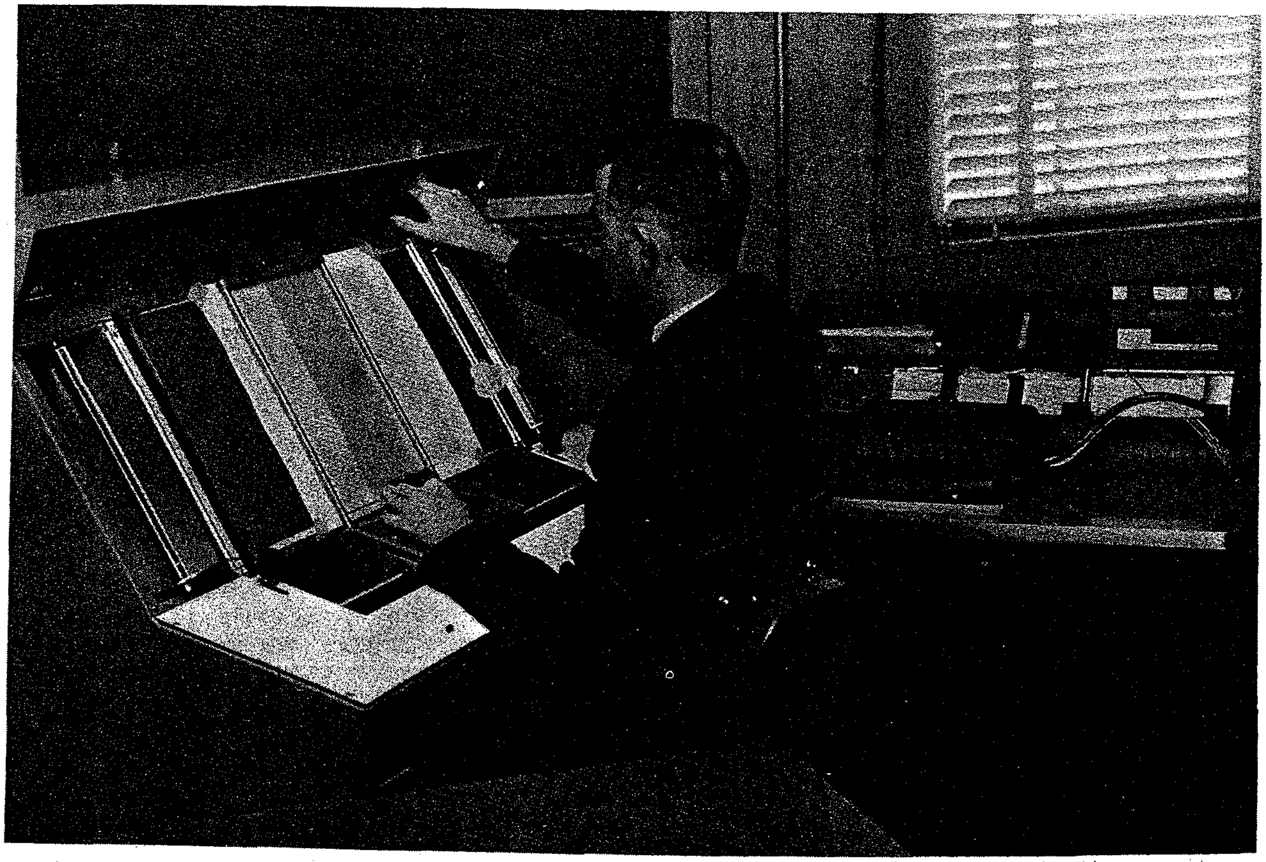

Figure 1. - Mr. Roy Hodges uses a Benson-Lehner Oscar Model K with IBM 026 card punch for archiving radar data.

DATE						TIME				±	i	i	θ			GAIN	j	j	j	j	j	j	j	j						C	C
1	2	3	4	5	6	7	8	9	10	11	12	13	14	15	16	17	18	19	20	21	22	23	24	25	26	27		77	78	79	80
0	5	1	0	6	4	0	8	5	9	+	4	8	0	8	0	1	5	8	6	2	6	7	6	7						0	0

May 10, 1964 Central Standard Time Echo data for ii address (row) 48

Elevation angle 8° Gain code 1 is 0 db (No attenuation)

Echo begins in 58 and ends in 62 Single echo in 67 Color code 0 0

Figure 2. - Explanation of digits on a single punch card containing radar data derived from PPI display.

Late in 1964, an inexpensive preliminary card check was developed which utilized a card sorter and a 407 tabulator for listing. This eliminated the need for the 7090 card checking program and provided other economies.

Most routine processing of NSSL radar data is done by students at the University of Oklahoma whose services are provided by a contract between the Weather Bureau and the Oklahoma University Research Institute.

3. COMPUTER PROCESSING OF DIGITIZED RADAR DATA

The computer programs prepared by Travelers Research Center for radar data handling are written for the IBM 7090 in Fortran IV. The assembly program, described by Kessler and Russo [1] was modified slightly under a contractual agreement with TRC. The alterations include a change in card format to the style shown in figure 2. The range normalizing routine was made optional to permit use of a calibrated STC circuit available on the NSSL radar (see paper by Dooley and Clark elsewhere in this report).

Figures 3, 4, and 5 illustrate an echo intensity distribution and the height of echo bases and tops as produced by the assembly programs. Illustrations of outputs of other programs are given elsewhere in this report.

All 1964 data were processed using the IBM 7090 and IBM 1401 at FAA's National Aviation Experimental Center in Atlantic City, N. J. All magnetic tapes produced by this processing are stored at the same facility. All punched cards and printouts are stored at NSSL, Norman, Okla.

The January 30, 1965 status of the processing is shown in table 1, and time and cost estimates can be derived from table 2.

As shown by the tables, 18 storm days between April 3 and June 12, 1964, have been processed. In addition, 4 storm days from October 12 through November 15 have been processed for special studies. These data represent 418 sequences and 148 hours of radar data. The storms average 19 sequences each; the maximum number of sequences for a 24-hour period is 64. In the four cases for which data were required for a special study, only one or two sequences were digitized.

Table 2 reports the time in hours and/or minutes required for processing the records. Man hours are shown for the tracing and digitizing of data, and the computer time is shown for each part of the program.

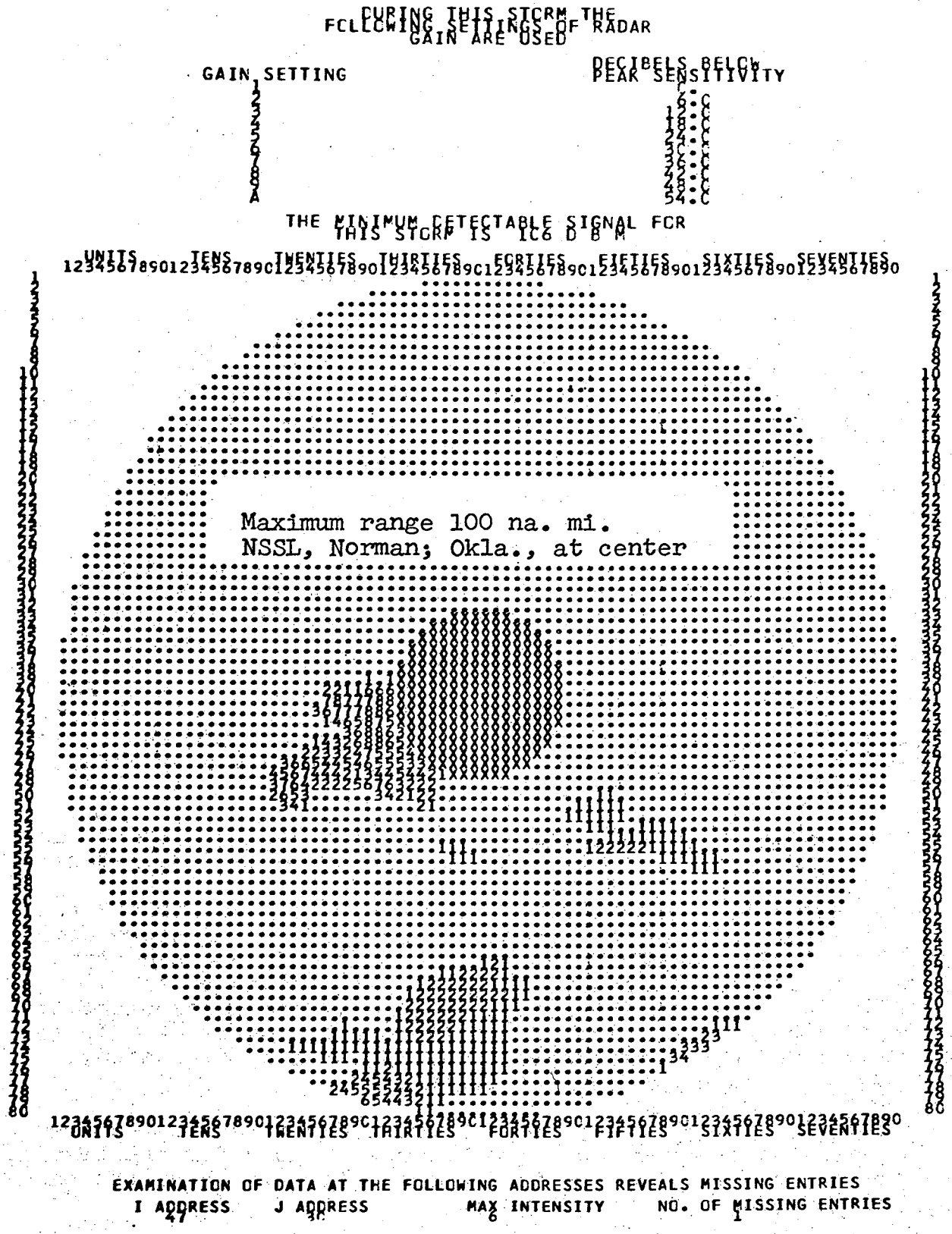

Figure 3. - Map of echo intensities, 1757 CST, April 23, 1964, as assembled by computer from punch cards.

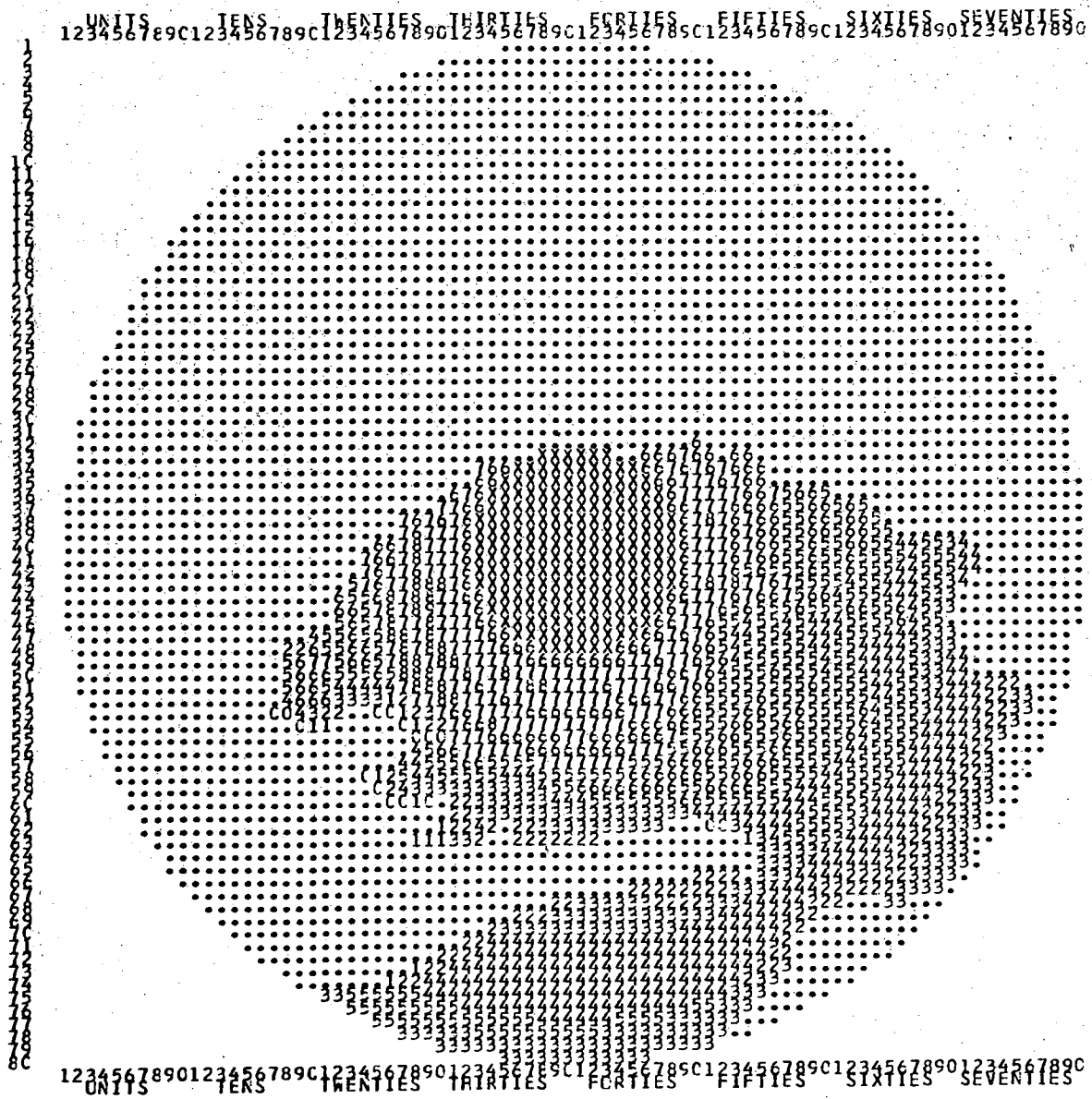

Figure 4. - Height of echo tops, April 23, 1964, 1729 CST, in units of 5,000 feet, as assembled from radar data prepared at NSSL for computer processing.

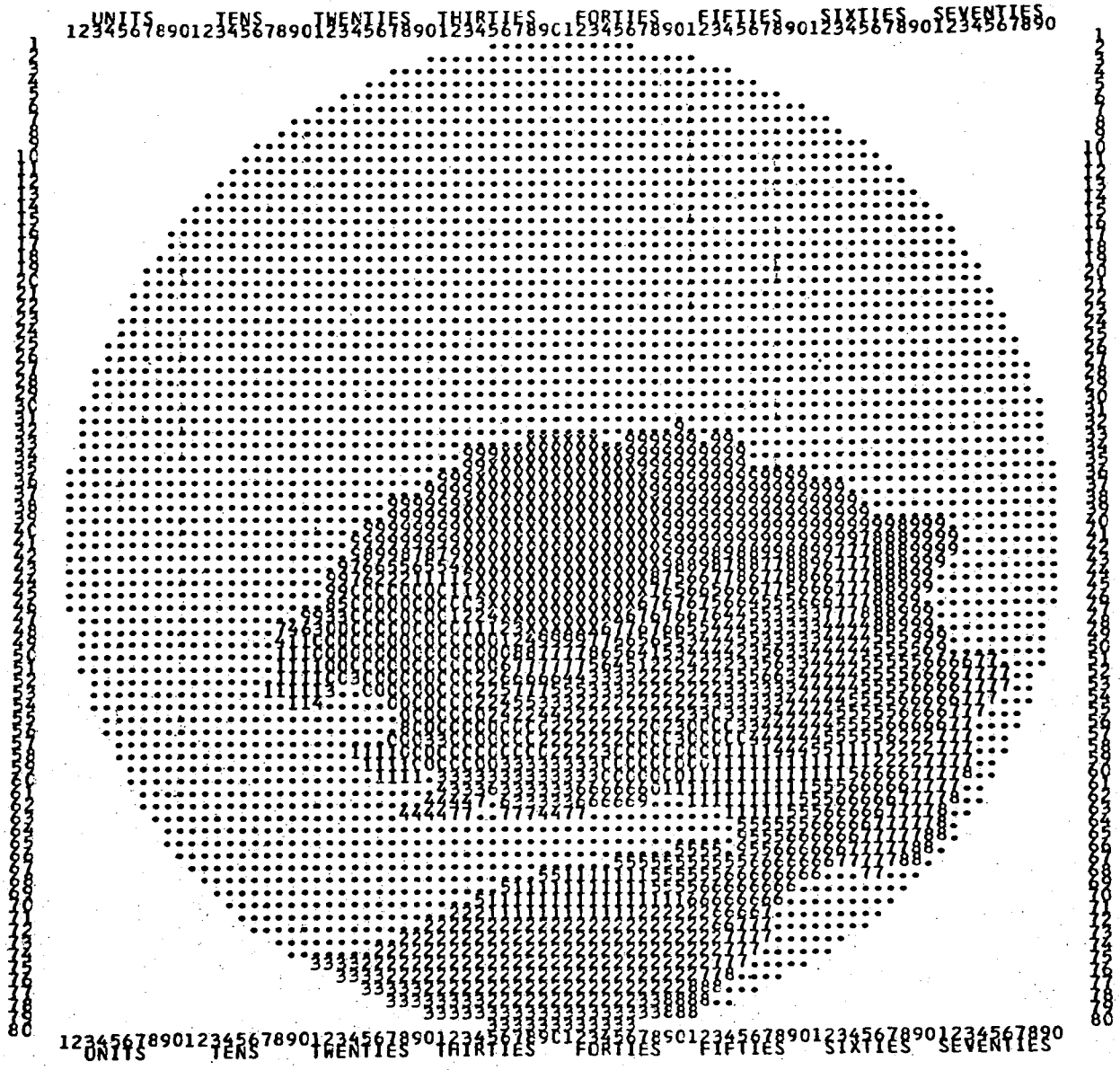

Figure 5. - Height of echo bases, April 23, 1964, 1729 CST, in units of 2,000 feet.

Table 2 - 1964 Processing Time

Date 1964	Data	Tracing and Digit. in Hours	Tracing and Digit. Time Per Seq.	Card Check 1401	Card Check 7090	Assembly CAPPI 1401	Assembly CAPPI 7090	Precip. 1401	Precip. 7090	Stat. Prop. 1401	Stat. Prop. 7090
April											
3	NRO WSR-57	143	4	2:00	1:10	1:40	1:50	0:15	0:30	1:30	3:30
3	NRO WSR-57 & Mesonetwork	130	5	--	--	1:50	2:35	--	--	1:00	4:20
4	NRO WSR-57	108	4-1/2	1:20	0:45	1:20	1:15	--	--	--	--
12	NRO WSR-57	2	2	--	--	0:10	0:10	--	--	--	--
23	NRO WSR-57	137	5-1/2	--	--	0:45	1:30	0:15	0:30	0:45	1:40
26	NRO WSR-57	1	1	0:10	0:10	0:10	0:10	--	--	--	--
May											
1	NRO WSR-57	35	4	0:20	0:25	0:25	0:40	0:35	0:15	1:00	2:40
9	NRO WSR-57	223	5	1:10	1:45	1:15	2:10	0:40	1:00	1:00	4:10
10	NRO WSR-57	191	6	1:00	1:15	1:00	1:50	0:20	0:30	0:50	2:45
14	NRO WSR-57	43	4-1/3	0:20	0:30	--	--	--	--	--	--
15	NRO WSR-57	3	1-1/2	0:10	0:10	--	--	--	--	--	--
21	NRO WSR-57	74	5	0:20	0:30	--	--	--	--	--	--
22	NRO WSR-57	148	5	0:30	1:00	--	--	--	--	--	--
29	NRO WSR-57	197	5-1/2	--	--	0:25	0:45	0:20	0:40	0:30	1:45
June											
4	NRO WSR-57	42	4	0:15	0:30	--	--	--	--	--	--
5	NRO WSR-57	67	5	0:15	0:30	0:20	0:40	0:10	0:20	0:40	1:15
11	NRO WSR-57	102	4	0:40	1:00	0:45	1:15	0:20	0:30	1:00	2:00
12	NRO WSR-57	105	4	1:00	1:15	1:00	1:00	0:15	0:30	1:00	2:00
Oct											
12	NRO WSR-57, MPS-4	51	5	0:45	0:45	--	--	--	--	--	--
Nov											
3	OKC,NRO WSR-57	9	4-1/2	0:15	0:20	0:15	0:30	--	--	--	--
14-15	OKC WSR-57	172	4	1:00	2:00	1:10	2:20	0:45	1:00	1:15	4:10
	TOTALS:	1988		11:30	13:00	12:30	18:40	3:55	5:45	10:30	30:35

The average time required to trace, digitize, and correct each sequence was approximately 4 hours. The time varied from 1 to 5-1/2 hours according to the scope coverage, and statistical properties of the radar data.

4. ADDITIONAL ANALOG-TO-DIGITAL PROCESSING PROGRAMS

A. Aviation Data

Acceleration of an F-11 aircraft normal to its line of flight was recorded on 65-mm. film during the 1964 program of in-storm turbulence observations. The Benson-Lehner Oscar Model K with card punch was used for reading and recording these data with precision to the nearest thousandth part of the acceleration of gravity. The data have been listed with a 407 tabulator and used with radar data for the turbulence studies reported by Lee elsewhere in this report.

Turbulence data recorded on the F-100 aircraft have been processed under auspices of the Aeronautical Systems Division, USAF, Wright-Patterson AFB, Ohio.

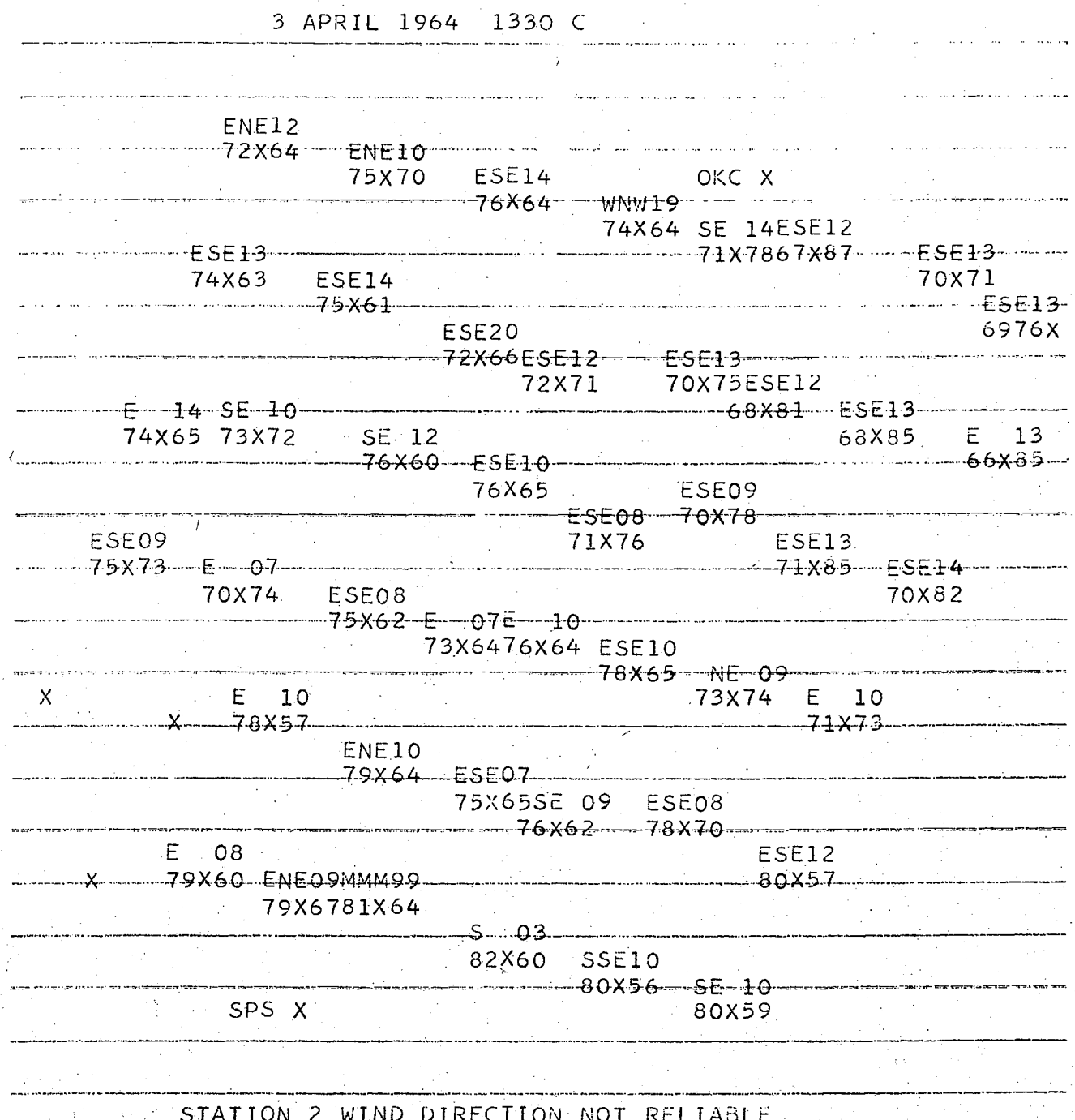

Figure 6. - Map of mesonetwork data, April 3, 1964, 1330 CST, assembled from punch cards by a tabulator. Reading a station model clockwise from top right, there is listed wind speed in knots, relative humidity, temperature, and wind direction.

B. Mesonetwork Data

The NSSL mesonetwork is discussed in detail by Sanders elsewhere in this report. The network was an expanded version of the NSSP Beta network of preceding years, and many data-processing methods in earlier use were continued. Time corrections were accurately apportioned to every part of every record. Improved procedures for checking and time annotating were established by the mesonetwork supervisor and closely coordinated with the Data Reduction Unit.

A program planned for extensive use during 1965 involves readout of analog data to punch cards with the Benson-Lehner equipment and use of a tabulator for automatic plotting of weather data in a format suitable for visual inspection and map analysis. One of a large number of possible listings of the mesoscale surface network data is illustrated in figure 6. Microbarograms, hygrothermograms, rain gage charts, and wind records of the 1964 season are cataloged, microfilmed, and stored at NSSL.

The records produced by data processing are needed for applied and basic research in severe storm analysis and forecasting and they are important for studies of communications and data processing in the national weather system.

REFERENCE

Kessler, Edwin and John A. Russo, "A Program for the Assembly and Display of Radar-Echo Distributions," Journal of Applied Meteorology, Vol. 2, No. 5, Oct. 1963, pp. 582-593.

RADAR DATA ACQUISITION TECHNIQUES

Charles G. Clark and J. T. Dooley

1. INTRODUCTION

A WSR-57 radar system is used at NSSL for research oriented to Weather Bureau missions. The radar was new when acquired in 1962 and installed on a 75 ft. tower adjacent to NSSL offices. The radar has operated routinely for three years without a major breakdown. Although no basic modifications to this radar have been made, it has been continually modernized by the addition of improved control, processing, and data recording systems. This paper reviews the WSR-57 radar program as it existed during 1964.

2. DATA GATHERING FEATURES OF THE WSR-57 SYSTEM

A simplified block diagram of the NSSL WSR-57 radar system is shown in figure 1. The received signal is range normalized by the Sensitivity Time Control (STC) at the preamplifier. The linear receiver output is displayed directly on three PPI scopes and an RHI scope. The output of the log IF strip is processed by a multichannel contour circuit, and displayed on a type VK-2 PPI repeater.

As shown in figure 1, the WSR-57 attenuator strip is located between the preamplifier and the IF linear amplifier. Attenuation is accomplished by preset, precision resistors controlled by sealed relays. This system has been very reliable in routine use at NSSL. The received signal can be attenuated automatically, in steps of 3n db., where n is an integer, to a maximum of 66 db.

A component for automatic control of the antenna elevation-angle was designed and built by D. Sirmans [1] with parts costing less than $100. This utilizes a resistance network which alters the stator voltage of the antenna control synchro-mechanism.

The WSR-57 system is normally operated automatically, with a step-sequence of receiver sensitivity at a low elevation angle, followed by azimuthal scans at successively higher elevation angles, with continuous photography of the PPI displays. The flexibility built into controls for the automatic attenuator and antenna elevation circuits is indicated in table 1.

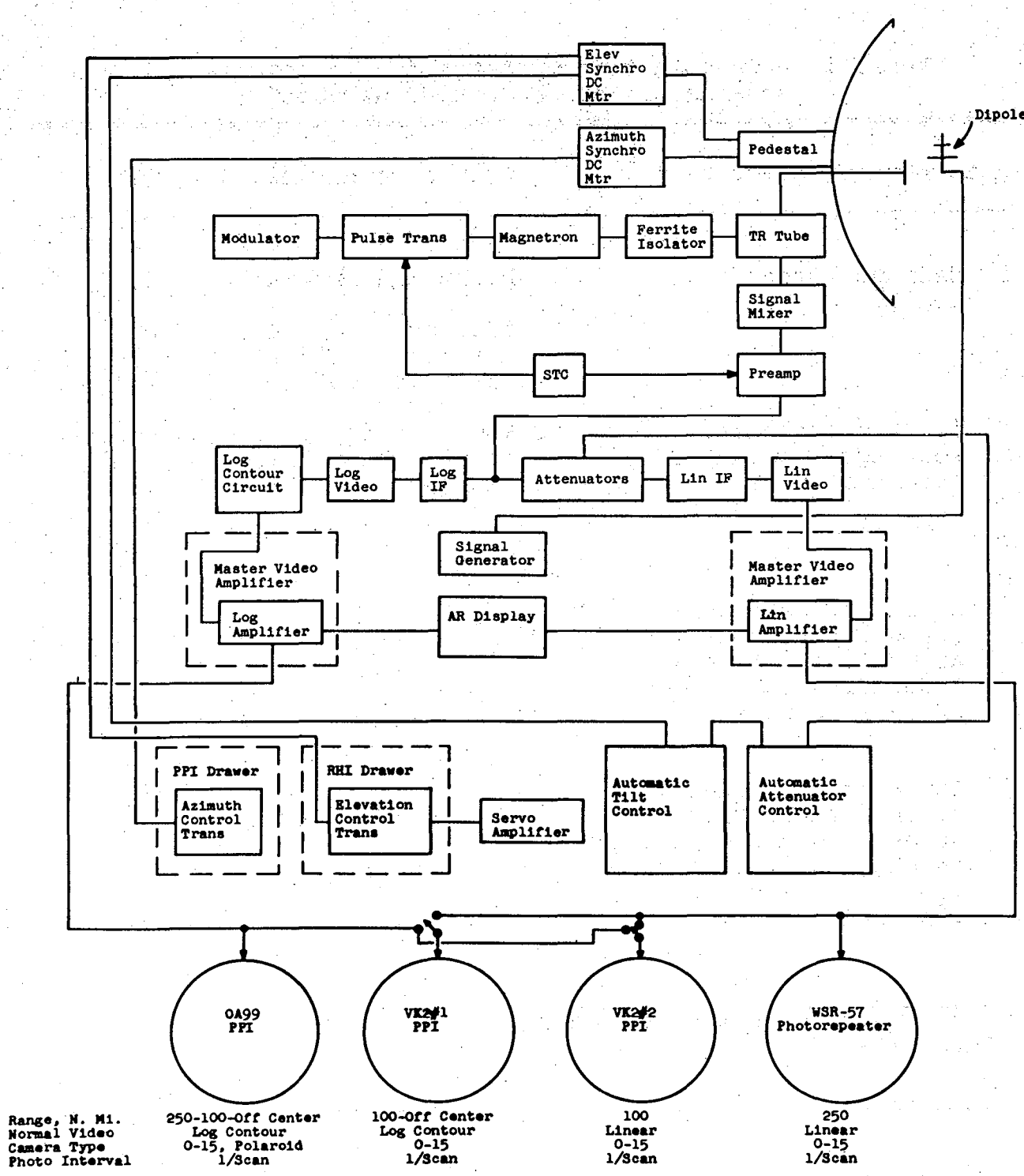

Figure 1. - Simplified block diagram of NSSL's WSR-57 system.

Table 1. - Capabilities of Automatic Attenuator and Antenna-Elevation Control Circuits

Auto Attenuator Control	Auto Antenna Tilt Control
1. Maximum attenuation 66 db.	1. Four tilt programs -
	Program A B C D Interval 1° 2° 3° Preset Max Tilt 10° 20° 20° 14°*
2. First 6 attenuator settings - amount of attenuation can be controlled by push buttons.	2. Number of steps can be reduced as desired with corresponding increase in cycling rate.
3. Number of attenuation steps can be selected as desired with corresponding variations of cycling rate.	
4. Attenuation sequence on any or all tilt steps with corresponding changes in cycling rate (normal attenuation on 0° only).	

*Preset program tilts at 1° intervals through 6° then 2° intervals to 14°.

A program objective is to monitor the echo intensity distribution continuously in time throughout the atmospheric space. However, it is also important to collect three-dimensional data at a rate at least commensurate with the growth of new echoes. Limitations of the antenna scan rate, and other more fundamental restrictions suggest a compromise between resolution in space sampling and speed in cycling.

Figure 2 shows, as a function of accumulated time, how much of the atmospheric volume within 100 n. mi. range is sampled to a height of 60,000 ft. when one antenna scan in azimuth is made at each elevation indicated in Tilt Program D (table 1). Figure 2 also illustrates that only about 90 percent of the volume can be sampled efficiently. In recent NSSL practice, this sequence of elevation steps follows a series of attenuation steps at 6 db. intervals at 0° elevation. The combined series of PPI photographs is digitized and computer-processed to yield the low-altitude distributions of echo intensity, and the approximate heights of echo tops and bases, as discussed and illustrated on pp. 111 ff in this report.

3. WSR-57 SYSTEM CALIBRATION

The transmitted power, and other indicators of system performance, are monitored as part of a monthly preventive maintenance schedule.

A dipole is mounted inside the radome and connected by a coaxial cable to a signal generator on the radar console. The coupling loss between dipole and signal generator is measured monthly by using a test signal and directional coupler on the antenna pedestal and comparing simultaneous MDS readings at the console and at the TR box in the radome.

Daily MDS calibrations are made by PPI photography of the test signal transmitted through the dipole with stepped attenuation of the test signal output. From 15 db. above the A-scope MDS, the test signal is attenuated 2 db. per PPI scan until the signal disappears on the PPI scope. The MDS on film is read to within 2 db.

At present, the receiver sensitivity is never adjusted through the receiver gain. If the A-scope MDS is below -105 dbm, operations are discontinued and maintenance performed. The MDS is stable within 2 db., as revealed by a series of thrice-daily calibrations for one week.

The MDS determined by photography of conventional PPI's is not the same for the average power of steady test signals as for fluctuating weather signals. The average weather echo PPI thresholds may be somewhat below the thresholds for steady power; the exact value depends on the CRT settings and decisions of the film reader. Signal processing techniques to provide precise PPI displays of distributions of average weather echo power are being developed.

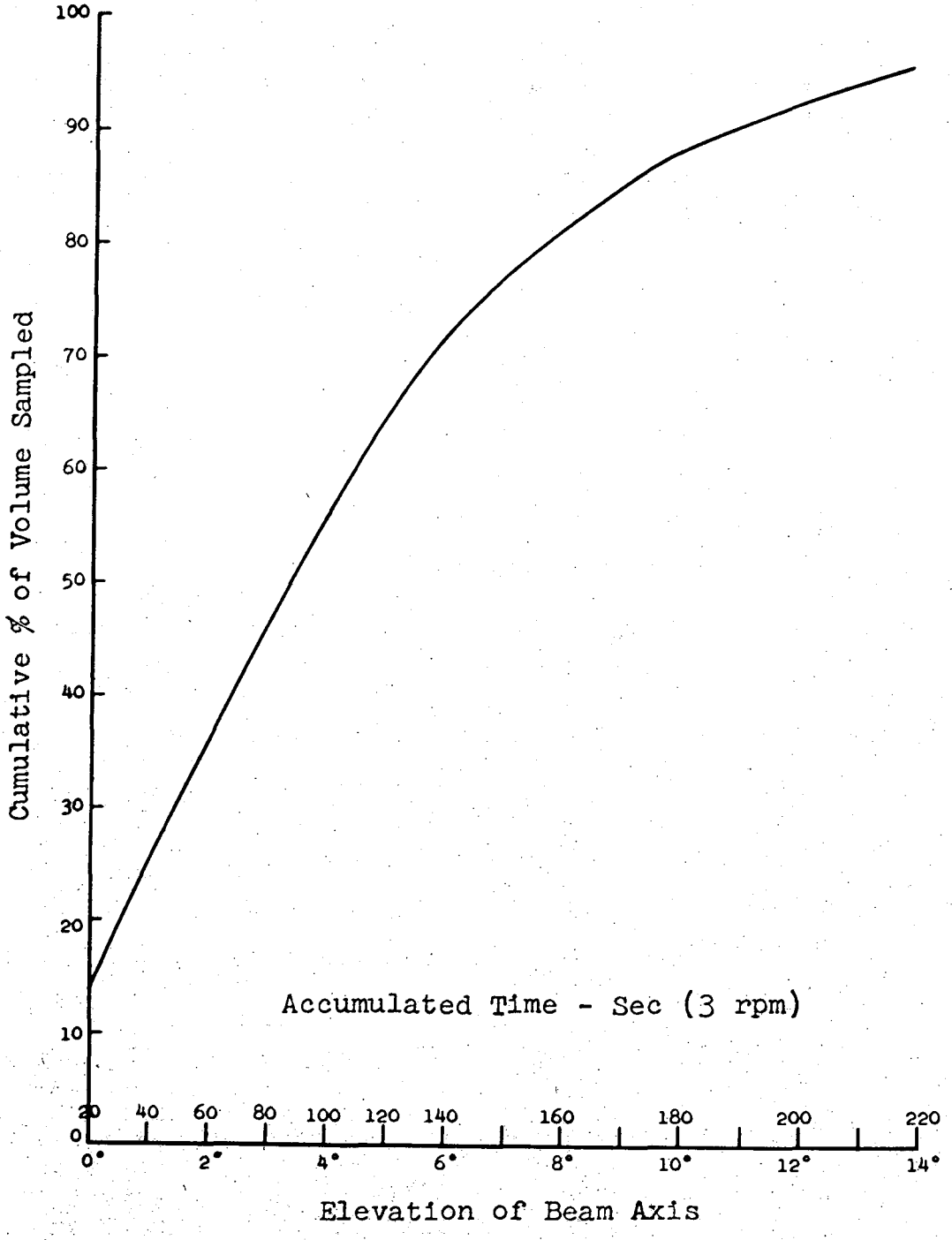

Figure 2. - Time required to scan indicated percentages of the atmospheric volume within 100 miles and below 60,000 feet.

There is also daily monitoring of the sensitivity time control (STC), adjusted to normalize all echo intensities to 100 n. mi. according to the well known inverse-range-squared law. This calibration is based on maintaining constant A-scope amplitude of a constant test signal whose range (delay) is stepped by measured increments while the I.F. attenuation is varied in steps of 3 db. The height of the test signal is compared to the amplitude of range marks also displayed on the A-scope, and STC variations within 1 db. are easily detected. When STC correction deviates more than an estimated 1 db. from the inverse R^2 law, the STC is readjusted.[1]

Known sources of calibration error in the NSSL WSR-57 system before photography are controlled by the means described above to within ± 2 db.

4. PPI PHOTOGRAPHY

The MDS recorded on film depends upon the cathode ray tube (PPI or RHI) setting and the characteristics of the film used. The receiver noise level can be suppressed at the PPI CRT by adjusting the intensity control; then the signal strength must be much above the noise level to register on film. Sweep intensity was controlled during 1963-64 to keep high contrast between echo and no echo.

The usual technique of PPI adjustment involves (1) reduction of the video gain; (2) establishment of the PPI sweep intensity at threshold visibility; (3) increase of the video gain to the maximum which does not produce "blooming" of the display. This technique is subjective. However, when several operators are in the darkened radar room for a considerable period they usually adjust the PPI display to yield similar photographic MDS's. The spread of results of one test with three operators was only 1 db.

The suppression of the film MDS below the receiver MDS has varied between 2 and 8 db. and averages about 6 db. The variations are monitored by photographing the test signal and comparing threshold intensities on film with the MDS defined by visual examination of the A-scope. However, variations of the film MDS complicate data processing, even when the variations are accurately monitored. Analyses of the 1963 data show that the variable film MDS is associated with voltage drifts in the CRT sweep intensity control.

---

[1] Daily temperature variations up to 70°F. in the radome adversely affected STC stability until an improved circuit received from the USWB Instrumental Engineering Division was installed.

The CRT intensity is now monitored during radar operations with a photo cell whose sensitivity matches CRT florescence. Preliminary results indicate that this technique permits continuous accurate control of the film MDS with little effect from ambient light sources or subjective factors. A thorough, technical treatment of this PPI display problem can be found in reports of the Stormy Weather Group, McGill University [2].

During 1963-64, Kodak Plus-X, emulsion type 4231, 35 mm. film was used in the 0-15 cameras for photographing the CRT displays. The sensitivity of the Plus-X film and the radiant energy characteristics of the CRT's P-7 phosphor are shown in figure 3 (curves a and b, respectively). The emission spectrum shows that maximum CRT radiation is at 4400 Ångstroms. This corresponds to florescent excitation of the phosphor. A secondary peak at 5500 Ångstroms is the florescence-induced phosphorescence, a persistent emission. Persistence is unwanted in CRT photography because diffusion of the florescent excitation within the phosphor causes defocussing of the original image, and because programs using serial photography at steps of receiver gain or antenna elevation angle may be associated with ghost images from preceding radar scans.

The phosphorescence spectrum can be effectively filtered by the 47B filter, figure 3 (curve c). However, this filter reduces the CRT's transmitted light by 50 percent. Reduction of the CRT image intensity can be compensated for by increased f-stop (with decreased depth of field) or increased exposure time (with decreased data-gathering rate).

Modern film emulsions incorporate many features and special emulsions which are particularly suitable for photorecording PPI displays. A new film well suited for PPI photography is Eastman Dacomatic S0266 now in use at NSSL. The sensitivity of the Dacomatic S0266 and the radiant energy of the CRT are shown in figure 3 (curve d). Due to the sensitivity of Dacomatic, a 47B filter is not needed. Thus a smaller lens aperature can be used than with Plus-X with associated reduction of focussing problems.

Table 2 compares Dacomatic S0266 with Plus-X. Increased speed and resolution of Dacomatic is associated with simplified processing, since this film can be developed under a red safelight.

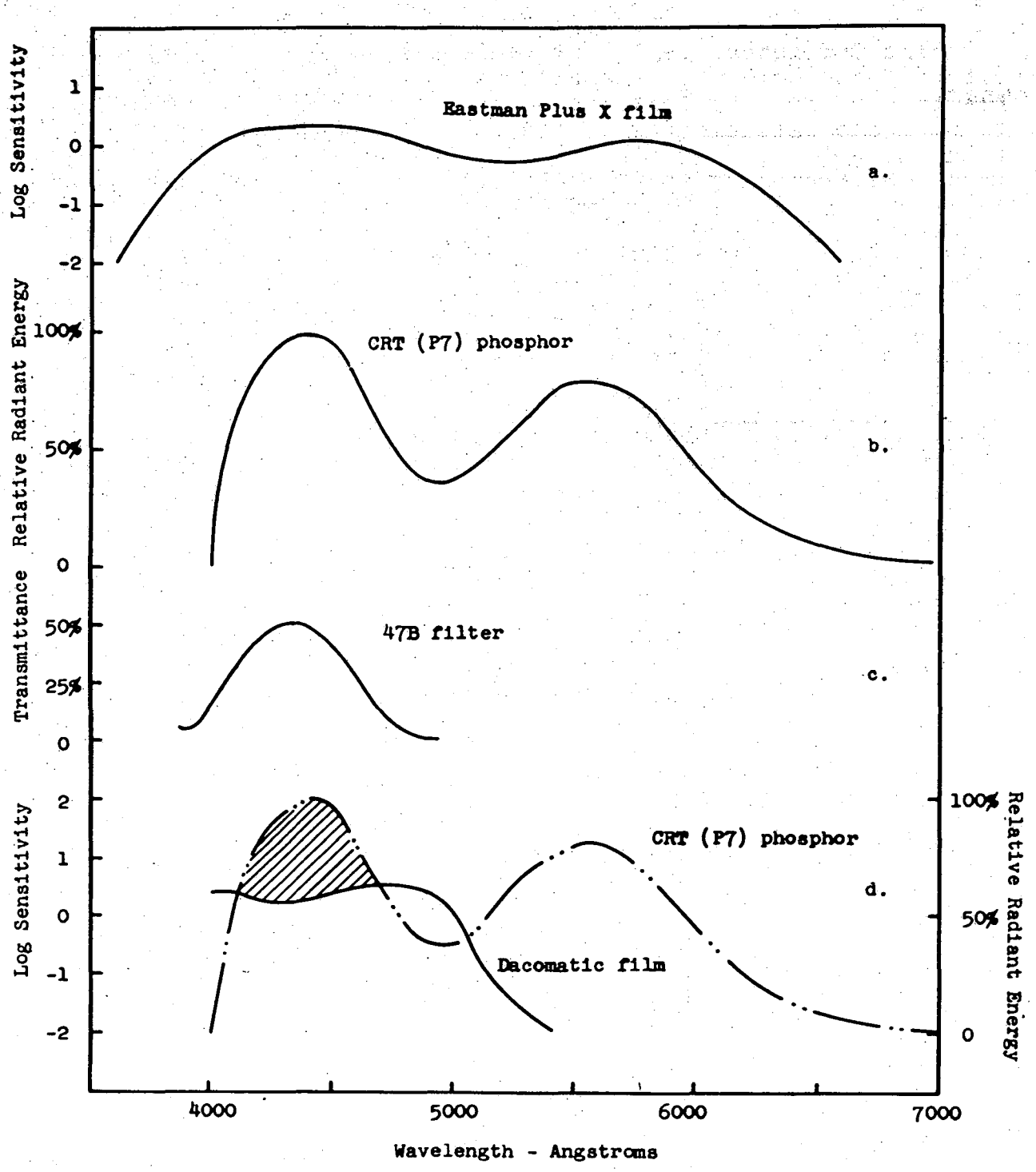

Figure 3. - Film, filter, and CRT characteristics.

Table 2. - Comparison of Kodak Dacomatic and Plus-X*

Characteristics	Plus-X 4231	Dacomatic-S0266
Color Sensitivity	Panchromatic (All color sensitive)	Monochromatic (Blue light only)
f-stop	2.8 with 47B filter	5.6 without filter
Resolving Power	About 100 lines/mm.	About 200 lines/mm.
Safelight	Total Darkness	Red Series 1

*Film was evaluated by exposure to type VK-2 PPI scope with P-7 phosphor operated with WSR-57 radar, with one PPI scan/20 sec. An O-15 camera was used with a hood at a focal distance of 25 in.

5. THE PRESENT DATA COLLECTION PROGRAM IN RELATION TO THE FUTURE

The data collection system described in this paper contains many interim techniques. The system will be upgraded as improved means for signal processing are developed. Components which provide some integration of the fluctuating weather echoes will permit accurate display and recording of many steps of signal intensity during one azimuth scan of the radar antenna. At this time, the relatively simple system described above provides systematic collection of comprehensive data, invaluable for the meteorological studies discussed elsewhere in this report.

REFERENCES

1. Watts, W. L., D. Sirmans, and J. T. Dooley, "WRL Techniques with Field Station Applications," Progress Report No. 13, WSR-57 Radar Program, U. S. Weather Bureau, 1963.

2. Legg, T. H., "The Quantitative Display of Radar Weather Patterns on a Scale of Gray," Scientific Report MW-31, Stormy Weather Group, McGill University, June 1960.

NSSL MESOSCALE NETWORK OF SURFACE STATIONS

Leslie D. Sanders

ABSTRACT

In an attempt to acquire new knowledge of surface circulation patterns of severe thunderstorms and other mesoscale weather phenomena, special networks of recording stations have been operated by NSSP and NSSL since 1961. A brief history of these operations is followed by a detailed description of the present 52-station mesonetwork operated by NSSL in south-central Oklahoma during the spring severe storm season.

1. INTRODUCTION

From the beginning of the National Severe Storms Project in 1961, surface networks for study of mesoscale features of severe convective storms have constituted an integral part of the data collection program. Surface networks on two scales have been operated by NSSP and NSSL.

An "Alpha" network of approximately 200 stations, recording barometric pressure, temperature, relative humidity, and rainfall, was established in 1961 as shown by figure 2 in [1]. The Alpha network was a continuation, with numerous station relocations, of the original "Pressure Jump Network" established in Nebraska, Kansas, and Oklahoma in 1950 under the supervision of M. Tepper [2]. All stations were equipped with 12-hr. microbarographs, and the majority of the stations were equipped with 12-hr. hygrothermographs and 24-hr. recording precipitation gages. The Alpha network stations were 30 to 50 mi. apart and covered all of Oklahoma and those portions of Kansas and Texas lying between 30° 30' and 38° 30' N. Lat. The 200-station network was operated during March-June 1961 and 1962. During the 1963 season, it was reduced to 130 stations in Oklahoma and in Texas north of 31.5° N., and the entire network was discontinued June 30, 1963 in order to concentrate research activities on the smaller-scale Beta network.

The current NSSL mesonetwork was established in spring 1961 with 36 stations in south-central Oklahoma. The network grid spacing is on the "Beta" scale of approximately 10 x 15 n. mi., with stations on a 6 x 6 grid oriented nearly WNW-ESE and NNE-

SSW.[1] This orientation maximizes areal coverage of storms and the time continuity of their records for the usual cases of storm orientation and motion. A detailed index and description of the 1961 Beta network has appeared earlier in this preprint series [3]. The network was operated during the season of maximum incidence of severe thunderstorms, March to June, inclusive, from 1961 through 1964.

Five stations were added to the northwestern corner of the network at the beginning of the 1963 spring season. These were placed to encompass a dense network of 170 recording rain gages operated in the Washita watershed by the U.S. Department of Agriculture, Soil and Water Conservation Research Division, Agricultural Research Service (ARS), Chickasha, Okla. Records from this rain gage network are available for research use through the cooperation of ARS. The 1963 mesonetwork is shown as figure 4 in [4].

The network was further expanded by the addition of six stations on the western side during March and April 1964, bringing the total to 47 stations in a 6 x 8 array, with a station omitted on the southwestern corner.

Five additional stations were established on March 1, 1965 on the northern side of the network. These stations, on a WNW-ESE line through Oklahoma City were added to extend the N-S coverage of squall line systems, and are the first step in providing mesonetwork coverage encompassing the site of a tall television tower in northern Oklahoma City which is to be instrumented by NSSL during 1965. When the tower installation is completed, four additional stations are planned; one near the base of the tower, and three in the next grid row north of the tower.

The 1965 mesonetwork operated by NSSL is shown in figure 1. Figure 2 shows in detail the rain gage network operated by the Agricultural Research Service.

2. INSTRUMENTATION

The "Beta" mesonetwork stations are all identically equipped to record wind speed and direction, barometric pressure, temperature, relative himidity, and precipitation.

---

[1]Beta network spacing of 5 x 7.5 mi. was suggested by T. Fujita and H. A. Brown in "Design of a Three-Dimensional Meso-Meteorological Network," Quarterly Report No. 4, 1 January - 30 April, 1960, Contract DA-36-039 SC-78901, Department of the Army Project 3A99-07-001-04-01.

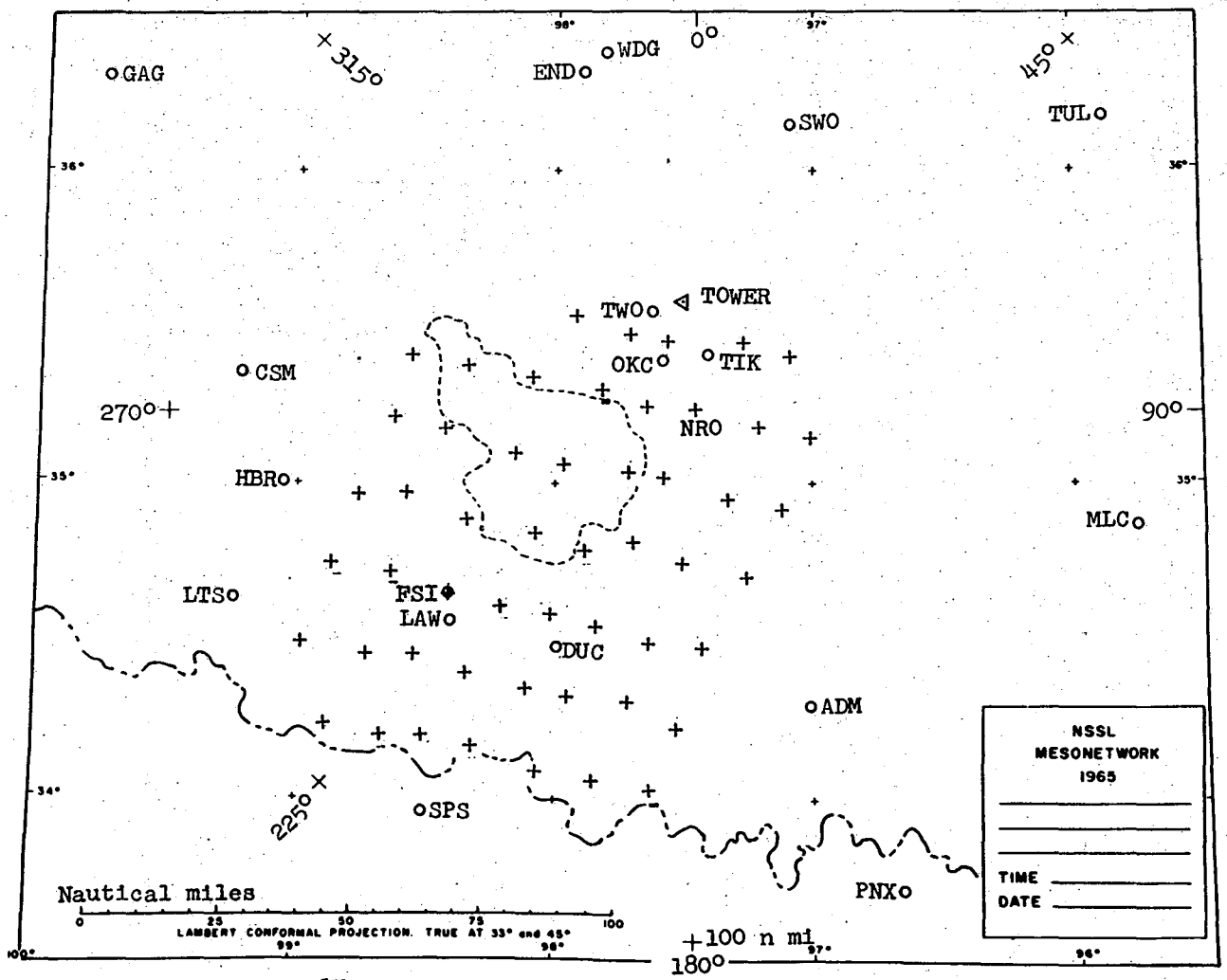

Figure 1. - 1965 NSSL Mesonetwork. Network stations are shown by crosses; other weather reporting stations by circles. Upper-air soundings are made at WBAS, Oklahoma City (OKC), Tinker AFB (TIK) and U. S. Army 26th Artillery at Fort Sill (FSI). Dashed line outlines the rain gage network operated by the Agricultural Research Service. Location of WKY-TV tower to be instrumented in 1965 is shown by the triangle.

Wind sensors consist of standard Weather Bureau F420C-1 wind speed transmitters and F005 wind direction transmitters mounted 22 ft. above ground on a guyed 10-in. triangular steel tower (fig. 3). Wind speed is recorded in knots as a continuous trace on an Esterline-Angus DC-voltmeter type analog-event recorder at a chart speed of 3 in./hr. Wind direction is recorded by 8 event pens actuated once each minute for a period of about 10 sec. During actuation all direction contacts made by the direction transmitter are recorded. It is usually practical to interpolate directions to 16 compass points. Wind recorder charts are changed weekly by the network field manager and an assistant. Calibration of wind speed transmitters and orientation of direction transmitters are checked at the beginning and end of each operating season.

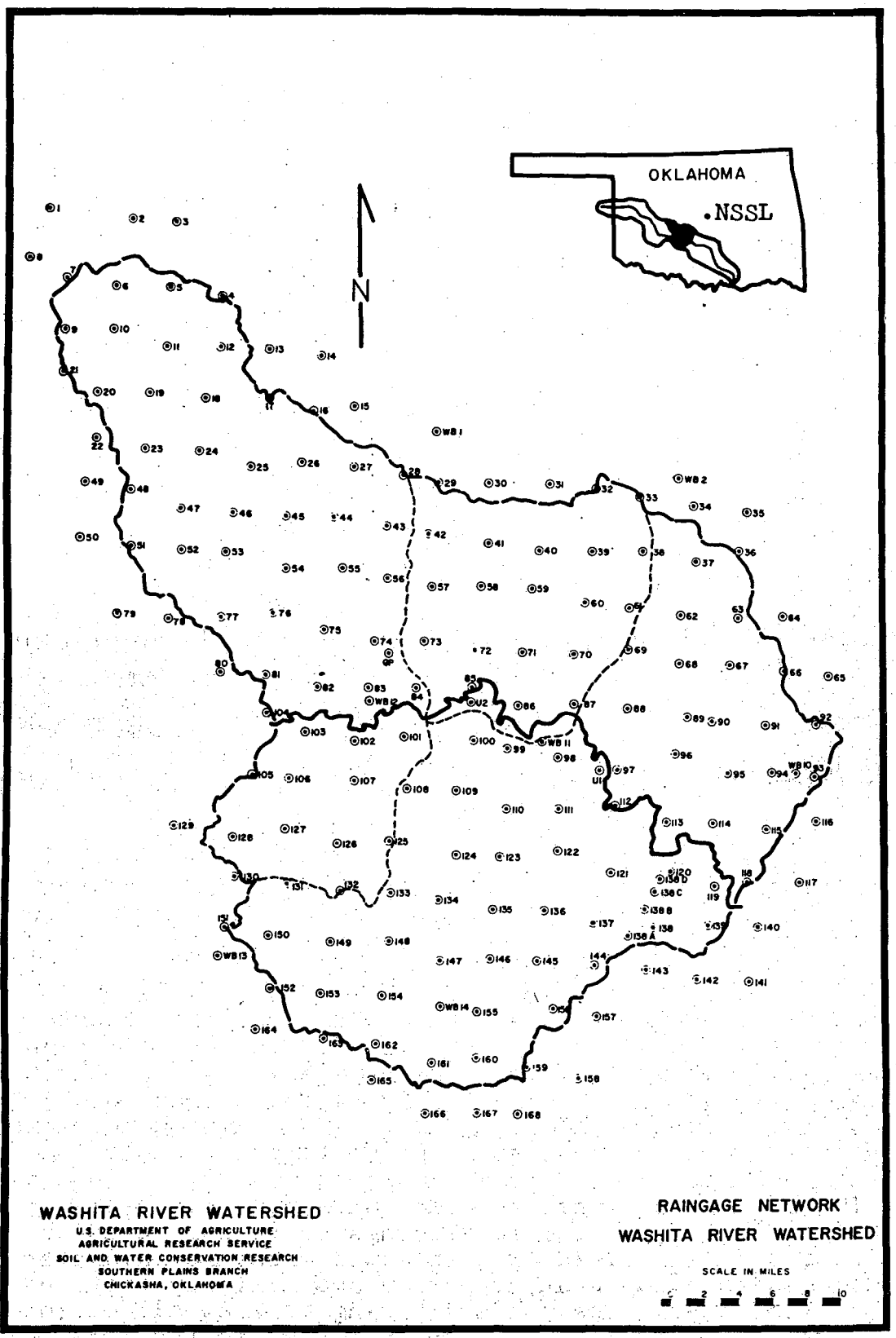

Figure 2. - Agricultural Research Service rain gage network in Washita watershed.

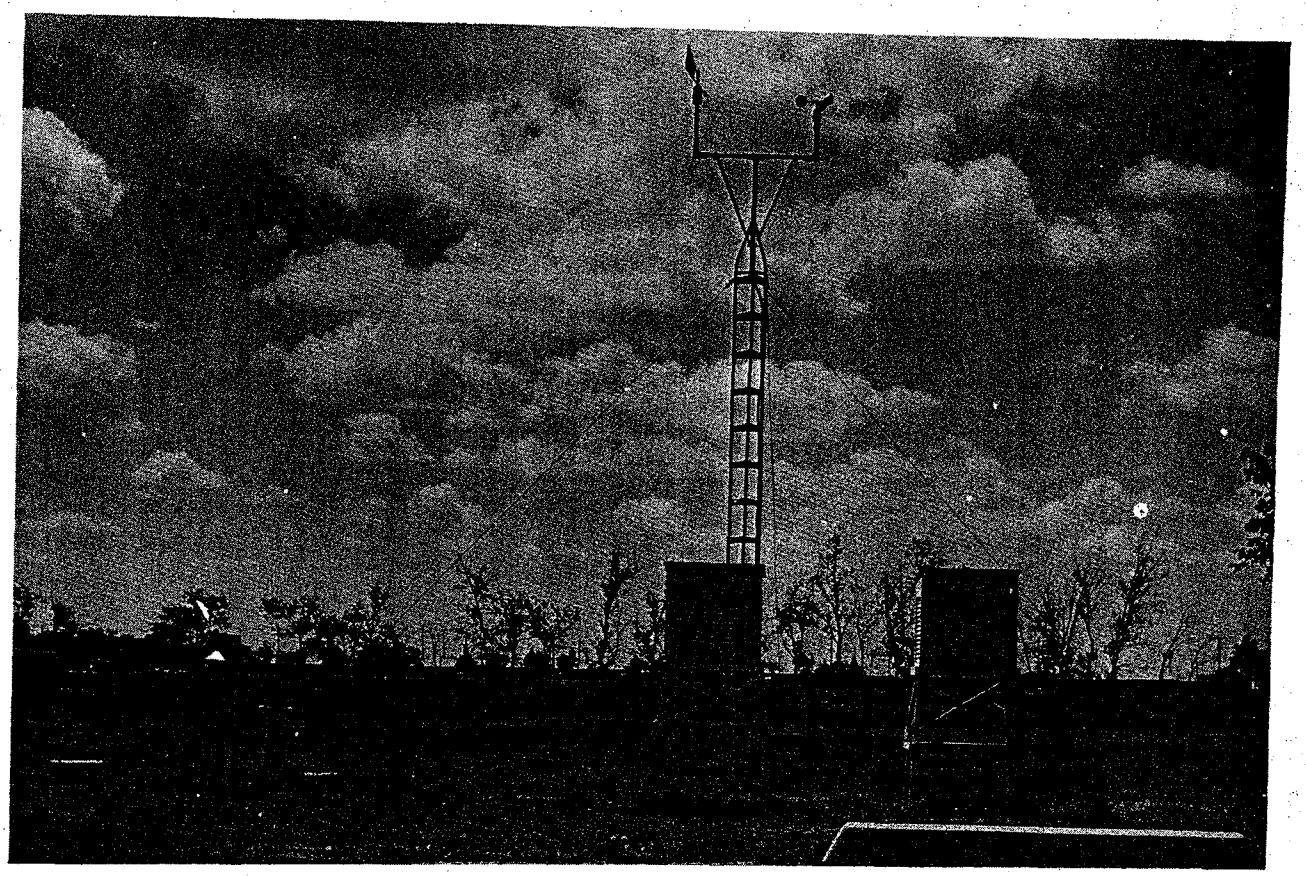

Figure 3. - Mesonetwork installation at Norman (3F). Extra instrument shelter, and two smaller rain gages are property of Oklahoma University Atmospheric Research Laboratory, and are not part of a typical installation.

Barometric pressure is recorded on Friez or Instruments Corp. microbarographs with scale magnified 2-1/2 to 1. All microbarographs have 12-hr. gears giving approximately 1 in. of chart travel per hour. Pressure can be read to the nearest 0.005 in. Hg, and time resolved to about 1/2 min. The damping mechanisms are disconnected to permit fast response to the rapid pressure changes characteristic of severe thunderstorms. From 1961 through 1964, pressures were recorded on a relative basis only. Pressure analyses thus required readings to be corrected to conform to a smoothed field of a selected pressure parameter measured at surrounding Weather Bureau and military stations. During the 1965 operations, we are trying to keep all microbarographs adjusted to station pressure by comparing them bi-weekly with a portable Kollsman precision aneroid barometer. If successful, this will simplify pressure reduction and analysis

procedures. Preliminary results are encouraging.

Temperature and relative humidity measurements are made with Belfort or Friez hygrothermographs (10° to 110° F. range) mounted in shelters about 4-1/2 ft. above ground. Hygrothermographs have a Bourdon tube temperature element and a hair hygrometer element. Instruments are serviced and adjusted immediately before installation in the field. Psychrometric comparisons are made in the field each week using portable aspirated psychrometers. Instruments are adjusted if errors exceed 2°F. or 10 percent relative humidity; otherwise the comparisons serve as a basis for determining corrections to be applied to indicated chart values. Analysis of psychrometric comparisons made in 1964 shows that the probably errors of temperature and relative humidity are ± 1°F. and ± 6 percent. The magnitude of the relative humidity error is dependent on the recent history of humidity conditions experienced. Temperatures and relative humidities are read to the nearest 0.5°F. and 1 percent. As with the microbarograph, 12-hr. gears are used, giving 2 traces per 24 hours, with charts changed daily.

Precipitation gages are of the weighing-recording type with 6-in., or 12-in. dual traverse capacity, and a 1:1 scale ratio. As with the hygrothermograph and microbarograph, the rain gages are operated with 12-hr. gears, giving a time scale of slightly less than 1 in./hr. Charts are changed daily whether or not precipitation has occurred. The rain gages are unshielded.

3. TIME SYNCHRONIZATION

The use of mesonetwork records for detailed analyses, which may include synoptic analyses at time intervals as short as 5 min., requires precise timing of the recorder charts. Observers cannot be relied upon to give the required precision.

During the operational seasons of 1962-1964, inclusive, an electric timer operating through a relay was used to switch a fixed voltage into the wind-speed circuit twice daily, thus placing time reference marks on the wind record. The relay simultaneously activated solenoids which jogged the pen arms on the other three recorders. This provided cross referencing in relative time of the various charts at a given station. Absolute time reference was obtained by using chronometers to determine the weekly "on" and "off" times of the wind recorder chart. This permitted correction of the indicated chart times for recorder clock error. Corrected times of the reference marks were then entered on each chart with an estimated precision of ± 1 min. This system had the fault of being entirely dependent on electric power for timer operation, and power failures are too frequent during severe storms when the records were most important.

Table 1. - NSSL Mesonetwork, March 1 - June 30, 1965

Station No.	Station Name	Latitude[2] o '	Longitude[2] o '	Approximate Elevation Ft.
2C	El Reno	35 32.6	97 55.6	1325
2D	Yukon	35 29.5	97 42.6	1270
2E	Oklahoma City	35 27.2	97 34.5	1200
2F	Choctaw	35 26.8	97 16.0	1235
2G	McLoud	35 24.7	97 05.9	1115
3A	Hydro	35 24.7	98 34.3	1645
3B	Lookeba	35 22.3	98 20.5	1440
3C	Cogar (Minco)	35 20.1	98 04.7	1425
3D	Tuttle	35 17.7	97 49.7	1310
3E	*Newcastle	35 15.2	97 39.2	1315
3F	Norman	35 14.2	97 27.7	1180
3G	Little Axe	35 11.4	97 12.6	1115
3H	Macomb	35 08.7	97 00.6	1025
4A	Alfalfa	35 13.1	98 37.0	1525
4B	Albert	35 10.7	98 24.5	1470
4C	Verden	35 06.3	98 08.6	1170
4D	Chickasha	35 04.2	97 58.1	1100
4E	Naples (Tabler)	35 02.6	97 42.5	1175
4F	Criner	35 01.3	97 35.0	1245
4G	Wayne	34 57.2	97 20.9	1105
4H	Rosedale	34 55.2	97 07.6	1010
5A	Sedan	34 58.0	98 45.6	1470
5B	Carnegie	34 58.3	98 34.6	1460
5C	Apache	34 53.4	98 18.2	1405
5D	Rocky Ford	34 50.7	98 04.4	1210
5E	Rush Springs	34 47.0	97 52.9	1315
5F	Bradley	34 48.8	97 42.7	1105
5G	Wallville	34 44.8	97 30.6	985
5H	Pauls Valley	34 42.4	97 16.0	1000
6A	Mountain Park	34 44.7	98 51.8	1495
6B	Cache	34 43.0	98 38.3	1510
6C	Fort Sill	34 39.2	98 24.0	1190
6D	Letitia	34 36.8	98 12.7	1125
6E	Marlow	34 35.6	98 01.1	1155
6F	Duncan Lake	34 33.4	97 50.8	1115
6G	County Line	34 30.1	97 37.9	1015
6H	Tatums	34 29.3	97 27.1	990
7A	Manitou	34 30.3	98 58.7	1255
7B	Chattanooga	34 28.0	98 43.9	1230
7C	Faxon	34 27.6	98 33.4	1095
7D	Walters Lake	34 24.4	98 20.8	1045
7E	Corum	34 21.5	98 07.4	1030
7F	Comanche	34 19.7	97 57.9	980
7G	Loco	34 19.0	97 43.9	995
7H	Wirt	34 14.0	97 31.8	960
8B	Hollister	34 14.7	98 53.8	1155
8C	*Grandfield	34 11.9	98 40.9	1105
8D	Randlett	34 12.2	98 30.5	1040
8E	Taylor	34 10.3	98 19.7	985
8F	Sugden	34 06.2	98 04.4	925
8G	Ryan	34 03.8	97 51.9	900
8H	Grady	34 01.3	97 38.1	885

*New location 3-1-65

[2]Geographical coordinates are believed accurate to within 0.1 min. Elevations are given to the nearest 5 ft. as determined from USGS topographic maps, and adjusted by hypsometry.

Prior to the beginning of the 1965 mesonetwork operations, a new timing system was devised to give hourly time marks, and to eliminate dependence on electric power. This system uses the 1-hr. gear of the wind recorder chart drive to close a microswitch and simultaneously place reference marks on all charts. The wind recorder chart, timed by chronometer, permits determination of the true time of the reference marks on all charts with an accuracy of 1 min. or less. While the system does not depend on commercial electrical power, neither does it provide an independent time source, and it would fail in the event of stoppage of the wind recorder chart drive. However, sixteen weeks' experience with this system has shown it to have advantages over the previous system. It permits more accurate time interpolation between the hourly marks and correction of time errors on hygrothermograph, microbarograph, and rain gage charts resulting from slight variations of length of the printed charts. The 1965 records reveal that this error uncorrected may be as much as 3 to 5 min.

4. FIELD SERVICE PROGRAM

The network is serviced weekly by the field manager and one assistant. This requires about 7-1/2 man days per week. During these weekly visits, wind charts are timed by chronometer and changed and charts are collected; pressure, temperature, and relative humidity comparisons are made; performance of all equipment is checked; adjustments or repairs are made as required; and operating deficiencies are discussed with observers.

Storm damage and other equipment malfunctions which cannot be repaired at the regular visit are corrected during the last two days of each week.

5. TOPOGRAPHY AND EXPOSURE OF INSTRUMENTS

As indicated in table 1, the station elevations vary from about 800 ft. at the southeastern corner of the network near the Red River to about 1600 ft. MSL in the northwestern corner. The general topography of the area is shown in figures 3 and 4 of [3].

Exposure of hygrothermographs and rain gages is considered excellent. In a few instances the wind equipment is somewhat sheltered by terrain or nearby buildings (e.g., at Taylor (8C) the wind tower was extended to 30 ft. to minimize effect of eddies around a farmhouse with N-NW winds; at Cache (6B) the station is within the Wichita Mtns. Wildlife Refuge where terrain and trees give some unavoidable shielding of wind equipment). Most of the stations are situated at farms. The requirement for electricity to operate battery chargers and the need for easy access to equipment occasionally require slight compromises of ideal exposure.

6. RECORDS PROCESSING AND DATA REDUCTION

Records are processed by Oklahoma University students under contract with the Oklahoma University Research Institute. Processing involves determining the true time of time marks and annotating charts accordingly, monitoring charts for observer errors and instrument malfunction, and microfilming and binding all records.

Experience has shown the time error of the spring-wound wind recorder chart drive to be linear over a 7-day period. The weekly chronometer comparisons are thus used to determine the true time of all "hourly" time marks on the wind charts. Each mark is labeled with the corrected time in minutes. These times are then transferred to the time reference marks on the microbarograph, hygrothermograph, and rain gage charts. The charts are then sorted, microfilmed, and bound by days. The seven-day wind chart rolls are cut into 24-hr. sections (0000 to 2400 CST), folded and bound.

All original records are retined at NSSL. Microfilm of the records is also retained, and can be made available to qualified researchers.

Procedures are being developed for digitizing synoptic data from the records by the use of trace reading equipment. As illustrated in the paper by Gray and Wilk on p. 111 of this report, the data can be printed automatically at locations corresponding to grid positions, ready for analysis.

REFERENCES

1. J. T. Lee, "A Summary of Field Operations and Data Collection by the National Severe Storms Project in Spring 1961," NSSP Report No. 5, U.S. Weather Bureau, March 1962.

2. M. Tepper, "Pressure Jump Lines in Midwestern United States," U.S. Weather Bureau Research Paper No. 37, 1954, 70 pp.

3. T. Fujita, "Index to the NSSP Surface Network," NSSP Report No. 6, U.S. Weather Bureau, April 1962.

4. J. T. Lee, L.D. Sanders, and D.T. Williams, "Field Operations of the National Severe Storms Project in Spring 1963," NSSP Report No. 20, U.S. Weather Bureau, January 1964.